

**ULTRACOLD BOSONS IN A MULTI-DIMENSIONAL, TILTED,
DOUBLE-WELL TRAP: POTENTIAL DECOHERENCE,
TUNNELING RESONANCES, AND
TWO-LEVEL PHENOMENA**

by

Dimitri R. Dounas-Frazer

A thesis submitted to the Faculty and the Board of Trustees of the Colorado School of Mines in partial fulfillment of the requirements for the degree of Master of Science (Applied Physics).

Golden, Colorado

Date _____

Signed: _____
Dimitri R. Dounas-Frazer

Approved: _____
Dr. Lincoln D. Carr
Assistant Professor of Physics
Thesis Advisor

Golden, Colorado

Date _____

Dr. James A. McNeil
Professor and Head,
Department of Physics

ABSTRACT

We study the quantum dynamics of ultracold bosons in a tilted double-well potential by exact diagonalization of one- and two-level Bose-Hubbard-like Hamiltonians. In the one-level approximation, the atoms occupy the ground level of each well. This assumption is relaxed in the two-level approximation which allows atoms to occupy both the ground and first excited levels. Furthermore, for two- and three-dimensional potentials, bosons occupying the excited level can have nonzero angular momentum, thus introducing additional degrees of freedom to these systems.

The stationary states of the one-level Hamiltonian consist of both harmonic oscillator-like and Schrödinger cat-like states. When the barrier between wells is high, cat-like states dominate the spectrum. A small potential difference between wells, or tilt, causes the collapse of the cat-like states and suppresses tunneling between wells. Such small imperfections in the trapping potential therefore constitute an additional source of decoherence, called *potential decoherence*. However, unlike for other forms of decoherence, *tunneling resonances* occur when the tilt can be exactly compensated by atom-atom interactions. At resonance, cat-like eigenstates reappear and a fraction of the atoms tunnel between wells. Tunneling at resonance is both much faster and less sensitive to tilt than in the symmetric case. Furthermore, tunneling resonances constitute a dynamic scheme for the creation of robust few-atom superposition states in a many-body system.

In the two-level approximation, the ground and excited energy levels are coupled by atom-atom interactions. The one-level approximation is valid when the interaction energy is much less than the energy level spacing, i.e., when coupling can be neglected.

In this regime, the eigenstates of the two-level Hamiltonian have definite occupation of each level and states in which all atoms occupy the ground level are well described by the one-level approximation. However, even when the coupling is weak, the two-level eigenstates undergo eigenvalue crossings when either the number of atoms or the interaction energy is greater than some critical value. Eigenvalue crossings cause cat-like states with nonzero occupation of the excited level to emerge among the lowest-lying eigenstates. When the atom-atom interactions are strong and coupling can no longer be neglected, atoms occupying the ground and first excited levels become entangled.

TABLE OF CONTENTS

ABSTRACT	iii
LIST OF FIGURES	vii
ACKNOWLEDGMENT	ix
Chapter 1 INTRODUCTION	1
1.1 Applications of Ultracold Atoms in Multi-Well Potentials	3
1.2 Theoretical Studies of Ultracold Atoms in Double-Well Potentials	5
1.3 Overview	7
Chapter 2 BACKGROUND: ULTRACOLD ATOMS IN A DOUBLE-WELL	10
2.1 Bose-Einstein Condensation	10
2.2 Effects of Reduced Dimensionality	13
2.3 Optical Lattices	14
2.4 Double-Well Potentials	16
2.4.1 Localized Single-Particle Wavefunctions	19
2.5 Multidimensional One- and Two-Level Hamiltonians	25
Chapter 3 ONE-LEVEL APPROXIMATION	36
3.1 One-Level Hamiltonian	37
3.2 Entanglement Measures	38
3.3 Characterization of Energy Eigenstates	40
3.3.1 Harmonic-Oscillator-Like States	41
3.3.2 Schrödinger-Cat-Like States	44
3.3.3 Medium Barrier	47
3.3.4 Potential Decoherence	51
3.4 Dynamics: Quantum Sloshing	54
3.4.1 Sloshing of Non-Interacting Bosons	55
3.4.2 Modulated Oscillations in the Presence of a Low Barrier	58
3.4.3 Ultra-slow Tunneling Through a High Barrier	60
3.4.4 Tunneling Resonances	62

3.5	Summary	65
Chapter 4	TWO-LEVEL APPROXIMATION	67
4.1	Two-Level Hamiltonians	67
4.2	Counting Fock States	70
4.3	Characterization of Stationary States	72
4.3.1	Eigenvalue Crossings: Decoupled Energy Levels	72
4.3.2	Shadows of Schrödinger's Cat	80
4.3.3	Eigenvalue Crossings: Weakly Coupled Energy Levels	85
4.4	Summary	90
Chapter 5	CONCLUSIONS AND OUTLOOK	92
	REFERENCES	96
	APPENDIX A HOPPING STRENGTHS	102
	APPENDIX B HARMONIC-OSCILLATOR-LIKE STATES	104
	APPENDIX C SCHRÖDINGER CAT-LIKE STATES	111
C.1	Cat-Like States in a Symmetric Potential	112
C.2	Potential Decoherence	114
C.3	Tunneling Resonances	115
	APPENDIX D LOCALIZATION OF A SINGLE PARTICLE IN A TILTED SQUARE TWO-WELL POTENTIAL	117
	APPENDIX E EXACT SOLUTIONS FOR THE ONE-LEVEL APPROXIMA- TION	121
E.1	One Atom	122
E.2	Two Atoms	123
	APPENDIX F MATLAB CODE FOR GENERATING TWO-LEVEL HAMIL- TONIANS	125
F.1	MultiModeMultiplicity.m	127
F.2	Colindex.m	127
F.3	Operators.m	129
F.4	Params.m	147
F.5	TwoLevelHamiltonian.m	148

LIST OF FIGURES

2.1	Schematic of a double-well potential	16
2.2	Localized wavefunctions: Harmonic oscillator approximation	21
2.3	Localized wavefunctions: Superpositions of eigenfunctions	24
2.4	Pictorial representation of the one-dimensional Hamiltonian	29
2.5	Pictorial representation of the two-dimensional Hamiltonian	30
2.6	Pictorial representation of the three-dimensional Hamiltonian	31
3.1	Eigenstate amplitudes: Harmonic oscillator-like states	42
3.2	Eigenstates and eigenvalues: Harmonic oscillator-like states	42
3.3	Entanglement measures: Harmonic oscillator-like states	43
3.4	Eigenstate amplitudes: Schrödinger cat-like states	45
3.5	Eigenstates and eigenvalues: Schrödinger cat-like states	45
3.6	Entanglement measures: Schrödinger cat-like states	46
3.7	Eigenstate amplitudes: Medium barrier	48
3.8	Eigenstates and eigenvalues: Medium barrier	48
3.9	Energy level diagram	49
3.10	Entanglement measures: Medium barrier	50
3.11	Potential decoherence and tunneling resonances	53
3.12	Quantum sloshing of non-interacting bosons	56
3.13	Damped tunneling in the low barrier regime	59
3.14	Tunneling resonances in a few-atom system	61

3.15	Tunneling periods in a many-body system	63
4.1	Eigenstate amplitudes: Non-interacting case	74
4.2	Energy eigenvalues: Non-interacting case	75
4.3	Eigenstate amplitudes: High barrier and weak coupling	82
4.4	Energy eigenvalues: High barrier and weak coupling	83
4.5	Eigenstate amplitudes: Shadows of Schrödinger cat states	86
4.6	Energy eigenvalues: Shadows of Schrödinger cat states	87
4.7	Eigenvalue crossings	88
F.1	Time required to generate and diagonalize the two-level Hamiltonian	126

ACKNOWLEDGMENT

The last five years of my life have been dedicated to the study of physics and mathematics at the Colorado School of Mines. I am greatly indebted to the professors at CSM, and indeed to the institution itself, for the education I received. Through the guidance and wisdom of these men and women, I have developed a spiritual appreciation for these disciplines; mathematics in particular has become a form of introspection for me.

I was first introduced to the world of theoretical physics by my current advisor, Lincoln Carr. While Lincoln taught me quite a bit of physics, I also learned a few things about the scientific community in general (especially the importance of public speaking!). Most important, however, is what I learned through his example. Lincoln has a genuine interest in the education and welfare of his students, a quality which I sincerely admire. Thank you for taking me on as your student.

Ann Hermundstad and I started working on this research project as senior undergraduates at CSM. Together, we made a great team. Ann is much more than a colleague, though. She is also my poetry buddy, my snow-shoeing companion, a fellow sugar fiend, and a good friend.

Five years is not a short time, and in that time I had the pleasure of meeting a number of great professors at CSM. Specifically, I would like to thank Jim McNeil and David Wood for serving on my thesis committee; Jeff Squier and Orlen Wolf for giving me a job in the electronics lab; Ed Cecil for convincing me to volunteer in Mexico; Paul Martin and Mahadevan Ganesh for supporting my decision to pursue physics; and Luis Tenorio for giving me a real, working, honest to goodness slide-rule.

Of course, I cannot overlook Toni Lefton, who encouraged me to scribble poetry in the margins of my textbooks. What is math if not poetry written in numbers?

My friend Meagan Carroll has a saying: “It takes a village to raise a Dimitri.” Over the years, my friends have provided me with all the comforts of modern society: warm meals, warm clothes, and a warm bed. Without the kindness of these people, I would have starved or frozen by now. I am eternally grateful to my friends Bridget Lawrence and Katie Hayden, whose compassion and wrath know no bounds; to Steve Jones, with whom I used to get into as much trouble as possible and with whom I now enjoy infrequent but intense philosophical discussions; to Dan Adams, whose grandparents forced us to be friends; to Erik “Magnus” Pfeif, whose friendship is unfaltering; and to everybody at 1006 13th Street who has put up with my excessive free loading: Lisa Mauger, Roger Brown, Megan Hottovy, Brian McLachlan, and Matt Bowles. I would also like to thank my fellow adventurers (whether in the hills or on the road): Thomas Wells, Ryan O’Kuinghttons, and Brian Hesselberg.

As any college student will readily admit, the love and support of one’s family is paramount to success. While my parents have always encouraged my education, they have also listened patiently as I recounted my near-death experiences on knife-edge ridges and at desert truck stops. These are truly amazing parents!

Finally, I must mention that Golden, Colorado, is one of the best cities on Earth. It was in this city that I adopted a philosophy of life which continues to bring me much happiness today. I owe thanks to Clear Creek and to the Table Mountains for providing endless hours of free entertainment: swimming, tubing, hiking, biking, and climbing. Thank you for teaching me that a poor man can always enjoy a cold river on a hot afternoon. (The Coors Brewery, on the other hand, taught me that water isn’t everything it’s cracked up to be.)

Some people never go crazy. What truly horrible lives they must live.

-Charles Bukowski

Chapter 1

INTRODUCTION

In 1925, Einstein generalized the statistics of photons developed by Bose [1] to a system of non-interacting, massive bosons [2, 3]. He concluded that below a critical temperature, a finite fraction of the particles condense into the same single-particle quantum state, forming what is now known as a Bose-Einstein condensate (BEC). Seventy years later, the first BECs were created experimentally in dilute gases of rubidium [4], sodium [5], and lithium [6], and quickly became the subject of an explosion of exciting research. Soon after the experimental realization of Bose-Einstein condensation, the interference of two spatially separate BECs was observed [7] demonstrating the coherence of Bose condensed atoms. *Atom lasers*, sources of coherent matter waves, were extracted from BECs first as a series of pulses [8, 9] and later continuously [10]. Today, the versatility of BECs has led to applications in a wide range of fields, including quantum information processing, gravimetry, and quantum atom optics.

Recently, ultracold atoms in optical lattices and multi-well potentials have received much attention due to the tunability of their experimental parameters. An optical lattice is made by standing waves of laser light. Multi-well potentials, on the other hand, can be created using lasers of various frequencies and geometries (see Chapter 2). The depth of the wells is easily controlled by varying the intensity of the laser light. Such control has been used to demonstrate the Mott-insulator-to-superfluid transition in a BEC with repulsive interactions trapped in a three-

dimensional optical lattice [11, 12]. Moreover, the strength and even the sign of atom-atom interactions can be tuned using a Feshbach resonance [13, 14]. Ultracold atoms in optical lattices therefore constitute designer solid state crystals and provide an ideal medium for the observation of a vast range of quantum many-body phenomena, including macroscopic quantum tunneling through a potential barrier [9] and “dynamical” tunneling between separate stable regions in phase space [15, 16].

The Mott-insulator-to-superfluid transition is one example of a *quantum phase transition* [11, 12, 17]. Like classical phase transitions, a system that passes through a quantum phase transition undergoes a fundamental change in its macroscopic properties. For instance, a system of cold atoms in an optical lattice in the superfluid phase is characterized by delocalized atoms with long-range phase coherence. This is in contrast to the Mott insulator phase in which the occupation of each lattice site is exact and the atoms do not exhibit phase coherence across the lattice [11, 12]. Unlike classical phase transitions, quantum phase transitions occur at zero temperature. Phase transitions in a classical system are driven by thermal fluctuations and therefore cannot occur at zero temperature. However, Heisenberg’s uncertainty principle states that fluctuations in quantum systems are present even at zero temperature. These fluctuations can induce transitions between different quantum phases and bring about a qualitative change in the correlations in the ground state of the system [17].

Our research is a theoretical investigation of two outstanding issues in quantum many-body theory: macroscopic quantum tunneling and quantum superpositions of macroscopically distinct states, or *Schrödinger cats*. We study the quantum dynamics of many interacting bosons in a double-well potential at zero temperature. A novel method for the observation of the tunneling of a few atoms through a high barrier in the presence of many bosons is proposed. In addition, we demonstrate that the

existence of stationary Schrödinger cat-like states depends strongly on the details of the trapping potential. Such phenomena provide a stringent test for the validity of quantum mechanics in many-body systems. Furthermore, we find eigenvalue crossings in the double-well system which suggest the possibility of phase transitions in the infinite lattice [17].

1.1 Applications of Ultracold Atoms in Multi-Well Potentials

In 1999 Brennen *et al.* showed that neutral atoms trapped in an optical lattice can be used to implement quantum logic gates [18]. Recent studies have focused on lattices of double-wells with the goal of realizing one- and two-qubit gates [19, 20]. In these two-well systems, *tilt*, a potential difference between wells, is applied dynamically and multi-band effects play a vital role in the desired logical operations. Systems of cold atoms in optical lattices are therefore a promising candidate for quantum computation. Coherent processing of *optical* information is possible in systems of BECs in double-well potentials. Ginsberg *et al.* have demonstrated that optical information can be transferred between two spatially separate BECs through the conversion of an optical pulse into a traveling matter wave; a slow light pulse stored in one BEC was subsequently retrieved from a completely different condensate [21]. This remarkable experiment has implications in both classical and quantum information processing.

Bose-Einstein condensates in multi-well potentials are also revolutionizing the field of gravimetry [22]. Atom-chip-based sensors use BECs in double-well potentials to make sensitive measurements of gravity. Local gravitational field gradients introduce tilt to an otherwise symmetric double-well potential. The resulting atom population imbalance is determined by analyzing the interference patterns of the BECs [23, 24]. Another approach to gravimetry uses optical lattices instead of

double-well potentials. Cold strontium atoms in a lattice will undergo Bloch oscillations in the presence of a gravitational field. In this case, the strength of the field is determined by measuring the Bloch frequency [25]. The unprecedented sensitivity of these effective gravimeters will allow researchers to search for deviations from Newtonian gravity at very small distances.

Recently, Gati *et al.* demonstrated that fluctuations in the relative phase of two BECs in a double-well potential can be used as a primary noise thermometer to measure temperatures below the critical temperature of the condensate. In this regime, standard time of flight measurements cannot be applied due to the lack of a directly visible thermal component. The noise thermometer was used to measure the heating of a Bose gas. Their experiment demonstrated that the heat capacity of a Bose gas vanishes at zero temperature [26, 27].

Systems of ultracold atoms in tilted optical lattices allow the direct study of quantum transport phenomena, including Landau-Zener tunneling and Wannier-Stark ladders [28, 29, 30]. These systems are analogous to electrons in a periodic crystal potential where tilt plays the role of an external electric field. Landau-Zener tunneling refers to interband tunneling in the presence of a strong field. However, when the field is weak, Landau-Zener tunneling is negligible and a Bloch band splits into equally spaced energy levels called Wannier-Stark ladders [28]. Wannier-Stark ladders in optical lattices were observed experimentally in 1996 [29] and recent theoretical studies have focused on Landau-Zener-like tunneling rates [30]. Clearly, ultracold atoms provide a new experimental context in which to study quantum transport on a lattice.

Because ultracold atoms in optical lattices mimic traditional solid state systems, they can be used to create atom analogs of solid state materials and devices. This new field, dubbed “atomtronics,” exploits the superfluid and insulating regimes of the

Bose-Hubbard Hamiltonian. The analogs of n-type and p-type semiconductor materials can be achieved by raising and lowering individual sites in an optical lattice [31]. Moreover, transistor-like behavior of a BEC has been demonstrated theoretically in a three-well trap [32]. Unlike traditional solid-state devices, the experimental parameters of atomtronic devices are easily controllable.

Interest in systems of ultracold atoms in multi-well potentials is not limited to practical applications; such systems also provide a unique opportunity to study fundamental quantum mechanics in finite-sized systems. In particular, a double-well is one of the simplest potentials that gives rise to many-body phenomena, such as macroscopic quantum tunneling and Schrödinger cats. In the context of a double-well potential, a Schrödinger cat describes a state in which one BEC simultaneously occupies both wells. Spatially separate BECs in a two-well potential have recently been created [33] and tunneling times on the order of 50 ms have been observed [34]. Although Schrödinger cats have not yet been observed experimentally, many theoretical schemes for their creation in a double-well potential have been proposed.

1.2 Theoretical Studies of Ultracold Atoms in Double-Well Potentials

The success of experiments with ultracold atoms in double-well potentials has sparked an equally ambitious pursuit of a theoretical description of these systems. Smerzi *et al.* showed that the semi-classical dynamics of a BEC in a double-well potential can be modeled as a classical nonrigid pendulum [35]. The dynamics can also be mapped onto the Lipkin-Meshkov-Glick (LMG) model for mutually interacting spin- $\frac{1}{2}$ particles embedded in a magnetic field [36]. Under this mapping, tilt is modeled by the presence of a parallel field [37]. A quantum dimer, i.e., a double-well potential, coupled to a heat bath can also be used to study vibrations in water molecules [38].

In this model, the two oxygen-hydrogen stretching modes are coupled to the relative angle between the bonds.

The tunneling dynamics of the double-well system have been studied in various regimes [39, 35, 40] and ultralong tunneling times [41] have been attributed to the phenomenon of self-trapping observed in recent experiments [34]. The response of a BEC in a double-well potential to a sudden change in barrier height was analyzed [42] in an attempt to better understand the “contrast resonance” observed by Tuchman and Kasevich under similar experimental conditions [43]. Spekkens and Sipe studied the transition of the ground state of a repulsive BEC in a double-well potential from a single to a fragmented condensate as the barrier was increased [44], analogous to the superfluid-to-Mott-insulator transition in a lattice [11].

Other double-well models have focused on the creation of Schrödinger cat-like states by dynamically reversing the sign of the atomic s -wave scattering length via a Feshbach resonance [45] or by ramping the potential barrier [46]. Past studies have also focused on decoherence effects in double-well potentials. Huang *et al.* showed that decoherence due to interactions of atoms with the electromagnetic vacuum can cause the collapse of Schrödinger cat-like states [45]. Thermal effects [47] and dissipation [48] constitute other sources of decoherence and can suppress tunneling between wells [49, 50, 51].

To describe these double-well systems, a Hubbard-like Hamiltonian has often been employed [26, 35, 36, 39, 40, 41, 42, 44, 45, 46]. However, these studies not only assume that the trapping potential is symmetric, but effects of excited levels are completely neglected. A *multi-level* picture of a *tilted* two-well potential is especially relevant to the creation of a quantum computer from neutral atoms [19, 20], atom-chip-based gravity sensors [23, 24], and to the study of quantum transport phe-

nomena [28, 29, 30]. Although Tonel *et al.* have investigated the behavior of the ground state in a tilted double-well with one allowed energy level [52], mean-field studies have indicated that a two-level approximation is needed when the interactions between particles are strong [53]. Thus, the current experimental context of double-well potentials has created an urgent need for a new theoretical analysis of the many-body double-well problem.

1.3 Overview

We use one- and two-level Hubbard-like Hamiltonians to investigate the behavior of ultracold bosons in a tilted double-well potential. That is, we relax two assumptions commonly made in previous studies of similar systems: the symmetric trap assumption and the one-level assumption. Furthermore, we allow atoms to have nonzero orbital angular momentum, thus introducing additional degrees of freedom into our system which are not found in other studies.

We find that tilt constitutes an additional source of decoherence in these systems, causing both the collapse of Schrödinger cat-like states and the suppression of tunneling between wells [54, 55]. We call this *potential decoherence*. Potential decoherence displays radically different behavior from other forms of decoherence. When the barrier is high, *tunneling resonances* occur for critical values of the tilt [54, 55]. At resonance, the potential difference between wells is exactly compensated by atom-atom interactions. Whereas tunneling through the barrier of a symmetric trap can be prohibitively slow [41], resonances can be used to achieve experimentally realistic tunneling times. Moreover, tunneling at resonance is also much less sensitive to potential decoherence than in the symmetric case. Robust few-atom superposition states are realized periodically by a many-body system tunneling at resonance [55].

The one-level assumption is valid if coupling of energy levels can be neglected. Although levels are only completely decoupled when there are no atom-atom interactions, coupling is negligible when the interactions are much weaker than the energy level spacing. Even in this regime, however, effects of the excited level are still important. Eigenvalue crossings, which cannot be described by a one-level approximation, occur when either the number of particles or the interaction energy is greater than a critical value [54]. Eigenvalue crossings cause states with definite occupation of the excited level to emerge among the lowest lying eigenstates. Crossings which involve the ground state energy of the double-well system can become points of non-analyticity in the ground state energy of the infinite lattice. Such points constitute quantum phase transitions [17]. This suggests that phase transitions involving excited energy bands may occur in an optical lattice even when the bands are weakly coupled.

In Chapter 2, we give a brief overview of Bose-Einstein condensation, optical lattices, multi-dimensional double-well potentials, and the localized wavefunction basis; angular momentum degrees of freedom are introduced in two- and three- dimensional systems; and we derive the one- and two-level Hamiltonians from first principles quantum field theory. The one-level system is analyzed in Chapter 3. Analytical techniques, including high order degenerate and non-degenerate perturbation theories, are used to investigate potential decoherence and tunneling resonances. We provide analytical expressions for the quantum sloshing of many bosons through the potential barrier. Analytical results are checked numerically for large systems by exact diagonalization of the one-level Hamiltonian. The one-level assumption is relaxed in Chapter 4 and the stationary states of the two-level Hamiltonian are characterized. We discuss eigenvalue crossings in systems described by one-, two-, and three-dimensional double-well traps and bounds on the use of a one-level approximation are presented.

Chapter 5 provides a summary of our results and an outlook for future extensions of this work. Proofs of analytic results as well as exact treatments of simple limiting cases can be found in Appendices A-E. Finally, algorithms for generating matrix representations of the one-, two-, and three- dimensional two-level Hamiltonians are presented in Appendix F.

Chapter 2

BACKGROUND: ULTRACOLD ATOMS IN A DOUBLE-WELL

As discussed in Chapter 1, many theoretical studies of ultracold bosons in double-well potentials use a Hubbard-like Hamiltonian. In this chapter, the fundamental physics of these systems is described, beginning with a brief review of Bose-Einstein condensation and the response of cold atoms to an optical standing wave. A definition of double-well potentials in one, two and three dimensions is followed by a description of localized single-particle wavefunctions. One- and two- level Hamiltonians in one, two, and three spatial dimensions are derived from first principles quantum field theory for weakly interacting bosons in an external potential.

2.1 Bose-Einstein Condensation

Bose-Einstein condensation in a uniform, non-interacting gas of N spinless bosons in thermodynamic equilibrium is a standard problem which is treated in many statistical mechanics textbooks [56]. In the Grand Canonical ensemble, the mean occupation number of the single-particle state $|\nu\rangle$ at some temperature T is given by the Bose-Einstein distribution function,

$$f_{\text{BE}}(\epsilon_\nu, \mu, T) = \frac{1}{e^{(\epsilon_\nu - \mu)/k_B T} - 1}, \quad (2.1)$$

where ϵ_ν is the energy of the state $|\nu\rangle$, μ is the chemical potential, and k_B is Boltzmann's constant. The chemical potential is determined as a function of the total

number of particles in the gas and the temperature by the requirement that the sum of the occupation numbers is equal to N . At high temperatures, the chemical potential is much less than the energy of the single-particle ground state $\epsilon_0 \equiv 0$ because the average occupation of any state is much less than unity. As the temperature is lowered, the mean occupation of states and hence the chemical potential increase. However, μ cannot exceed zero since $\mu > 0$ yields a negative occupation of the ground state which is nonphysical.

The number of allowed energy states in an energy range ϵ to $\epsilon + d\epsilon$ is given by $g(\epsilon)d\epsilon$, where $g(\epsilon)$ is the density of states. Because the density of states often varies as a power of the energy, we will consider densities of states of the form

$$g(\epsilon) = C\epsilon^{\alpha-1}, \quad (2.2)$$

where C and α are constants that depend on the details of the confining potential [57]. For a system of free particles in d dimensions, $\alpha = d/2$. If instead the particles are confined by a d -dimensional harmonic oscillator potential, the density of states varies with ϵ^{d-1} , i.e., $\alpha = d$.

The total number of particles in excited states is given by

$$N_{\text{ex}} = \int_0^{\infty} d\epsilon g(\epsilon) f_{\text{BE}}(\epsilon, \mu, T). \quad (2.3)$$

Equation (2.3) is maximized when $\mu = 0$. The number of particles in excited states is equal to the total number of particles in the gas at a temperature T_c determined by the equation

$$N_{\text{ex}} = N = \int_0^{\infty} d\epsilon g(\epsilon) f_{\text{BE}}(\epsilon, 0, T_c). \quad (2.4)$$

This integral can be evaluated in terms of gamma and zeta functions provided $\alpha > 1$.

The critical temperature is

$$k_B T_c = \frac{N^{1/\alpha}}{[C\Gamma(\alpha)\zeta(\alpha)]^{1/\alpha}}. \quad (2.5)$$

At temperatures less than T_c , the occupation of excited states is

$$N_{\text{ex}}(T) = \int_0^\infty d\epsilon g(\epsilon) f_{\text{BE}}(\epsilon, 0, T) = C\Gamma(\alpha)\zeta(\alpha)(k_B T)^\alpha. \quad (2.6)$$

The remaining particles must therefore occupy the single-particle ground state. The occupation of the ground state is

$$N_0(T) \equiv N - N_{\text{ex}}(T) = N \left[1 - \left(\frac{T}{T_c} \right)^\alpha \right]. \quad (2.7)$$

The rapid population of the ground state for $T < T_c$ is called *Bose-Einstein condensation*. The criterion for Bose-Einstein condensation can be understood by means of the one-particle density matrix,

$$\rho(\mathbf{r}, \mathbf{r}') \equiv \langle \hat{\Psi}^\dagger(\mathbf{r}') \hat{\Psi}(\mathbf{r}) \rangle, \quad (2.8)$$

where $\hat{\Psi}^\dagger(\mathbf{r})$ and $\hat{\Psi}(\mathbf{r})$ are the bosonic creation and annihilation operators. By definition, the one-particle density matrix $\rho(\mathbf{r}, \mathbf{r}')$ is Hermitian and therefore has a complete orthonormal basis $\{\chi_j(\mathbf{r})\}$ such that

$$\rho(\mathbf{r}, \mathbf{r}') = \sum_j \lambda_j \chi_j^*(\mathbf{r}') \chi_j(\mathbf{r}). \quad (2.9)$$

In the context of the non-interacting Bose gas, the eigenfunctions χ_j are the single-particle wavefunctions and the eigenvalues λ_j are the corresponding occupation num-

bers. At zero temperature in a gas of non-interacting bosons, the eigenvalue for the lowest excited single-particle state is equal to N and all others vanish. A system in which the interactions are nonzero is said to exhibit Bose-Einstein condensation if one of the eigenvalues is of order N while all others are finite in the limit $N \rightarrow \infty$ [57, 58].

The diluteness condition for a weakly interacting Bose gas is

$$\bar{n}a_s^3 \ll 1, \quad (2.10)$$

where \bar{n} is the average density of the gas and a_s is the s -wave scattering length of the atoms. Although the system is said to be “weakly interacting” when condition (2.10) is met, the interaction energy can be on the order of the kinetic energy in this regime and dilute gases can therefore exhibit non-ideal behavior [59].

2.2 Effects of Reduced Dimensionality

Condensation of a non-interacting Bose gas in a three-dimensional harmonic trap, corresponding to $\alpha = 3$, requires that $T < T_{3D}$, where the critical temperature is given by

$$k_B T_{3D} = \hbar\omega_{3D} \left[\frac{N}{\zeta(3)} \right]^{1/3} \approx 0.94 \hbar\omega_{3D} N^{1/3}. \quad (2.11)$$

Here $\hbar\omega_x$, $\hbar\omega_y$, and $\hbar\omega_z$ are the oscillator energies and $\omega_{3D} \equiv (\omega_x\omega_y\omega_z)^{1/3}$. To achieve two-dimensional Bose-Einstein condensation, corresponding to $\alpha = 2$, the trapping frequency ω_z in the third dimension must satisfy

$$\hbar\omega_{2D} \ll k_B T_{2D} < \hbar\omega_z, \quad (2.12)$$

where $\omega_{2D} \equiv (\omega_x \omega_y)^{1/2}$ and the critical temperature is given by

$$k_B T_{2D} = \hbar \omega_{2D} \left[\frac{N}{\zeta(2)} \right]^{1/2} \approx 0.78 \hbar \omega_{2D} N^{1/2}. \quad (2.13)$$

In a one-dimensional harmonic trap, $\alpha = 1$ and the integral (2.4) diverges. Therefore, Bose-Einstein condensation cannot occur in the thermodynamic limit. However, macroscopic occupation of the ground state is possible in a finite system provided

$$\omega_x \ll \omega_{\perp}, \quad (2.14)$$

where we assume the trapping frequencies in the transverse directions are the same, $\omega_y = \omega_z \equiv \omega_{\perp}$. The critical temperature in one dimension is approximately [60]

$$k_B T_{1D} \simeq \hbar \omega_x \frac{N}{\ln(N)}. \quad (2.15)$$

Thus, Bose-Einstein condensation is possible in one- and two- dimensional harmonic traps with very large anisotropy [57, 59].

2.3 Optical Lattices

Bose-Einstein condensates in optical lattices are ideal systems for the study of many-body quantum mechanics, as we saw in Chapter 1. Here we consider the response of an atom coupled to a classical, single-mode laser of frequency ω_l and wavenumber k_l forming a standing wave in one dimension [57, 61, 62, 63]. In the dipole approximation, the interaction between the atom and the laser light is

$$\hat{H}_{\text{dipole}} = -\boldsymbol{\mu} \cdot \mathbf{E}(\hat{x}, t), \quad (2.16)$$

where $\boldsymbol{\mu}$ is the electric dipole moment of the atom, \mathbf{E} is the electric field, and \hat{x} is the position operator. For a real standing wave, the applied electric field has the form

$$\mathbf{E}(\hat{x}, t) = \text{Re}\{\mathbf{E}_0(\hat{x})e^{i\omega_l t}\}. \quad (2.17)$$

An atom initially in the electronic ground state $|g\rangle$ will be coupled by the laser light to an excited internal state $|e\rangle$. The energy difference between these two states is $\hbar\omega_{eg}$. Conventional perturbation theory can be used to determine the change ΔE_g in the ground-state energy. The shift in energy, known as the ac-Stark effect, is given by

$$\Delta E_g(x) = -\hbar\Omega_R(x)^2/\delta, \quad (2.18)$$

where we have introduced the *detuning* $\delta \equiv \omega_l - \omega_{eg}$ and the *effective Rabi frequency* $\hbar\Omega_R(x) \equiv |\langle e|\boldsymbol{\mu} \cdot \mathbf{E}_0(\hat{x})|g\rangle|$. In deriving Equation (2.18), we have neglected the finite lifetime of the ground and excited states due to spontaneous emission of photons. Furthermore, we assume that the frequency ω_l is close to resonance so that the ground state $|g\rangle$ is not coupled to excited states other than $|e\rangle$. The condition for the validity of Equation (2.18) is $|\delta| \gg \Omega_R$.

The energy shift ΔE_g has the form of an effective potential acting on the atom. The resulting potential is

$$V_{\text{lattice}}(x) \equiv -\hbar\Omega_R^2(x)/\delta = -(\hbar\Omega_0^2/\delta) \sin^2(k_l x) = -V_0 \sin^2(k_l x), \quad (2.19)$$

where the spatial dependence of a 1D standing wave gives $\Omega_R(x) = \Omega_0 \sin(k_l x)$ and the lattice depth is defined as $V_0 \equiv \hbar\Omega_0^2/\delta$. The potential (2.19) is referred to as an *optical lattice*. The depth of the lattice V_0 can be tuned by simply adjusting the intensity of the laser light. This potential can be modified using different laser

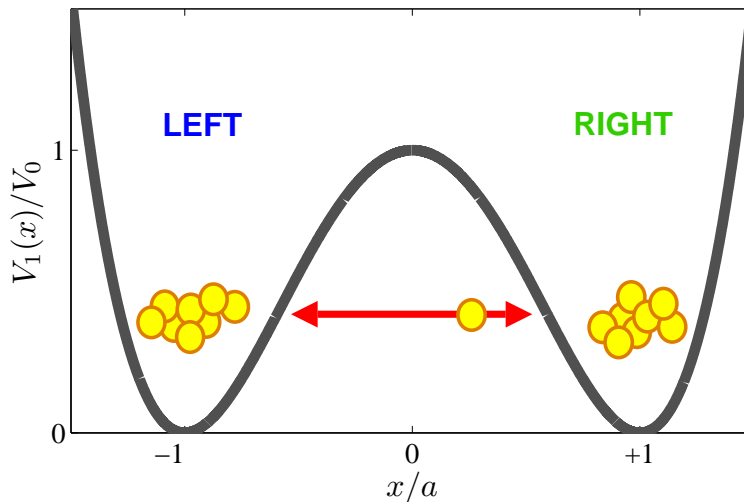


Figure 2.1. *Schematic of a double-well potential.* We study the behavior of ultracold bosons in a double-well potential. Shown is a sketch of atoms occupying a one-dimensional double-well. The labels *left* and *right* will be used throughout our presentation. Minima occur at $x = \pm a$ and the barrier has height V_0 at $x = 0$. Atoms can tunnel between wells through the barrier, as indicated by the arrow.

geometries [63] to obtain, for instance, a lattice of double-wells [19].

2.4 Double-Well Potentials

Double-well potentials are a simple limiting case of optical lattices which nevertheless exhibit rich quantum behavior. We study the behavior of ultracold bosons, with mass M and s -wave scattering length a_s , experiencing a double-well potential. In this section, we explicitly define double-well potentials in one, two, and three dimensions.

Let $V_1 : \mathbb{R} \rightarrow [0, \infty)$ represent an arbitrary one-dimensional (1D) double-well potential. We assume the following.

1. V_1 is infinitely differentiable and can therefore be expanded in a Taylor series.

This assumption is physically realistic since double-well traps are made using counter propagating beams [19] or superpositions of periodic and harmonic potentials [34].

2. $V_1'(x) = 0$ if and only if $x \in \{-a, 0, a\}$ for some $a > 0$; $V_1'(x) > 0$ for $x \in (-a, 0) \cup (a, \infty)$ and $V_1'(x) < 0$ for $x \in (-\infty, -a) \cup (0, a)$; $V_1''(x) = 0$ if and only if $x \in \{-b, b\}$ for some $0 < b < a$; and $V_1''(x) > 0$ for $x \in (-\infty, -b) \cup (b, \infty)$ and $V_1''(x) < 0$ for $x \in (-b, b)$. These assumptions guarantee that V_1 is a double-well potential with absolute minima at $x_L \equiv -a$ and $x_R \equiv +a$ and a local maximum value of $V_0 \equiv V_1(0)$ at $x = 0$.
3. $V_1(\pm a) = 0$, thus establishing a reference for zero energy. The height of the barrier between wells is then V_0 .
4. the double-well is symmetric, that is, $V_1(-x) = V_1(x)$ for $x \in \mathbb{R}$. In practice, it can be very difficult to create a perfectly symmetric double-well potential. This assumption will later be relaxed in order to study the effects of a small potential difference between wells.

A schematic of a double-well potential is shown in Figure 2.1. The distance a is analogous to the lattice constant for an infinite lattice and should not be confused with the s -wave scattering length a_s of the atoms. We define the *recoil energy* E_r by $E_r \equiv \hbar^2/Ma^2$. The dimensionless quantity V_0/E_r provides a useful measure of the barrier size and is standard in experiments on optical lattices.

We also study two- and three-dimensional double-well potentials of the form

$$V_2(x, y) = V_1(x) + V_\perp(y) \quad \text{and} \quad V_3(x, y, z) = V_1(x) + V_\perp(y) + V_\perp(z), \quad (2.20)$$

where the single-well potential $V_\perp : \mathbb{R} \rightarrow [0, \infty)$ satisfies the following assumptions.

1. V_{\perp} is infinitely differentiable and can therefore be expanded in a Taylor series.
2. $V'_{\perp}(x) = 0$ if and only if $x = 0$; $V'_{\perp}(x) > 0$ for $x > 0$ and $V'_{\perp}(x) < 0$ for $x < 0$; and $V''_{\perp}(x) > 0$ for $x \in \mathbb{R}$. These assumptions guarantee that V_{\perp} is a single-well potential with a global minimum at the origin.
3. $V''_{\perp}(0) = V''_1(\pm a)$ and $V_{\perp}(0) = 0$. As we will see, this assumption ensures that V_d is well approximated by a d -dimensional isotropic harmonic oscillator near the minima.

In higher dimensions, $\mathbf{x}_L \equiv (x_L, 0, 0)$ and $\mathbf{x}_R \equiv (x_R, 0, 0)$ are the minima of the double-well potential. Expanding V_d in a Taylor series about $\mathbf{x} = \mathbf{x}_j$, we find that, to second order,

$$V_d(\mathbf{x} - \mathbf{x}_j) \approx \frac{1}{2}M\omega^2\mathbf{x}^2, \quad (2.21)$$

for $j \in \{L, R\}$. That is, each well of the double-well potential resembles a d -dimensional, isotropic, simple harmonic oscillator with frequency

$$\omega \equiv \sqrt{V''_1(a)/M}. \quad (2.22)$$

The harmonic oscillator length $a_{\text{ho}} = \sqrt{\hbar/M\omega}$ is related to the double-well potential V_1 by

$$a/a_{\text{ho}} = [V''_1(a)a^2/E_r]^{1/4}. \quad (2.23)$$

In the many-body system, we will show that off-site interactions can be neglected if $a \gtrsim 2a_{\text{ho}}$, that is, if the condition

$$[V''_1(a)a^2/E_r]^{1/4} \gtrsim 2, \quad (2.24)$$

is satisfied. A lower bound on V_0 ,

$$V_0 > \frac{d+2}{2}\hbar\omega = \frac{d+2}{2}\sqrt{E_r V_1''(a)a^2}. \quad (2.25)$$

can be achieved by requiring that the first excited level of the isotropic oscillator is lower than the barrier height. Together, Equations (2.24) and (2.25) imply the necessary condition

$$V_0/E_r \gtrsim 2(d+2). \quad (2.26)$$

In the double-well experiments of [34], the barrier height V_0 is approximately $11E_r$. A much larger barrier, $V_0 \approx 2000E_r$, is used in the gravity-sensor experiments of [23]. Barrier heights ranging between 10 and 40 recoils are used in the experiments of [19]. Clearly, condition (2.26) is experimentally feasible.

2.4.1 Localized Single-Particle Wavefunctions

We now turn our attention to the construction of localized wavefunctions in a d -dimensional double-well potential V_d . For $j \in \{L, R\}$, the localized wavefunctions

$$\phi_d^{(\ell, m)}(\mathbf{x} - \mathbf{x}_j) \equiv \langle \mathbf{x} | j, \ell, m \rangle_d, \quad (2.27)$$

can be approximated by the eigenfunctions of the d -dimensional, isotropic, simple harmonic oscillator (2.21) with corresponding energy eigenvalues $(\ell + d/2)\hbar\omega$. This approximation is valid when $a \gg a_{\text{ho}}$. However, we do not restrict ourselves to this approximation. Here $\ell \in \{0, 1\}$ is called the *energy level index* since the energy of the state $|j, \ell, m\rangle_d$ depends only on the value of ℓ . Because an isotropic oscillator potential is central, it is possible to construct eigenfunctions which are also eigenfunctions of the z - and the total angular momentum operators \hat{L}_z and \mathbf{L}^2 [64]. The index m counts

the quanta of angular momentum in the z -direction.

In one dimension, we have

$$\begin{aligned}\phi_1^{(0,0)}(x) &= a_{\text{ho}}^{-1/2} \pi^{-1/4} e^{-x^2/2a_{\text{ho}}^2}, \\ \phi_1^{(1,0)}(x) &= a_{\text{ho}}^{-1/2} 2^{1/2} \pi^{-1/4} (x/a_{\text{ho}}) e^{-x^2/2a_{\text{ho}}^2},\end{aligned}\tag{2.28a}$$

where a_{ho} is given by Equation (2.23). In two and three dimensions, the eigenfunctions are given by

$$\begin{aligned}\phi_2^{(0,0)}(s, \phi) &= a_{\text{ho}}^{-1} \pi^{-1/2} e^{-s^2/2a_{\text{ho}}^2}, \\ \phi_2^{(1,\pm 1)}(s, \phi) &= a_{\text{ho}}^{-1} \pi^{-1/2} (s/a_{\text{ho}}) e^{-s^2/2a_{\text{ho}}^2} e^{\pm i\phi},\end{aligned}\tag{2.28b}$$

and

$$\begin{aligned}\phi_3^{(0,0)}(r, \theta, \phi) &= a_{\text{ho}}^{-3/2} \pi^{-3/4} e^{-r^2/2a_{\text{ho}}^2}, \\ \phi_3^{(1,0)}(r, \theta, \phi) &= a_{\text{ho}}^{-3/2} 2^{1/2} \pi^{-3/4} (r/a_{\text{ho}}) e^{-r^2/2a_{\text{ho}}^2} \cos(\theta), \\ \phi_3^{(1,\pm 1)}(r, \theta, \phi) &= a_{\text{ho}}^{-3/2} \pi^{-3/4} (r/a_{\text{ho}}) e^{-r^2/2a_{\text{ho}}^2} \sin(\theta) e^{\pm i\phi},\end{aligned}\tag{2.28c}$$

where we have introduced the plane polars (s, ϕ) and the spherical polars (r, θ, ϕ) defined by $s = \sqrt{x^2 + y^2}$, $r = \sqrt{x^2 + y^2 + z^2}$, $\theta = \cos^{-1}(z/r)$, and $\phi = \tan^{-1}(y/x)$.

The localized wavefunctions are shown in Figure 2.2.

The coordinate representation of \hat{L}_z is

$$\hat{L}_z = -i\hbar \frac{\partial}{\partial \phi}.\tag{2.29}$$

One can show [64] that $\phi_d^{(\ell, m)}$ are eigenfunctions of \hat{L}_z with z -component of angular momentum equal to $m\hbar$, that is,

$$\hat{L}_z \phi_d^{(\ell, m)} = m\hbar \phi_d^{(\ell, m)} \quad \text{for } d \in \{1, 2, 3\}.\tag{2.30}$$

It is in this context that the index m of the localized states $|j, \ell, m\rangle_d$, given by (2.27),

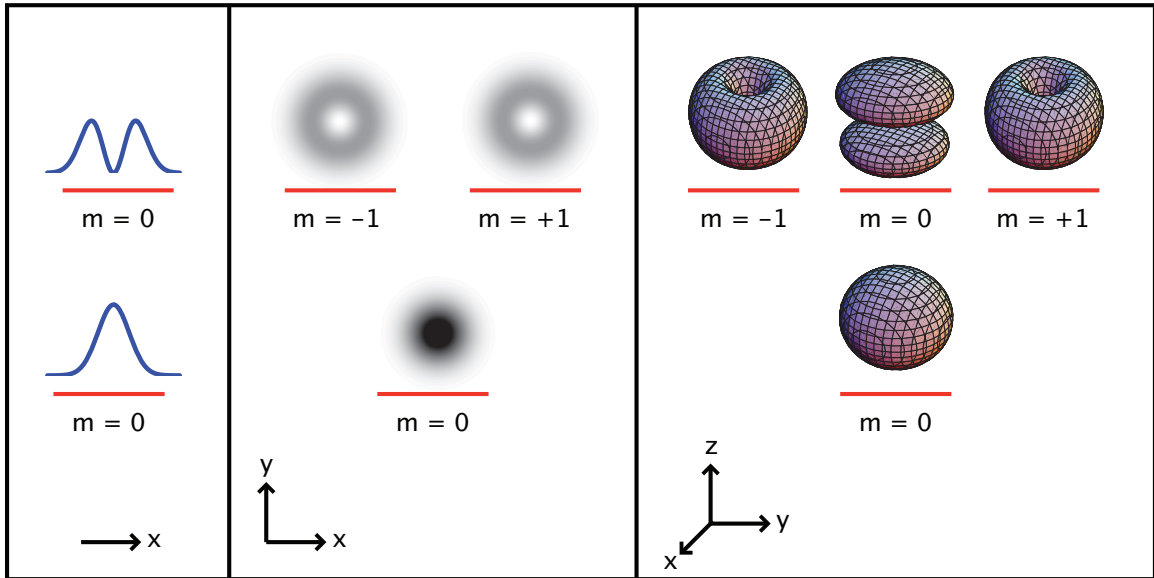


Figure 2.2. *Localized wavefunctions: Harmonic oscillator approximation.* In the harmonic oscillator approximation, the localized wavefunctions are assumed to be eigenfunctions of the simple harmonic oscillator with frequency $\omega = \sqrt{V_1''(a)/M}$. Shown are the localized probability densities $|\phi_d^{(\ell,m)}|^2$, given by Equation (2.28), offset by the energy of the corresponding level. The left-most panel corresponds to the one-dimensional case, the middle panel to two dimensions, and the right-most panel to three dimensions. In one dimension, the angular momentum of the localized states is always zero. On the other hand, in two and three dimensions the degenerate wavefunctions of the excited level are eigenfunctions of the orbital angular momentum operators. This choice of wavefunctions introduces new degrees of freedom into the two-level Hubbard-like Hamiltonian.

is called the *angular momentum index*. We emphasize that neither j nor ℓ should be mistaken as the “total angular momentum”; $j \in \{L, R\}$ and $\ell \in \{0, 1\}$ are the well and energy level indices, respectively. The allowed values of m do, however, depend on the value of ℓ . When $\ell = 0$, there is no angular momentum, i.e., $m = 0$. When $\ell = 1$, the allowed values of m depend on the dimensionality d : $m = 0$ in 1D, $m \in \{-1, +1\}$ in 2D, and $m \in \{-1, 0, +1\}$ in 3D.

Analogous to the creation of Wannier functions in a lattice [62, 63], wavefunctions localized in the left and right wells can be constructed by taking appropriate superpositions of symmetric and antisymmetric eigenstates of the single-particle Hamiltonian. The Hamiltonian for a single particle of mass M in a double-well potential is

$$\hat{H}_{\text{double-well}} \equiv \frac{\hat{\mathbf{p}}^2}{2M} + V_d(\hat{\mathbf{x}}). \quad (2.31)$$

Because V_d is separable, the eigenstates are products of the one-dimensional eigenstates, that is, $|n_x, n_y, n_z\rangle = |n_x\rangle \otimes |n_y\rangle \otimes |n_z\rangle$, with corresponding energy eigenvalues $\varepsilon_{n_x, n_y, n_z} = \varepsilon_{n_x} + \varepsilon_{n_y} + \varepsilon_{n_z}$.

Consider the eigenstates $|n_x\rangle$ of the 1D potential V_1 . When condition (2.25) is met, the four lowest lying states occur in nearly degenerate pairs of symmetric and antisymmetric states, as in Figure 2.3(a). The left- and right-localized states are

$$\begin{aligned} |L, 0, 0\rangle_1 &= (|0_x\rangle + |1_x\rangle)/\sqrt{2}, & |R, 0, 0\rangle_1 &= (|0_x\rangle - |1_x\rangle)/\sqrt{2}, \\ |L, 1, 0\rangle_1 &= (|2_x\rangle + |3_x\rangle)/\sqrt{2}, & |R, 1, 0\rangle_1 &= (|2_x\rangle - |3_x\rangle)/\sqrt{2}, \end{aligned} \quad (2.32a)$$

where the state $|j, \ell, m\rangle_d$ was defined in Equation (2.27). The 1D localized wavefunctions, given by $\phi_1^{(\ell, 0)}(x - x_j) \equiv \langle x | j, \ell, 0 \rangle_1$, are shown in Figure 2.3(b). In 2D and 3D, we construct localized wavefunctions which are eigenfunctions of the z - and total

angular momentum operators. The two- and three- dimensional states are

$$\begin{aligned} |j, 0, 0\rangle_2 &= |j, 0, 0\rangle_1 \otimes |0_y\rangle, \\ |j, 1, \pm 1\rangle_2 &= (|j, 1, 0\rangle_1 \otimes |0_y\rangle \pm i|j, 0, 0\rangle_1 \otimes |1_y\rangle) / \sqrt{2}, \end{aligned} \quad (2.32b)$$

and

$$\begin{aligned} |j, 0, 0\rangle_3 &= |j, 0, 0\rangle_2 \otimes |0_z\rangle, \\ |j, 1, 0\rangle_3 &= |j, 0, 0\rangle_2 \otimes |1_z\rangle, \\ |j, 1, \pm 1\rangle_3 &= |j, 1, \pm 1\rangle_2 \otimes |0_z\rangle, \end{aligned} \quad (2.32c)$$

where $j \in \{L, R\}$. The energy of the state $|j, \ell, m\rangle_d$ is defined as

$$E_d^\ell \equiv {}_d\langle j, \ell, m | \hat{H}_{\text{double-well}} | j, \ell, m \rangle_d. \quad (2.33)$$

In one dimension, the level energies depend only on ℓ and are given by

$$E_1^0 = \frac{\varepsilon_{1_x} + \varepsilon_{0_x}}{2} \quad \text{and} \quad E_1^1 = \frac{\varepsilon_{3_x} + \varepsilon_{2_x}}{2}. \quad (2.34)$$

Likewise, in two-dimensions the energies E_2^ℓ are

$$E_2^0 = E_1^0 + \varepsilon_{0_y} \quad \text{and} \quad E_2^1 = \frac{1}{4} (E_1^0 + E_1^1 + \varepsilon_{0_y} + \varepsilon_{1_y}). \quad (2.35)$$

Finally, in three dimensions we find that

$$E_3^0 = E_2^0 + \varepsilon_{0_z} \quad \text{and} \quad E_3^1 = E_2^0 + \varepsilon_{1_z} = E_2^1 + \varepsilon_{0_z}. \quad (2.36)$$

In 3D, E_3^1 is independent of m provided $E_1^0 = \varepsilon_{0_y} = \varepsilon_{0_z}$ and $E_1^1 = \varepsilon_{1_y} = \varepsilon_{1_z}$. Since we assume that $V_1''(x_{L,R}) = V_1''(0)$, the conditions $E_1^0 \approx \varepsilon_{0_y}$ and $E_1^1 \approx \varepsilon_{1_y}$ are satisfied for large V_0/E_r .

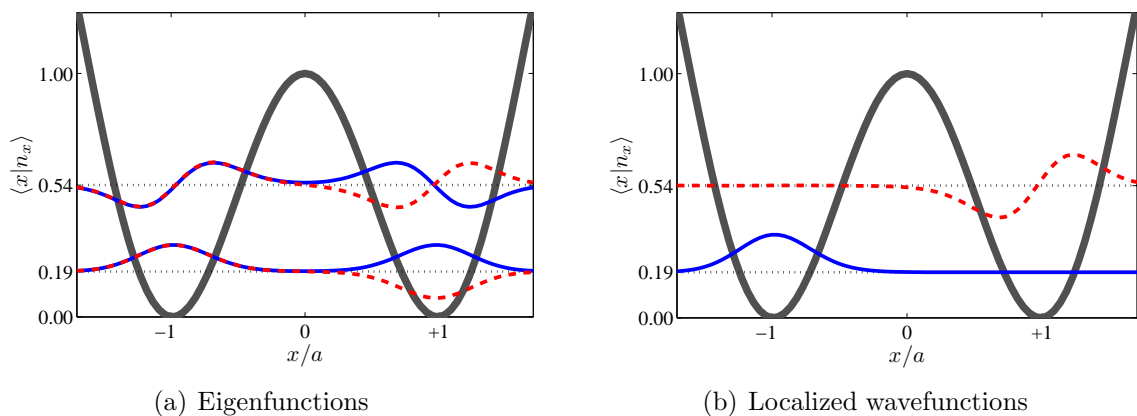


Figure 2.3. *Localized wavefunctions: Superpositions of eigenfunctions.* (a) Shown are the first four eigenfunctions $\langle x | n_x \rangle$ of a double-well $V_1(x)$ in arbitrary units. The eigenfunctions are offset by the corresponding eigen energy and are plotted in alternating solid blue and dashed red lines for clarity. The lowest eigenstates occur in nearly degenerate pairs of symmetric and antisymmetric states. (b) Spatially localized states can be constructed by superpositions of the appropriate eigenstates. Shown are the states $\langle x | L, 0, 0 \rangle_1$ (solid blue line) and $\langle x | R, 1, 0 \rangle_1$ (dashed red line) offset by the corresponding energy. In both (a) and (b), the double-well potential is indicated in black for reference.

2.5 Multidimensional One- and Two-Level Hamiltonians

In terms of the bosonic annihilation and creation field operators $\hat{\Psi}(\mathbf{x})$ and $\hat{\Psi}^\dagger(\mathbf{x})$, the second-quantized Hamiltonian for a system of N interacting bosons of mass M confined by an external potential $V_d(\mathbf{x})$ at zero temperature is given by

$$\begin{aligned} \hat{H}_d = & \int d\mathbf{x} \hat{\Psi}_d^\dagger(\mathbf{x}) \left(-\frac{\hbar^2}{2M} \nabla_d^2 + V_d(\mathbf{x}) \right) \hat{\Psi}_d(\mathbf{x}) \\ & + \frac{1}{2} \int d\mathbf{x} \hat{\Psi}_d^\dagger(\mathbf{x}) \left[\int d\mathbf{x}' \hat{\Psi}_d^\dagger(\mathbf{x}') V_{\text{int}}(\mathbf{x} - \mathbf{x}') \hat{\Psi}_d(\mathbf{x}') \right] \hat{\Psi}_d(\mathbf{x}), \end{aligned} \quad (2.37)$$

where $V_{\text{int}}(\mathbf{x} - \mathbf{x}')$ is the two-body interatomic potential. At low densities, only binary collisions are relevant. In the low energy limit, these collisions are characterized only by the s -wave scattering length of the atoms. Then the two-body potential can be replaced by the effective interaction [59]

$$V_{\text{int}}(\mathbf{x} - \mathbf{x}') = g_d \delta^{(d)}(\mathbf{x} - \mathbf{x}'), \quad (2.38)$$

where the coupling constant g_d depends on the s -wave scattering length a_s of the particles and $\delta^{(d)}(\mathbf{x} - \mathbf{x}')$ is the d -dimensional Dirac delta distribution. In the s -wave limit, the second-quantized Hamiltonian (2.37) reduces to [57, 61, 62, 63, 65]

$$\hat{H}_d = \int d\mathbf{x} \hat{\Psi}_d^\dagger(\mathbf{x}) \left(-\frac{\hbar^2}{2M} \nabla_d^2 + V_d(\mathbf{x}) \right) \hat{\Psi}_d(\mathbf{x}) + \frac{g_d}{2} \int d\mathbf{x} \hat{\Psi}_d^\dagger(\mathbf{x}) \hat{\Psi}_d^\dagger(\mathbf{x}) \hat{\Psi}_d(\mathbf{x}) \hat{\Psi}_d(\mathbf{x}). \quad (2.39)$$

For a d -dimensional trapping potential $V_d(\mathbf{x})$, the coupling constants are

$$g_1 = (2\hbar\omega_\perp)a_s, \quad g_2 = \left(\sqrt{8\pi\hbar^3\omega_z/M} \right) a_s, \quad \text{and} \quad g_3 = (4\pi\hbar^2/M)a_s, \quad (2.40)$$

where g_1 and g_2 are obtained by projecting onto the mean-field ground state in the transverse directions [66]. The 1D and 2D transverse trapping frequencies ω_\perp and ω_z must be sufficiently high to reduce the dimensionality of the single-particle wavefunctions, as described in Section 2.2, but should not be near any potential resonances [67].

The field operators can be expanded in terms of the localized single-particle wavefunctions [65],

$$\hat{\Psi}(x) = \sum_{j,\ell,m} \hat{b}_j^{(\ell,m)} \phi_d^{(\ell,m)}(\mathbf{x} - \mathbf{x}_j), \quad (2.41)$$

for $j, j' \in \{L, R\}$ and $\ell \in \{0, 1\}$. The allowed values of m depend on the values of both d and ℓ , as discussed in the previous section. The localized wavefunctions $\phi_d^{(\ell,m)}(\mathbf{x} - \mathbf{x}_j) = \langle \mathbf{x} | j, \ell, m \rangle_d$ are given by Equation (2.32). For the lattice, $\phi_d^{(\ell,m)}(\mathbf{x} - \mathbf{x}_j)$ would be Wannier functions. The simplest description of many bosons in a double-well potential is achieved by making the *one-level approximation*. In this approximation, $\ell = 0$ and all atoms occupy the lowest energy level in each well. However, the first excited level plays an important role in many applications of these systems [19, 20] and cannot be neglected when the interactions are strong [53, 54]. Therefore, we also consider a *two-level approximation* in which $\ell \in \{0, 1\}$, that is, the atoms are allowed to occupy both the lowest and first excited energy levels in each well.

In $d \in \{1, 2, 3\}$ spatial dimensions, the two-level Hamiltonian \hat{H}_d is

$$\begin{aligned} \hat{H}_1 = & \sum_{\ell} \left\{ \hat{H}_1^{(\ell,0)} + E_1^\ell \hat{N}^{(\ell,0)} \right\} + 2U_1^{11} \sum_j \left\{ \sum_{\ell \neq \ell'} \left[\hat{n}_j^{(\ell,0)} \hat{n}_j^{(\ell',0)} \right] \right\} \\ & + U_1^{11} \sum_j \left\{ \left(\hat{b}_j^{(0,0)\dagger} \hat{b}_j^{(1,0)} \right)^2 + \text{h.c.} \right\}, \end{aligned} \quad (2.42a)$$

$$\begin{aligned}
\hat{H}_2 &= \sum_{\ell,m} \left\{ \hat{H}_2^{(\ell,m)} + E_2^\ell \hat{N}^{(\ell,m)} \right\} - J_2^{-11} \sum_{j \neq j'} \left\{ \hat{b}_j^{(1,-1)\dagger} \hat{b}_{j'}^{(1,+1)} + \text{h.c.} \right\} \\
&+ 2U_2^{11} \sum_j \left\{ \sum_{(\ell,m) \neq (\ell',m')} \left[\hat{n}_j^{(\ell,m)} \hat{n}_j^{(\ell',m')} \right] \right\} \\
&+ 2U_2^{11} \sum_j \left\{ \left(\hat{b}_j^{(0,0)\dagger} \right)^2 \hat{b}_j^{(1,-1)} \hat{b}_j^{(1,+1)} + \text{h.c.} \right\}, \tag{2.42b}
\end{aligned}$$

$$\begin{aligned}
\hat{H}_3 &= \sum_{\ell,m} \left\{ \hat{H}_3^{(\ell,m)} + E_3^\ell \hat{N}^{(\ell,m)} \right\} - J_3^{-11} \sum_{j \neq j'} \left\{ \hat{b}_j^{(1,-1)\dagger} \hat{b}_{j'}^{(1,+1)} + \text{h.c.} \right\} \\
&+ 2U_3^{11} \sum_j \left\{ \sum_{(\ell,m) \neq (\ell',m')} \left[\epsilon_{\ell m}^{\ell' m'} \hat{n}_j^{(\ell,m)} \hat{n}_j^{(\ell',m')} \right] \right\} \\
&+ U_3^{11} \sum_j \left\{ \left(\hat{b}_j^{(0,0)\dagger} \hat{b}_j^{(1,0)} \right)^2 + \text{h.c.} \right\} \\
&+ U_3^{11} \sum_j \left\{ \left[2 \left(\hat{b}_j^{(0,0)\dagger} \right)^2 + \left(\hat{b}_j^{(1,0)\dagger} \right)^2 \right] \hat{b}_j^{(1,-1)} \hat{b}_j^{(1,+1)} + \text{h.c.} \right\}, \tag{2.42c}
\end{aligned}$$

where

$$\hat{H}_d^{(\ell,m)} \equiv -J_d^{|\ell|} \sum_{j \neq j'} \hat{b}_j^{(\ell,m)\dagger} \hat{b}_{j'}^{(\ell,m)} + U_d^{|\ell|} \sum_j \hat{n}_j^{(\ell,m)} \left(\hat{n}_j^{(\ell,m)} - 1 \right), \tag{2.42d}$$

is the one-level Hamiltonian and

$$\epsilon_{\ell m}^{\ell' m'} \equiv \begin{cases} 1/2, & \ell = \ell' = |m + m'| = 1 \\ 1, & \text{otherwise} \end{cases}, \tag{2.42e}$$

for all allowed values of j , ℓ , and m . The operators $\hat{b}_j^{(\ell,m)}$ and $\hat{b}_j^{(\ell,m)\dagger}$ satisfy the usual bosonic annihilation and creation commutation relations, $\hat{n}_j^{(\ell,m)} \equiv \hat{b}_j^{(\ell,m)} \hat{b}_j^{(\ell,m)}$ are number operators, and $\hat{N}^{(\ell,m)} \equiv \hat{n}_L^{(j,m)} + \hat{n}_R^{(j,m)}$.

Single particles in the ℓ th energy level with z angular momentum $m\hbar$ tunnel between wells with hopping strength $J_d^{\ell|m|}$ and pairs of particles interact in the same well with interaction energy $U_d^{\ell|m|}$. Interactions can be either repulsive, $U_d^{\ell|m|} > 0$, or attractive, $U_d^{\ell|m|} < 0$. While the hopping strengths J_d^{10} and $J_d^{\pm 11}$ are greater than J_d^{00} , the interaction energies U_d^{10} and U_d^{11} are smaller in magnitude than U_d^{00} . Interactions of two atoms in different levels of the same well are on the order of U_d^{00} and cannot be neglected. Furthermore, while single-atom transitions between energy levels are forbidden by the orthogonality of the localized wavefunctions, two atoms can hop together between energy levels such that the z -component of the on-site angular momentum is conserved. Thus the energy levels are coupled by the interaction energy U_d^{11} . Energy levels only become completely decoupled when $U_d^{11} = 0$, but the effects of coupling are negligible for $N|U_d^{00}| \ll 2\Delta E_d^{10}$. For clarity, pictorial interpretations of \hat{H}_1 , \hat{H}_2 , and \hat{H}_3 , are provided in Figures 2.4, 2.5, and 2.6.

The hopping strengths $J_d^{\ell|m|}$ and J_d^{-11} given by

$$J_d^{\ell|m|} = - \int d\mathbf{x} \left[\phi_d^{(\ell,m)}(\mathbf{x} - \mathbf{x}_L) \right]^* \left(-\frac{\hbar^2}{2M} \nabla^2 + V(\mathbf{x}) \right) \phi_d^{(\ell,m)}(\mathbf{x} - \mathbf{x}_R), \quad (2.43a)$$

$$J_d^{-11} = - \int d\mathbf{x} \left[\phi_d^{(1,-1)}(\mathbf{x} - \mathbf{x}_L) \right]^* \left(-\frac{\hbar^2}{2M} \nabla^2 + V(\mathbf{x}) \right) \phi_d^{(1,+1)}(\mathbf{x} - \mathbf{x}_R), \quad (2.43b)$$

and interaction energies $U_d^{\ell|m|}$ given by

$$U_d^{10} = (3/4)U_d^{00} \quad \text{and} \quad U_d^{11} = (1/2)U_d^{00}, \quad (2.43c)$$

where

$$U_d^{00} = \frac{g_d}{2} \int d\mathbf{x} |\phi_d^{(0,0)}(\mathbf{x} - \mathbf{x}_L)|^4. \quad (2.43d)$$

In our derivation of the one- and two-level Hamiltonians, we have assumed that the

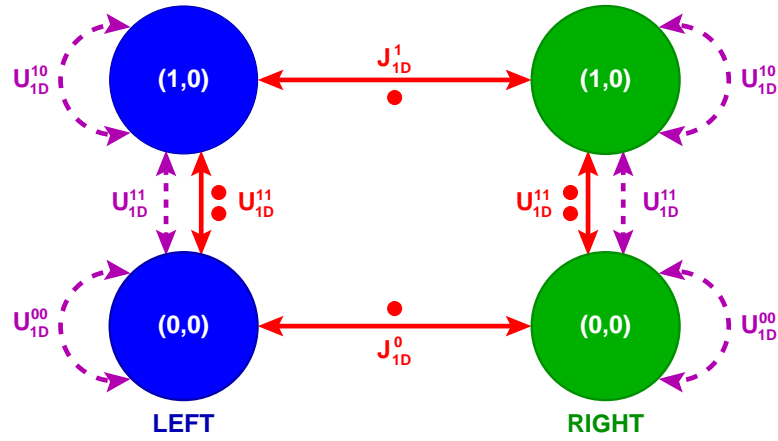


Figure 2.4. *Pictorial representation of the one-dimensional Hamiltonian \hat{H}_1 .* The allowed modes of the 1D system are depicted as circles. Blue and green circles correspond to modes in the left and right wells, respectively. The level index ℓ and the angular momentum index m are indicated by the ordered pair (ℓ, m) in the center of the circles. Tunneling processes are depicted as solid red lines. One or two dots are drawn near the lines corresponding to whether the transition involves one or two particles. Dashed magenta lines represent interactions between two atoms. The parameters which appear next to the lines are the coefficients of the corresponding process in the 1D Hamiltonian (2.42a). The 1D Hamiltonian consists of two one-level Hamiltonians coupled by the interaction energy U_1^{11} .

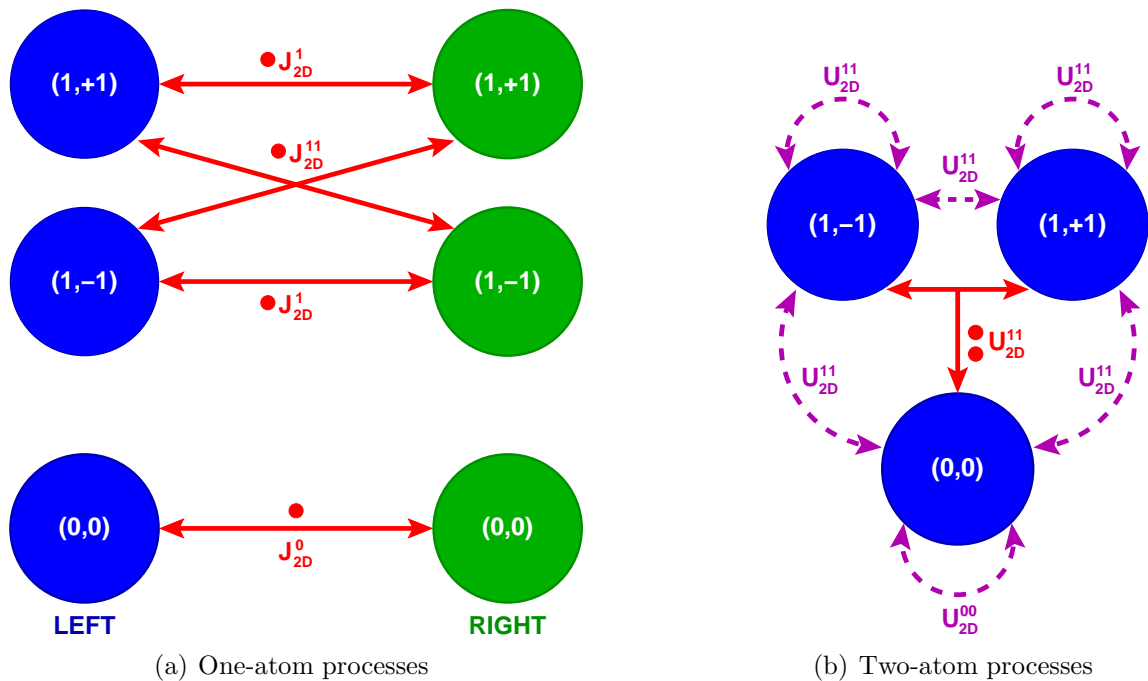


Figure 2.5. *Pictorial representation of the two-dimensional Hamiltonian \hat{H}_2 .* This diagram is similar to Figure 2.4 except that the one- and two-atom processes are depicted separately in (a) and (b), respectively. (a) A single atom can tunnel between wells provided it remains in the same energy level. However, as indicated by the diagonal lines, the atom need not remain in the same angular momentum state. (b) Within each well, a pair of atoms can hop from the $\ell = 0$ level to the $\ell = 1$ level with one atom entering angular momentum state $m = -1$ and the other entering state $m = +1$.

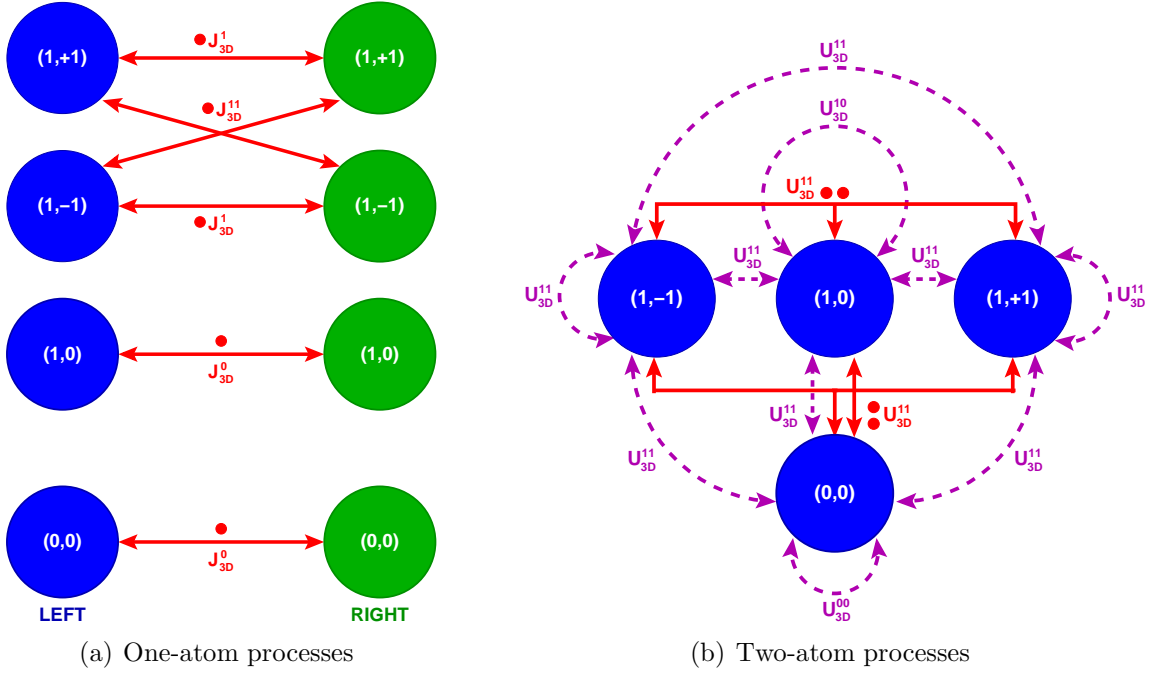


Figure 2.6. *Pictorial representation of the three-dimensional Hamiltonian \hat{H}_3 .* This diagram is similar to Figure 2.5. (a) The single-atom processes are essentially the same as in the one- and two- dimensional cases. One important difference is that the tunneling strength J_d^{10} of the excited level is greater than the tunneling strength J_d^{00} in 1D, whereas in 3D these energies are equal. (b) In addition to the two-atom processes present in the 1D and 2D Hamiltonians, two atoms in the same well can tunnel from the $m = 0$ state to the $m = \pm 1$ states all within the energy level $\ell = 1$.

off-site interaction terms, e.g.,

$$\frac{g_d}{2} \int d\mathbf{x} |\phi_d^{(0,0)}(\mathbf{x} - \mathbf{x}_L)|^2 |\phi_d^{(0,0)}(\mathbf{x} - \mathbf{x}_R)|^2,$$

are much smaller than U_d^{00} .

In the harmonic oscillator approximation, we find

$$U_d^{00} = \hbar\omega \frac{G_d}{\sqrt{2\pi}} \left(\frac{a_{\text{ho}}}{a}\right)^{2-d}, \quad (2.44)$$

where $\hbar\omega = \Delta E_d^{10}$ is the energy level spacing. The dimensionless coupling constants are defined as

$$G_1 \equiv a_s a / a_\perp^2, \quad G_2 \equiv a_s / a_z, \quad \text{and} \quad G_3 \equiv a_s / a. \quad (2.45)$$

Here $a_\perp = \sqrt{\hbar/M\omega_\perp}$ and $a_z = \sqrt{\hbar/M\omega_z}$ are the transverse trapping lengths in 1D and 2D, respectively (see Equations (2.12) and (2.14)). Off-site interactions scale like $U_d^{00} \exp[-(a/a_{\text{ho}})^2]$. If $a \gtrsim 2a_{\text{ho}}$, then $\exp[-(a/a_{\text{ho}})^2] \lesssim 0.02$ and the off-site terms are much smaller than U_d^{00} in magnitude. We can therefore neglect interactions between atoms in the left well with those in the right when condition (2.24) is met. Although off-site interactions have been neglected in the derivation of Hamiltonian (2.42), all other nonzero terms have been included. While the harmonic oscillator assumption was used to evaluate the interaction energies (2.43c), we have also evaluated these energies numerically for specific potentials.

From the definition (2.32) of the exact wavefunctions $\phi_d^{(\ell,m)}(\mathbf{x} - \mathbf{x}_j)$, one can show the relation

$$J_1^{00} = \frac{\varepsilon_{1x} - \varepsilon_{0x}}{2} \quad \text{and} \quad J_1^{10} = \frac{\varepsilon_{3x} - \varepsilon_{2x}}{2}. \quad (2.46a)$$

Furthermore, the 2D and 3D hopping strengths are related to J_1^{00} and J_1^{10} by

$$J_d^{00} = J_1^{00}, \quad J_d^{\pm 11} = (J_1^{10} \pm J_1^{00})/2, \quad J_3^{10} = J_1^{00}, \quad \text{for } d \in \{2, 3\}. \quad (2.46b)$$

It is therefore sufficient to compute only the 1D hopping parameters. In the harmonic oscillator approximation, the localized wavefunctions are given by Equation (2.28a) and the 1D hopping strengths have the form

$$J_1^{00} \approx \frac{1}{2} E_r \left\{ \left(\frac{a}{a_{\text{ho}}} \right)^2 \left[\left(\frac{a}{a_{\text{ho}}} \right)^2 - 1/2 \right] - 2V_0/E_r \right\} e^{-a^2/a_{\text{ho}}^2}, \quad (2.47a)$$

$$J_1^{10} \approx J_1^{00} \left[\left(\frac{a}{a_{\text{ho}}} \right)^2 - 1 \right] + \frac{1}{2} E_r \left\{ \left(\frac{a}{a_{\text{ho}}} \right)^6 - \frac{9}{2} \left(\frac{a}{a_{\text{ho}}} \right)^4 + \left(\frac{a}{a_{\text{ho}}} \right)^2 \right\} e^{-a^2/a_{\text{ho}}^2} \quad (2.47b)$$

where E_r is the recoil energy of the double-well and $a/a_{\text{ho}} \gtrsim 2$. Equation (2.47) is derived in Appendix A for an arbitrary double-well potential. Clearly, the hopping strengths have a decaying exponential dependence on $(a/a_{\text{ho}})^2$. Moreover, since J_1^{10}/J_1^{00} is on the order of $(a/a_{\text{ho}})^2$ and $J^{00}/\hbar\omega$ is on the order of $\exp[-(a/a_{\text{ho}})^2]$, we have

$$J_1^{00} \ll J_1^{10} \ll \hbar\omega = \Delta E_d^{10}. \quad (2.48)$$

Therefore, the hopping strength is greater in the $\ell = 1$ energy level than in the $\ell = 0$ energy level, as expected.

To model a potential difference of ΔV between the wells, we increase the energy of all the atoms in the left well and decrease the energy of the atoms in the right well by an amount $\Delta V/2$. The one-level Hamiltonian becomes

$$\hat{H}_d^{(\ell,m)} \rightarrow \hat{H}_d^{(\ell,m)} + \frac{\Delta V}{2} \left(\hat{n}_L^{(\ell,m)} - \hat{n}_R^{(\ell,m)} \right), \quad (2.49)$$

where ΔV is called the *tilt* of the double-well. The left well has a higher energy than the right well for $\Delta V > 0$, the right well has a higher energy for $\Delta V < 0$, and $\Delta V = 0$ indicates a symmetric double-well potential. Ultracold atoms in tilted double-well potentials are especially relevant to quantum information processing [19, 20], gravimetry [23, 24], and quantum atom optics [28, 29, 30].

Throughout our discussion, we will operate in Fock space. A state vector in Fock space has the form

$$|\Psi\rangle = \sum_{n_d=0}^{\Omega_d-1} c_{n_d} |n_d\rangle, \quad |n_d\rangle = \bigotimes_{\ell,m} |n_L^{(\ell,m)}, n_R^{(\ell,m)}\rangle_{(\ell,m)}, \quad (2.50)$$

where $n_j^{(\ell,m)}$ represents the number of atoms in the ℓ th energy level of the j th well with z angular momentum $m\hbar$. Here Ω_d is size of the Hilbert space $\{|n_d\rangle\}$. We work in the canonical ensemble, that is, we require the total number of particles $N = \sum_{j,\ell,m} n_j^{(\ell,m)}$ to be constant. Under this restriction, the size of the Hilbert space is given by

$$\Omega_d = \frac{(N + 2d + 1)!}{N!(2d + 1)!}. \quad (2.51)$$

For large N , the multiplicity Ω_d scales like N^{2d+1} . The stationary states of the two-level Hamiltonian are discussed in Chapter 4.

When the coupling between levels is very weak, $N|U_d^{00}| \ll 2\Delta E_d^{10}$, the effects of the excited level can be neglected and a one-level approximation, in which all particles occupy the ground level of each well, is valid. The one-level Hamiltonian is

$$\hat{H}_d^{(0,0)} \equiv -J_d^{00} \sum_{j \neq j'} \hat{b}_j^{(0,0)\dagger} \hat{b}_{j'}^{(0,0)} + U_d^{00} \sum_j \hat{n}_j^{(0,0)} (\hat{n}_j^{(0,0)} - 1) + \frac{\Delta V}{2} (\hat{n}_L^{(0,0)} - \hat{n}_R^{(0,0)}). \quad (2.52)$$

In this approximation, an arbitrary state vector in Fock space is given by

$$|\Psi\rangle = \sum_{n_L=0}^N c_{n_L} |n_L, N - n_L\rangle_{(0,0)}, \quad (2.53)$$

where n_L and $n_R = N - n_L$ represent the number of particles in the left and right wells, respectively. The size of the Hilbert space $\{|n_L, N - n_L\rangle_{(0,0)}\}$ reduces to $N + 1$. The one-level approximation is discussed in detail in Chapter 3. In the limit of an infinite number of wells, the one-level Hamiltonian reproduces the single-band Bose-Hubbard Hamiltonian for weakly interacting bosons in an optical lattice. That is, as the number of sites goes to infinity,

$$\hat{H}_d^{(0,0)} \rightarrow \hat{H}_{\text{BH}} \equiv -J \sum_{\langle j, j' \rangle} \hat{b}_j^\dagger \hat{b}_{j'} + U \sum_j \hat{n}_j (\hat{n}_j - 1) + \sum_j V_j \hat{n}_j \quad (2.54)$$

where $\langle j, j' \rangle$ indicates a sum over nearest neighbors.

Chapter 3

ONE-LEVEL APPROXIMATION

In this chapter, we study the behavior of N ultracold bosons in a tilted double-well potential in the one-level approximation. The stationary states fall into one of two categories: *harmonic oscillator-like states* or *Schrödinger cat-like states*. When the barrier between wells is low, all states are oscillator-like. Cat-like states dominate the spectrum in the high barrier limit. We show that Schrödinger cats are highly sensitive to imperfections in the trapping potential; cat-like states are easily localized when a small tilt is introduced. Thus, tilt constitutes a new source of decoherence, called *potential decoherence*. Potential decoherence is a unique form of decoherence because cat-like states reappear for critical values of the tilt, unlike for decoherence due to coupling to a thermal heat bath.

The evolution of a state in which all atoms initially occupy one well is studied in various parameter regimes. In the high and low barrier limits, the atoms undergo *quantum sloshing*, that is, all atoms tunnel through the potential barrier. Interactions damp the tunneling when the barrier is low; quantum revivals occur periodically at times determined solely by the interaction energy. Although tunneling is easily suppressed by potential decoherence, *tunneling resonances* occur for critical values of the tilt when the barrier is high. Resonances are caused by the reappearance of the cat-like eigenstates. At resonance, only a fraction of particles tunnel between wells.

3.1 One-Level Hamiltonian

The one-level Hamiltonian for N weakly interacting bosons in a tilted two-well potential is

$$\hat{H} = -J \sum_{j \neq j'} \hat{b}_j^\dagger \hat{b}_{j'} + U \sum_j \hat{n}_j (\hat{n}_j - 1) + \frac{\Delta V}{2} (\hat{n}_L - \hat{n}_R). \quad (3.1)$$

Equation (3.1) was derived in Chapter 2. Because there are no angular momentum degrees of freedom in the lowest energy level, the cumbersome sub- and super-scripts of Equation (2.52) have been dropped. Recall that the subscript $j \in \{L, R\}$ is the well index, J is the hopping strength, U is the interaction potential, and ΔV is the potential difference between wells, or tilt.

For convenience, we define the following operators,

$$\hat{H}_U \equiv U \sum_j \hat{n}_j (\hat{n}_j - 1), \quad \hat{H}_J \equiv -J \sum_{j \neq j'} \hat{b}_j^\dagger \hat{b}_{j'}, \quad \text{and} \quad \hat{H}_{\Delta V} \equiv \frac{\Delta V}{2} (\hat{n}_L - \hat{n}_R). \quad (3.2)$$

The Hamiltonian can then be written $\hat{H} = \hat{H}_U + \hat{H}_J + \hat{H}_{\Delta V}$. We identify two parameter regimes: $J \ll |U|$, the high barrier regime; and $J \gg N|U|$, the low barrier regime. When the barrier is high, \hat{H}_J can be treated as a perturbation to \hat{H}_U and vice versa for a low barrier.

As stated in Chapter 2, an arbitrary state vector in Fock space is given by

$$|\Psi\rangle = \sum_{n_L=0}^N c_{n_L} |n_L, N - n_L\rangle, \quad (3.3)$$

where n_L and $n_R = N - n_L$ represent the number of particles in the left and right wells, respectively. We require the total number of particles N to be constant. Under

this restriction, the Hamiltonian (3.1) reduces to an $(N + 1) \times (N + 1)$ tridiagonal matrix with elements

$$H_{ij} \equiv \langle i, N - i | \hat{H} | j, N - j \rangle = H_{ij}^{(U)} + H_{ij}^{(J)} + H_{ij}^{(\Delta V)}, \quad (3.4a)$$

where

$$H_{ij}^{(U)} = U (2(i - N/2)^2 + N(N/2 - 1)) \delta_{ij}, \quad (3.4b)$$

$$H_{ij}^{(J)} = -J \left(\sqrt{(i+1)(N-i)} \delta_{i,j-1} + \sqrt{(j+1)(N-j)} \delta_{i,j+1} \right), \quad (3.4c)$$

$$H_{ij}^{(\Delta V)} = \Delta V (i - N/2) \delta_{ij}, \quad (3.4d)$$

for $i, j \in \{0, 1, 2, \dots, N\}$.

3.2 Entanglement Measures

In order to characterize the entanglement of a state $|\Psi\rangle$, we utilize two entanglement measures adapted from standard definitions for chains of qubits: Meyer's measure of the impurity [68, 69] and the von Neumann entropy S , which, in our case, is equivalent to the Shannon entropy [70]. The impurity is given by

$$Q = \frac{N+1}{N} \left[1 - \frac{1}{2} (\text{Tr} \hat{\rho}_L^2 + \text{Tr} \hat{\rho}_R^2) \right] = \frac{N+1}{N} \left[1 - \sum_{n_L=0}^N |c_{n_L}|^4 \right], \quad (3.5)$$

where $\hat{\rho}_{L(R)} = \text{Tr}_{R(L)} |\Psi\rangle\langle\Psi|$ is the reduced density matrix. The entropy is

$$S = -\text{Tr} \hat{\rho}_L \log_{N+1} \hat{\rho}_L = -\text{Tr} \hat{\rho}_R \log_{N+1} \hat{\rho}_R = - \sum_{n_L=0}^N |c_{n_L}|^2 \log_{N+1} |c_{n_L}|^2. \quad (3.6)$$

Here $0 \leq Q, S \leq 1$ with $Q = S = 0$ if $|\Psi\rangle$ is a pure state and $Q = S = 1$ for a maximally mixed state. A pure state satisfies $c_{n_L} = \delta_{n_L, n'_L}$ for some $n'_L \in \{0, \dots, N\}$ whereas a maximally mixed state is defined by $c_{n_L} = 1/\sqrt{N+1}$ for every $n_L \in \{0, \dots, N\}$.

In particular, we are interested in using the impurity Q and the entropy S to characterize the entanglement of *partial Schrödinger cat states*. These states have the form

$$|\psi_{\text{cat}}^{\pm}; n_L\rangle = \frac{1}{\sqrt{2}}(|n_L, N - n_L\rangle \pm |N - n_L, n_L\rangle), \quad (3.7)$$

for $0 \leq n_L < N/2$. Here $n_L = 0$ represents the *extreme Schrödinger cat state* $|\psi_{\text{cat}}^{\pm}; 0\rangle = (|0, N\rangle \pm |N, 0\rangle)/\sqrt{2}$ in which all atoms simultaneously occupy both wells. For partial cat states, we find that

$$Q_{\text{cat}} = \frac{N}{2(N+1)} \quad \text{and} \quad S_{\text{cat}} = \log_{N+1}(2), \quad (3.8)$$

Unfortunately, the above measures do not distinguish between the states $|\psi_{\text{cat}}^{\pm}; n_L\rangle$ and, say, $|\psi_{\text{cat}}^{\pm}; n'_L\rangle$ where $n'_L \neq n_L$. Such a distinction is vital as the decoherence of a partial cat state $|\psi_{\text{cat}}^{\pm}; n_L\rangle$ is highly sensitive to the value of n_L [45, 54, 55], as we will demonstrate.

In order to better identify cat-like states, it is desirable to have a quantum measure whose value lies between 0 and 1 and which is maximized for partial cat states. In addition, the measure should distinguish between states $|\psi_{\text{cat}}^{\pm}; n_L\rangle$ and $|\psi_{\text{cat}}^{\pm}; n'_L\rangle$. As we will show, the quantity $\bar{P}_{\text{cat}}(n_c)$ defined by

$$\bar{P}_{\text{cat}}(n_c) = |\langle \Psi | \hat{P}_{\text{cat}}(n_c) | \Psi \rangle|, \quad (3.9)$$

where

$$\hat{P}_{\text{cat}}(n_c) \equiv \sum_{n_L=0}^{n_c} (|n_L, N - n_L\rangle\langle N - n_L, n_L| + \text{h.c.}) \quad \text{for } 0 \leq n_c \leq N/2. \quad (3.10)$$

is the *Schrödinger-cat projection operator*, satisfies these requirements. It is trivial to show that $\bar{P}_{\text{cat}}(n_c) = 0$ for pure states and that $\bar{P}_{\text{cat}}(n_c) = 1$ for partial cat states $|\psi_{n_L}\rangle$ such that $n_L \leq n_c$. That $0 \leq \bar{P}_{\text{cat}}(n_c) \leq 1$ follows directly from the unitarity of the operator $\hat{P}_{\text{cat}}(N/2)$. Partial cat states with $\bar{P}_{\text{cat}}(n_c) = 1$ have a minimum peak separation of $N - 2n_c$. We call the $\bar{P}_{\text{cat}}(n_c)$ the *cat measure*. The cat measure is only valid when the amplitudes $c_{n_L} = \langle n_L, N - n_L | \Psi \rangle$ are real. Our measure is similar to one proposed by Huang and Moore [45]. Their measure, however, does not distinguish between cat states and pure states. Recently, Korsbakken *et al.* proposed a measurement-based measure of cat states which we do not consider here [71].

3.3 Characterization of Energy Eigenstates

We begin our analysis of the one-level approximation with a characterization of the eigenstates $|\phi_k\rangle$ of the Hamiltonian (3.1). The energy eigenstates satisfy

$$\hat{H}|\phi_k\rangle = \varepsilon_k|\phi_k\rangle, \quad (3.11)$$

and can be expanded in terms of the number states $|n_L, N - n_L\rangle$ as

$$|\phi_k\rangle = \sum_{n_L=0}^N c_{n_L}^{(k)} |n_L, N - n_L\rangle. \quad (3.12)$$

Here $|c_{n_L}^{(k)}|^2$ is the probability of finding n_L particles in the left well when the system is in the k th excited state. The discrete probability amplitudes $c_{n_L}^{(k)}$ and the correspond-

ing energy eigenvalues ε_k are readily obtained by diagonalizing the matrix (3.4). The *eigenstate label* k is chosen to increase with increasing energy.

3.3.1 Harmonic-Oscillator-Like States

Consider a system of non-interacting bosons in a symmetric potential, that is, $U = \Delta V = 0$ and $\hat{H} = \hat{H}_J$. The probability amplitude of the k th excited state is

$$c_{n_L}^{(k)} = A_k H_k(n_L|N) \sqrt{P_{1/2}(n_L|N)}, \quad (3.13)$$

where $P_{1/2}(n_L|N)$ is the binomial distribution, $H_k(n_L|N)$ is a k th order discrete Hermite polynomial, and A_k is a normalization constant (see Appendix B). The corresponding energy eigenvalue is

$$\varepsilon_k = -J(N - 2k). \quad (3.14)$$

The eigenstates of the noninteracting Hamiltonian are called harmonic-oscillator-like states because the (discrete) probability amplitudes closely resemble the (continuous) eigenfunctions of the one-dimensional simple harmonic oscillator and the eigenvalues are linear in k . The ground state and several excited states are shown in Figure 3.1. All eigenstates and eigenvalues are shown in Figure 3.2. The ground state amplitude $c_{n_L}^{(0)}$, given by

$$c_{n_L}^{(0)} = \sqrt{P_{1/2}(n_L|N)} = \frac{1}{2^{N/2}} \sqrt{\frac{N!}{n_L!(N - n_L)!}}, \quad (3.15)$$

is a binomial distribution of number states, as in Fig. 3.1(a). This distribution represents a superfluid state with energy $\varepsilon_0 = -NJ$.

The oscillator-like states are significantly entangled, as can be seen in Figure 3.3.

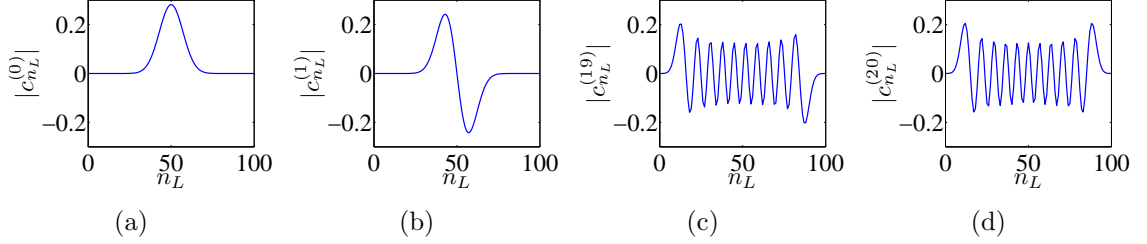


Figure 3.1. *Eigenstate amplitudes: Harmonic oscillator-like states.* Shown are the discrete probability amplitudes $c_{n_L}^{(k)}$ of the eigenstates $|\phi_k\rangle$ when $U = \Delta V = 0$ and $N = 100$ for (a) the ground state, (b) the first excited state, (c) the 19th excited state, and (d) the 20th excited state. These states are called oscillator-like because they resemble the continuous eigenfunctions of the 1D simple harmonic oscillator.

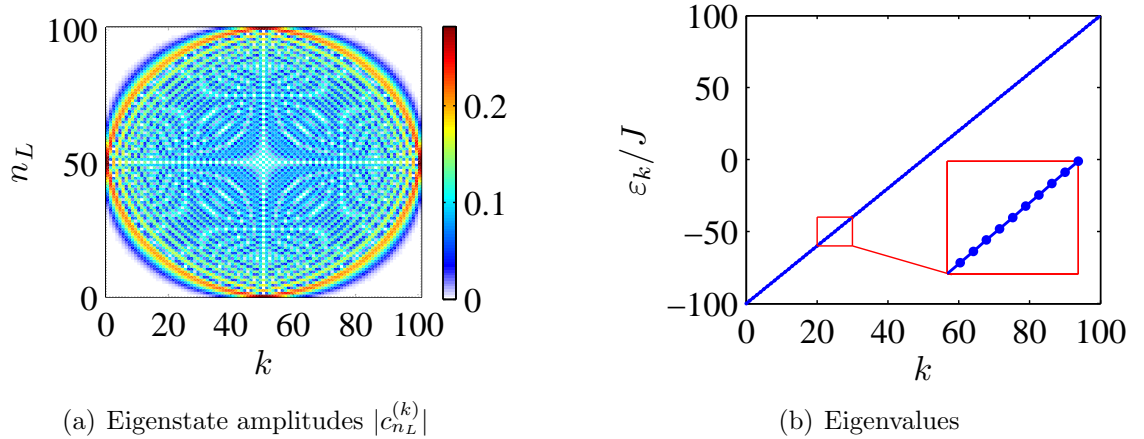


Figure 3.2. *Eigenstates and eigenvalues: Harmonic oscillator-like states.* (a) The eigenstate amplitudes $|c_{n_L}^{(k)}|$ of the Hamiltonian \hat{H} when $U = \Delta V = 0$ and $N = 100$ are plotted for all values of n_L and k . Amplitude is indicated by the colorbar. A vertical cross section of this plot produces curves similar to those of Fig. 3.1. (b) The eigenvalues ε_k of the same system as (a). The line serves as a guide to the eye. Just as in the 1D simple harmonic oscillator, the eigenvalues of the non-interacting systems are linear in k . The insert is a zoom of the indicated region.

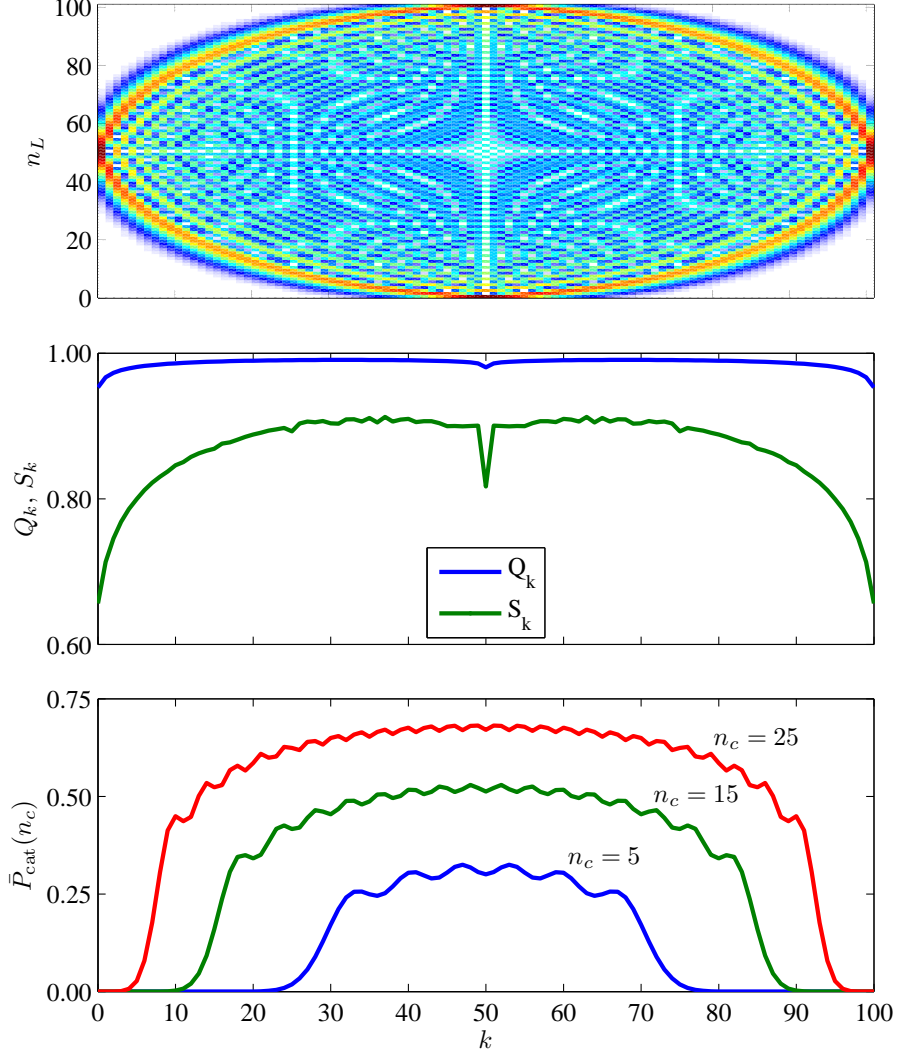


Figure 3.3. *Entanglement measures: Harmonic oscillator-like states.* Top panel: Shown are the probability amplitudes $|c_{n_L}^k|$ for all n_L and k for a system of $N = 100$ non-interacting atoms in a symmetric double-well. The color bar is the same as in Figure 3.2(a). Middle panel: The impurity and the entropy of the k th excited state, denoted Q_k and S_k , respectively, versus k . Eigenstates which lie in the middle of the spectrum are highly mixed and have an impurity close to unity. Bottom panel: Plotted is $\bar{P}_{\text{cat}}(n_c)$ for $n_c = 5$ (blue), $n_c = 15$ (green), and $n_c = 25$ (red). For small values of n_c , $\bar{P}_{\text{cat}}(n_c)$ is significantly less than unity.

Eigenstates which lie in the middle of the spectrum, such as Figure 3.1(c), have the highest impurity Q and entropy S because they are composed of a more even distribution of Fock states than the lowest and highest excited states. This is obvious in Figure 3.2; the middle of the spectrum has essentially no white regions, that is, there are no regions of zero probability. Because there are no eigenstates which resemble partial cat states, $\bar{P}_{\text{cat}}(n_c)$ is significantly less than unity over the entire spectrum.

3.3.2 Schrödinger-Cat-Like States

We now turn our attention to a symmetric potential in which the barrier is sufficiently high that no tunneling occurs, that is, $J = \Delta V = 0$. In this case, $\hat{H} = \hat{H}_U$ and the eigenstates and eigenvalues of the Hamiltonian (3.1) are given by

$$\hat{H}|n_L, N - n_L\rangle = \varepsilon_{n_L}|n_L, N - n_L\rangle, \quad (3.16)$$

with

$$\varepsilon_{n_L} = U [2(n_L - N/2)^2 + N(N/2 - 1)]. \quad (3.17)$$

Suppose now that the barrier is high but that the hopping strength is nonzero, that is, $0 < J \ll |U|$. In this case, we treat \hat{H}_J as a perturbation to \hat{H}_U . Because $\varepsilon_{N-n_L} = \varepsilon_{n_L}$, the states $|n_L, N - n_L\rangle$ and $|N - n_L, n_L\rangle$ are degenerate and we employ degenerate perturbation theory (see Appendix C).

To lowest order in $J/|U|$, the eigenstates have the form

$$|\phi_{\pm}; n_L\rangle = |\psi_{\pm}^{\text{cat}}; n_L\rangle \quad \text{for } 0 \leq n_L < N/2. \quad (3.18)$$

These represent symmetric (+) and antisymmetric (−) pairs of macroscopic super-

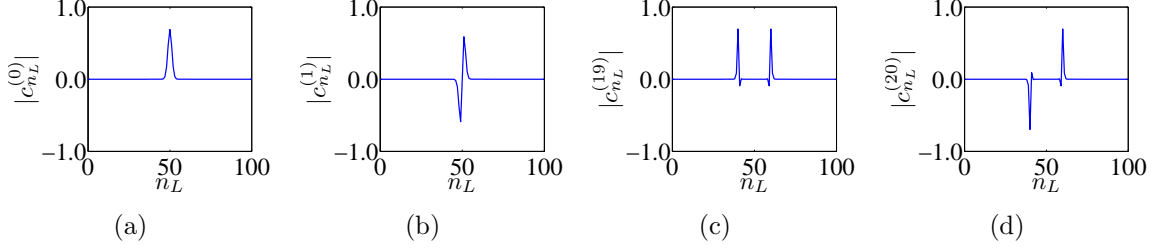


Figure 3.4. *Eigenstate amplitudes: Schrödinger cat-like states.* Shown are the discrete probability amplitudes $c_{n_L}^{(k)}$ of the eigenstates $|\phi_k\rangle$ when $J/U = 0.1$, $\Delta V = 0$, and $N = 100$ for (a) the ground state, (b) the first excited state, (c) the 19th excited state, and (d) the 20th excited state. The ground state is a Mott-insulator state in which exactly half the atoms occupy each well. Higher excited states are macroscopic superposition states which resemble partial Schrödinger cat states.

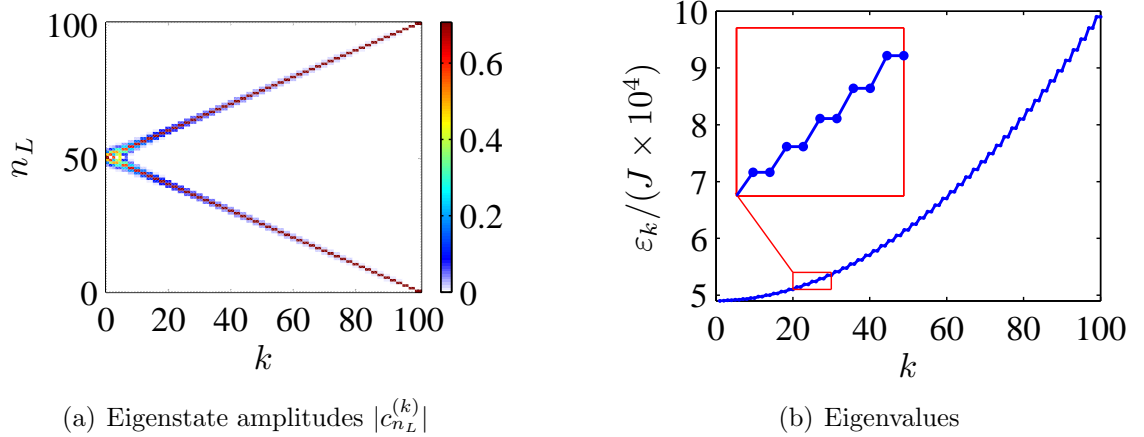


Figure 3.5. *Eigenstates and eigenvalues: Schrödinger cat-like states.* (a) The eigenstate amplitudes $|c_{n_L}^{(k)}|$ of the Hamiltonian \hat{H} when $J/U = 0.1$, $\Delta V = 0$, and $N = 100$ are plotted for all values of n_L and k . Amplitude is indicated by the colorbar. A vertical cross section of this plot produces plots similar to Fig. 3.4. The eigenstates are symmetric and antisymmetric macroscopic superpositions of different Fock states. (b) The eigenvalues ε_k of the same system as (a). The line serves as a guide to the eye. The eigenvalues occur in nearly degenerate pairs corresponding to symmetric and antisymmetric pairs of cat-like states. The energy increases quadratically with k . The insert is a zoom of the indicated region.

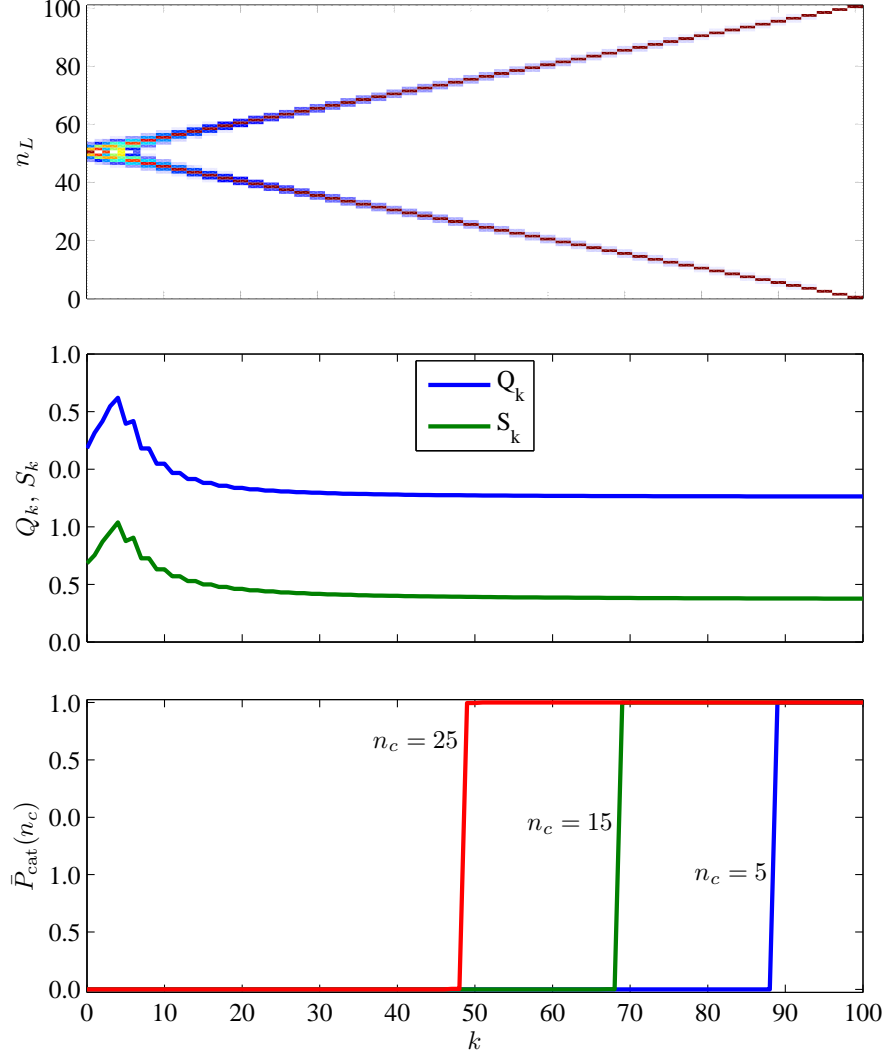


Figure 3.6. *Entanglement measures: Schrödinger cat-like states.* Top panel: Shown are the probability amplitudes $|c_{n_L}^k|$ for all n_L and k for a system of $N = 100$ atoms in a symmetric double-well with $J/U = 0.1$. Middle panel: The impurity and the entropy of the k th excited state, denoted Q_k and S_k , respectively, versus k . Excited states closely resemble partial cat states. For $k > 20$, $Q_k \simeq Q_{\text{cat}}$ and $S_k \simeq S_{\text{cat}}$. Bottom panel: Plotted is $\bar{P}_{\text{cat}}(n_c)$ for $n_c = 5$ (blue), $n_c = 15$ (green), and $n_c = 25$ (red). In this parameter regime, $\bar{P}_{\text{cat}}(n_c)$ can be used to determine the minimum peak separation of the cat-like eigenstates quite precisely. Cat-like states with $\bar{P}_{\text{cat}}(n_c) \simeq 1$ have a minimum peak separation of $N - 2n_c$.

position states, or partial Schrödinger cat states. The energy splitting between symmetric and antisymmetric pairs of states is

$$\Delta\varepsilon_{N-n_L} = 4U \frac{(N-n_L)!}{n_L![(N-2n_L-1)!]^2} \left(\frac{J}{2U}\right)^{N-2n_L}, \quad (3.19)$$

which is a very small number. For the special case $n_L = 0$, the eigenstates are extreme cat states of the form $|\psi_{\pm}^{\text{cat}}; 0\rangle$ with an energy level splitting

$$\Delta\varepsilon_N = 4U \frac{N}{(N-1)!} \left(\frac{J}{2U}\right)^N. \quad (3.20)$$

The ground state and several excited states are plotted in Figure 3.4. All eigenstates and corresponding eigenvalues are shown in Figure 3.5.

The impurity and the entropy of the cat-like eigenstates approach Q_{cat} and S_{cat} for highly excited states, as is evident in Figure 3.6. These measures obviously cannot be used to distinguish between cat-like states with different peak separations. However, $\bar{P}_{\text{cat}}(n_c)$ acts as an indicator for cat-like states with a separation greater than $N - 2n_c$.

3.3.3 Medium Barrier

When $J < N|U|$, the eigenstates can be either oscillator- or cat-like. For repulsive interactions, $U > 0$, the low-lying states are oscillator-like whereas higher lying states are cat-like. The ground state and several excited states are plotted in Figure 3.7. All eigenstates and corresponding eigenvalues are shown in Figure 3.8. In the oscillator-like region, the eigenvalues ε_k are approximately linear in k . The deviation from linear spacing is induced by the interaction energy U . In the cat-like region, on the other hand, the eigenvalues occur in nearly degenerate pairs which vary quadratically

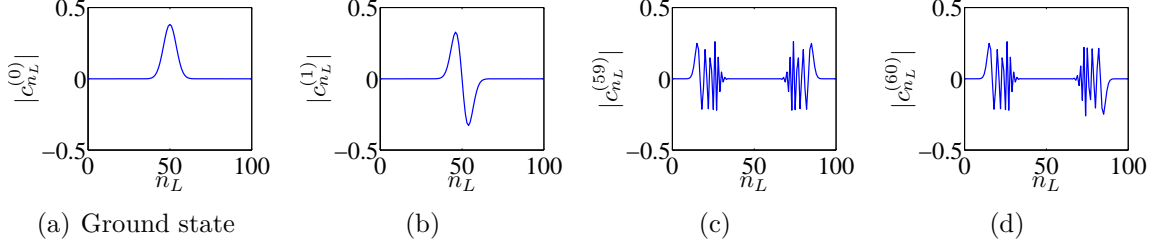


Figure 3.7. *Eigenstate amplitudes: Medium barrier.* Shown are the discrete probability amplitudes $c_{n_L}^{(k)}$ of the eigenstates $|\phi_k\rangle$ when $J/U = 10$, $\Delta V = 0$, and $N = 100$ for (a) the ground state, (b) the first excited state, (c) the 59th excited state, and (d) the 60th excited state. The lowest lying eigenstates are oscillator-like states. High-lying states occur in nearly degenerate pairs of partial cat-like states.

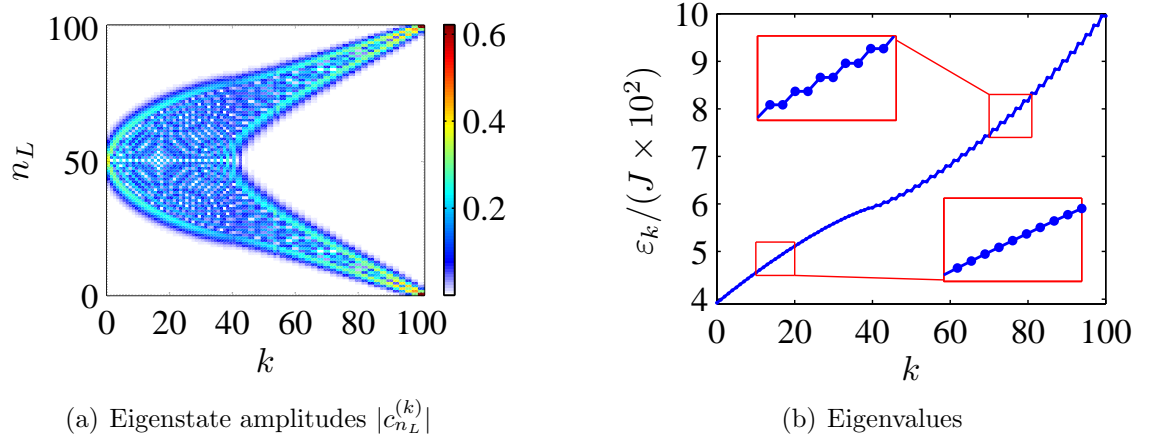


Figure 3.8. *Eigenstates and eigenvalues of the single-level Hamiltonian: Medium barrier.* (a) The eigenstate amplitudes $|c_{n_L}^{(k)}|$ of the Hamiltonian \hat{H} when $J/U = 10$, $\Delta V = 0$, and $N = 100$ are plotted for all values of n_L and k . Amplitude is indicated by the colorbar. A vertical cross section of this plot produces plots similar to Fig. 3.7. Low-lying states are oscillator-like whereas high-lying states are cat-like. The k axis is simply reversed when the interactions are attractive: $k \rightarrow N - k$ as $U \rightarrow -U$. (b) The eigenvalues ε_k of the same system as (a). The line serves as a guide to the eye. The eigenvalues display different dependence on k in the oscillator- and cat- like regions.

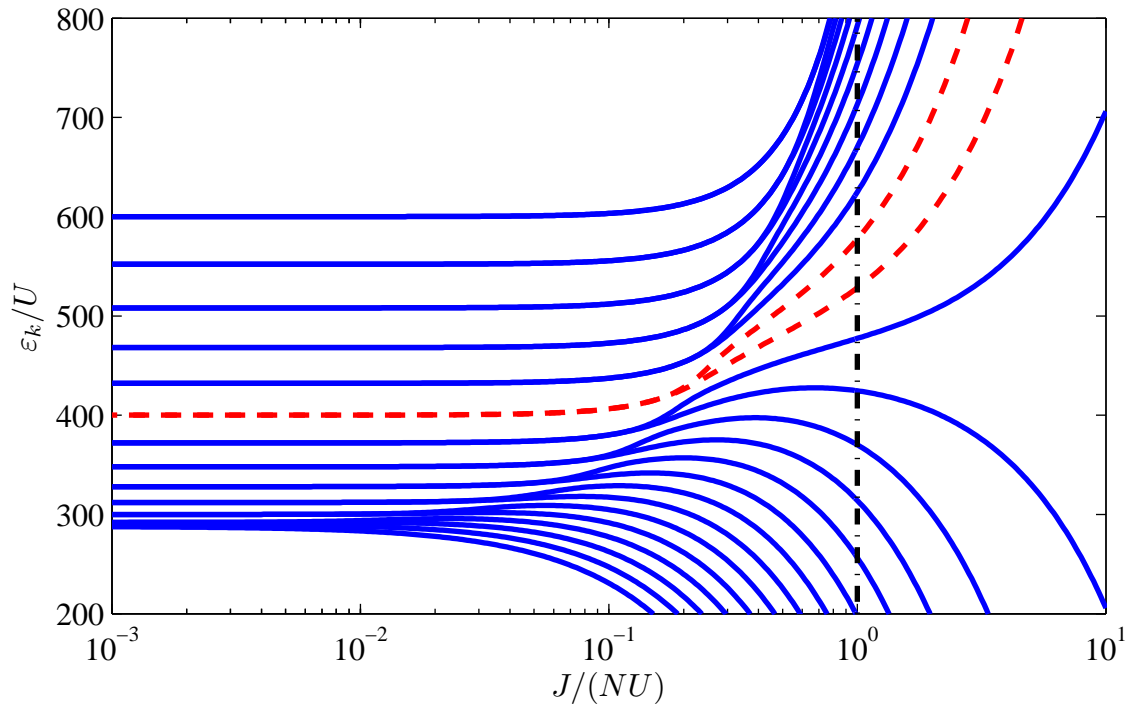


Figure 3.9. *Energy level diagram.* Energy eigenvalues versus J/NU for $N = 25$ particles. Energy is in units of U . When $J \ll |U|$, all the eigenvalues occur in nearly degenerate pairs corresponding to symmetric and antisymmetric pairs of entangled states. As J increases, the near degeneracies of the lowest lying states are lifted. However, the highly excited states are still cat-like provided $J \ll N|U|$. When $J \gtrsim N|U|$, there are no nearly degenerate pairs. All eigenstates are oscillator-like. Here the 14th and 15th energy eigenvalues are in red to assist identification of a nearly degenerate pair.

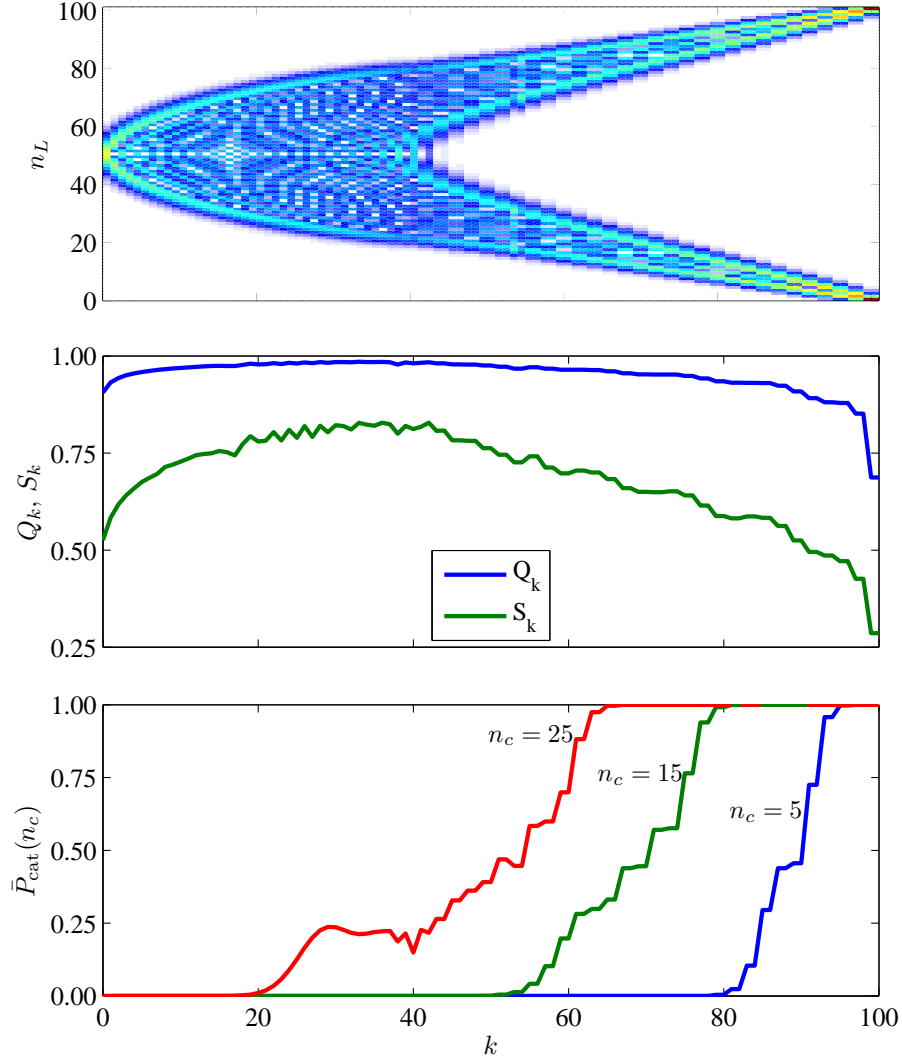


Figure 3.10. *Entanglement measures: Medium barrier.* Top panel: Shown are the probability amplitudes $|c_{n_L}^k|$ for all n_L and k for a system of $N = 100$ atoms in a symmetric double-well with $J/U = 10$. Middle panel: The impurity and the entropy of the k th excited state, denoted Q_k and S_k , respectively, versus k . The highest excited states are cat-like states. Cat-like eigenstates are less mixed and have a smaller impurity than oscillator-like states. Bottom panel: Plotted is $\bar{P}_{\text{cat}}(n_c)$ for $n_c = 5$ (blue), $n_c = 15$ (green), and $n_c = 25$ (red). This measure increases to unity in the cat-like region. Because the peaks of the cat-like states have a finite width, the rise to unity is not as sharp as in Figure 3.6.

with k . The peaks of the cat-like states have a finite width in this regime, as can be seen in Figures 3.7(c) and (d).

In Figure 3.9 the eigenvalues are plotted versus $J/N|U|$. When $J \ll |U|$, the eigenvalues occur in nearly degenerate pairs. As we have seen, the eigenstates are cat-like in this regime. As $J/N|U|$ increases, the degeneracies are lifted and oscillator-like states begin to emerge among the low lying states. When $J > N|U|$, all degeneracies have been lifted and oscillator-like states dominate the spectrum. Therefore, the highest lying states are cat-like when the condition $J \ll N|U|$ is met.

The impurity, entropy, and cat measure are plotted versus eigenstate label k in Figure 3.10. While both the impurity and the entropy behave differently in the oscillator- and cat-like regions, neither measure provides an obvious distinction between these two types of states. As expected, the cat measure is an excellent candidate for this purpose; states for which $\bar{P}_{\text{cat}}(n_c) \simeq 1$ are clearly cat-like, and oscillator-like states yield values of $\bar{P}_{\text{cat}}(n_c)$ significantly less than unity. Since the peaks of the cat-like states have a finite width in this regime, the rise to unity is not as abrupt as in the high barrier case (see Figure 3.6).

3.3.4 Potential Decoherence

Consider a symmetric potential, $\Delta V = 0$, with a high barrier, $J \ll |U|$. Because the level splitting between symmetric and antisymmetric pairs of cat-like states is so small, small perturbations can easily mix these states [45] and produce a localized state of the form $|n_L, N - n_L\rangle$. Indeed, entangled eigenstates are highly sensitive to tilt ΔV (see Appendix D). The probability densities of the localized eigenstates of a condensate in a slightly tilted potential are shown in Fig. 3.11(b). The entangled

eigenstates of Equation (3.18) are destroyed when

$$|\Delta V| \gtrsim \frac{2\Delta\varepsilon_{N-n_L}}{N-2n_L}, \quad (3.21)$$

where $\Delta\varepsilon_{N-n_L}$ is given by (3.19). Small imperfections in the external potential thus constitute a source of quantum decoherence, which is usually caused by coupling with an external system or thermal effects. In addition to dissipation and measurement, tilt therefore poses a further difficulty in the engineering of entangled states in experiments. Because condition (3.21) is minimized when $n_L = 0$, extreme Schrödinger cat states are the most sensitive to imperfections in the double-well, making them an unlikely candidate for experiments. Partial cat states, $n_L \neq 0$, on the other hand, are more robust with respect to tilt.

Despite their fragility, cat-like eigenstates reappear periodically for certain values of the tilt. These *tunneling resonances* occur when

$$\Delta V = \Delta V_p \equiv 2pU, \quad p \in \{1, 2, \dots, N-1\}. \quad (3.22)$$

While potential decoherence is caused by the slight misalignment of energy levels in the left and right wells, tunneling resonances occur when the potential difference can be exactly compensated by the repulsive (attractive) interaction of p particles in the lower (upper) well. To $(N-2n_L-p-1)$ th order in $J/|U|$, the energy eigenstates have the form

$$|\phi_{\pm}; n_L, p\rangle = \frac{1}{\sqrt{2}} (|n_L, N-n_L\rangle \pm |N-n_L-p, n_L+p\rangle), \quad (3.23)$$

where $0 \leq n_L < (N-p)/2$. The energy difference between the symmetric and anti-

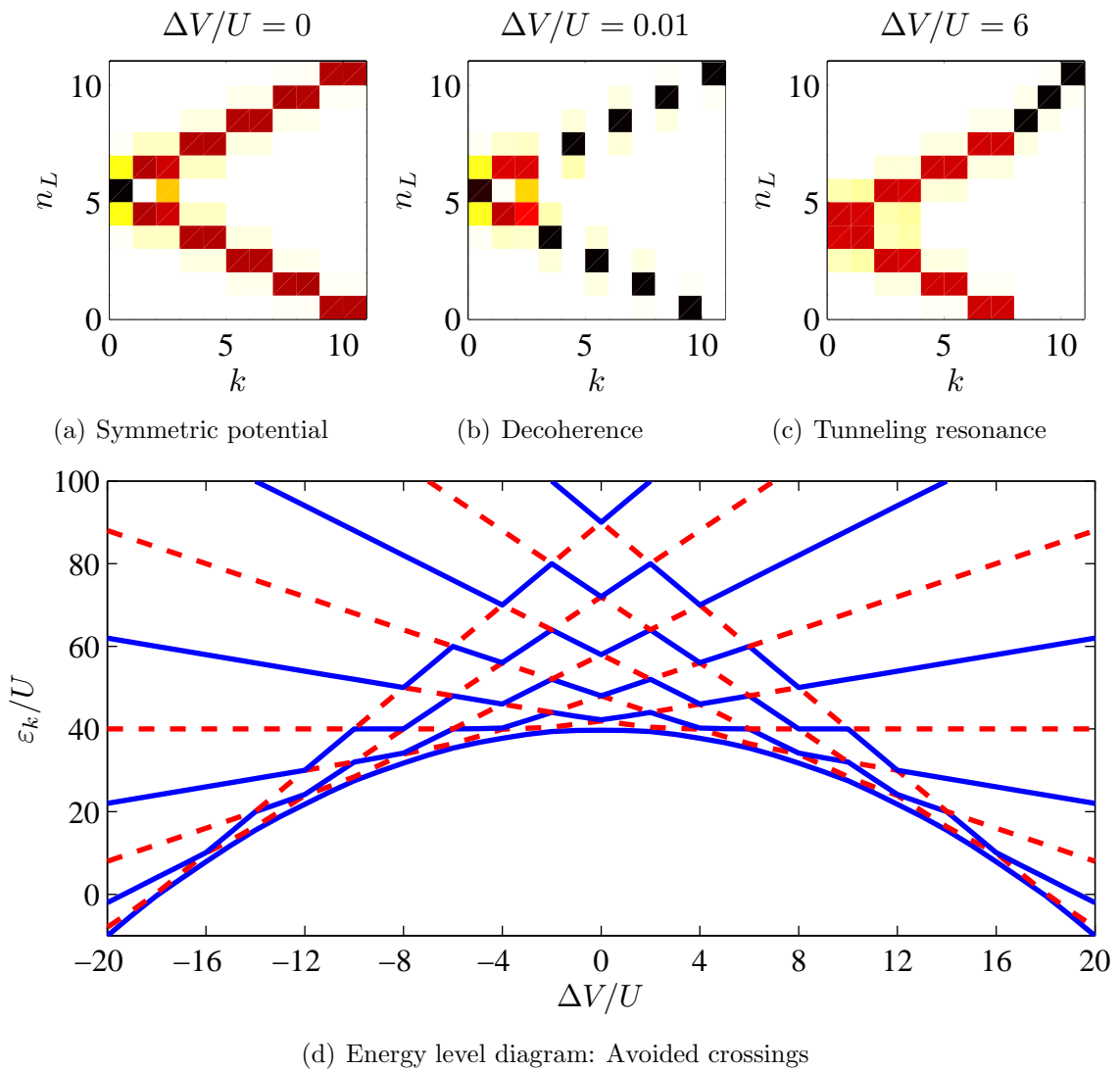


Figure 3.11. *Potential decoherence and tunneling resonances.* Eigenstate probability amplitudes for all eigenstates for $N = 10$, $J/U = 0.1$, and (a) $\Delta V/U = 0$, (b) $\Delta V/U = 10^{-2}$, and (c) $\Delta V/U = 6$. Here k is the eigenstate label, n_L is the number of particles in the left well, and the color indicates amplitude. The color bar is the same as in Figure 3.5(a). (b) The nearly degenerate pairs of entangled states are highly sensitive to tilt. (c) However, when $\Delta V = \Delta V_p \equiv 2pU$ the tilt is compensated by the interaction of p particles in the lower well and the lower entangled states reappear. (d) Avoided crossings in the energy eigenvalues indicate a reappearance of pairs of entangled eigenstates. The eigenvalues are shown alternatively in solid blue lines and dashed red lines to aid with visualization.

symmetric states $|\phi_{\pm}; n_L, p\rangle$ is $\Delta\varepsilon_{N-n_L}^p$. For the special case $n_L = 0$, the eigenstates are

$$|\phi_{\pm}; 0, p\rangle = \frac{1}{\sqrt{2}} (|0, N\rangle \pm |N-p, p\rangle), \quad (3.24)$$

with an energy splitting

$$\Delta\varepsilon_N^p = \frac{4U(J/2U)^{N-p}(N-p)}{(N-p-1)} \sqrt{\frac{N!}{p!(N-p)!}} \quad (3.25)$$

The reappearance of superposition states is shown in Figure 3.11(c) for $\Delta V = \Delta V_3$, i.e., $p = 3$. Because these states also occur in nearly degenerate pairs, the tunneling resonances are easily identified by avoided crossings in the energy eigenvalues, such as those displayed in Figure 3.11(d). The cat-like states (3.23) are destroyed when

$$|\Delta V - \Delta V_p| \gtrsim \frac{2\Delta\varepsilon_{N-n_L}^p}{N - 2n_L - p}. \quad (3.26)$$

A full discussion of potential decoherence and tunneling resonances can be found in Appendix C.

3.4 Dynamics: Quantum Sloshing

Quantum sloshing is the tunneling of all N atoms through the potential barrier. We consider the dynamics of a system in which all particles initially occupy the right well, i.e., $|\psi\rangle = |0, N\rangle$. This initial condition can be achieved experimentally by applying a positive tilt to the left well [34, 41]. At a later time $t > 0$, the system is described in the Schrödinger picture by the time-evolved state

$$|\psi(t)\rangle \equiv e^{-i\hat{H}t/\hbar}|\psi\rangle. \quad (3.27)$$

The probability of finding n_L particles in the left well at some time $t > 0$ is

$$P_{n_L}(t) \equiv |\langle n_L, N - n_L | \psi(t) \rangle|^2, \quad (3.28)$$

the average occupation of the left well is

$$\bar{n}_L(t) \equiv \langle \psi(t) | \hat{n}_L | \psi(t) \rangle, \quad (3.29)$$

and the average variance is

$$\sigma_{n_L}^2(t) \equiv \langle \psi(t) | \hat{n}_L^2 | \psi(t) \rangle - \bar{n}_L^2. \quad (3.30)$$

We will use $P_{n_L}(t)$, $\bar{n}_L(t)$, and $\sigma_{n_L}^2(t)$ to characterize the dynamics in three regimes: the non-interacting regime, $U = 0$; the low barrier regime, $J \gg N|U|$; and the high barrier regime, $J \ll |U|$.

3.4.1 Sloshing of Non-Interacting Bosons

We first consider the simple case of noninteracting particles, $U = 0$, in a symmetric potential, $\Delta V = 0$, to illustrate the problem. The probability of finding all particles in the right well, i.e., $n_L = 0$, is

$$P_0(t) = \cos^{2N}(Jt/\hbar). \quad (3.31)$$

The tunneling period is $T \equiv \pi\hbar/J$, which is independent of N . When $t = T/2$, the system is in state $|N, 0\rangle$ and all particles have tunneled into the left well. The average

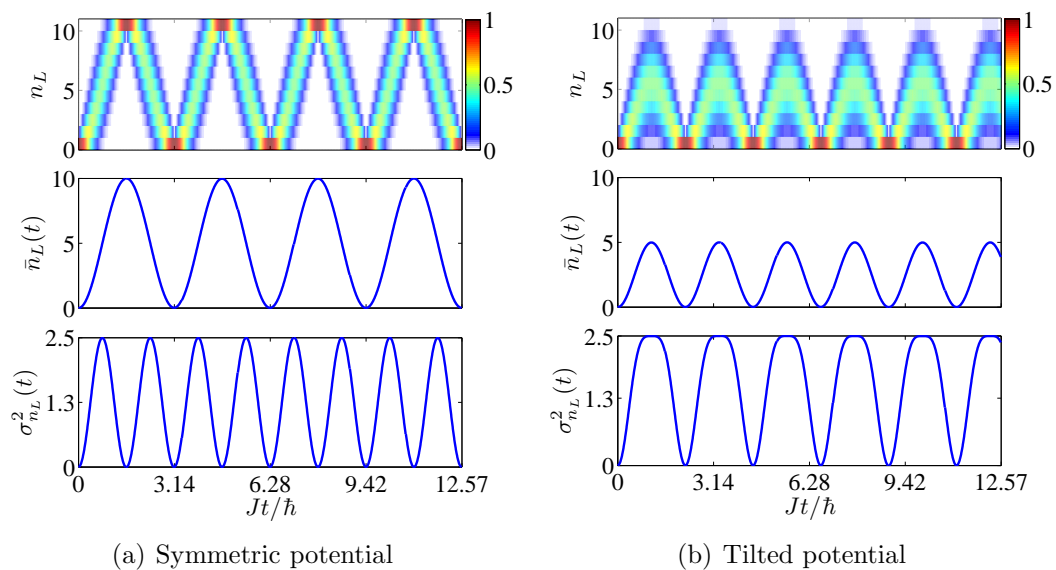


Figure 3.12. *Quantum sloshing of non-interacting bosons.* (a) Shown are the probability densities $P_{n_L}(t)$ for all number states when $N = 10$, $U = 0$, and $\Delta V = 2J$. Color indicates probability. Only $N/2 = 5$ particles tunnel between wells. (b) The tunneling amplitude and (c) the frequency of oscillation as a function of tilt. When $\Delta V > 2J\sqrt{N-1}$, tunneling is completely suppressed. Particles tunnel between wells faster in a tilted potential than in a symmetric potential.

occupation and variance of the left well are

$$\bar{n}_L(t) = N \sin^2(Jt/\hbar), \quad (3.32)$$

$$\sigma_{n_L}^2(t) = (N/4) \sin^2(2Jt/\hbar). \quad (3.33)$$

Equations (3.31) and (3.32) are proved in Appendix B and Equation (3.33) was obtained numerically. The probabilities $P_{n_L}(t)$ as well as the average occupation and variance, $\bar{n}_L(t)$ and $\sigma_{n_L}^2(t)$, are shown in Figure 3.12(a). The particles therefore tunnel sinusoidally between wells with a frequency $2J/\hbar$. The variance is greatest when $t = T/4$. At this time, the probability of finding n_L particles in the left well is

$$P_{n_L}(T/4) = \frac{1}{2^N} \frac{N!}{n_L!(N-n_L)!}. \quad (3.34)$$

The system is in a truncated coherent state, i.e., a binomial superposition of all number-states.

When $\Delta V \neq 0$, the occupation of the left well is

$$\bar{n}_L(t) = A \sin^2(\omega t/2), \quad (3.35a)$$

where the amplitude and frequency of oscillation are

$$A \equiv N/[1 + (\Delta V/2J)^2], \quad (3.35b)$$

$$\omega \equiv (2J/\hbar)\sqrt{1 + (\Delta V/2J)^2}. \quad (3.35c)$$

Equation (3.35) is proved for $N = 1$ in Appendix E and has been verified numerically for larger values of N . When $\Delta V = 2J$, only $N/2$ particles tunnel between wells. Figure 3.12(b) shows the probability densities $P_{n_L}(t)$, average number $\bar{n}_L(t)$,

and variance $\sigma_{n_L}^2(t)$ in this case. Tunneling between wells is completely suppressed when $|\Delta V| > 2J\sqrt{N-1}$. Tunneling is therefore highly sensitive to small tilt.

3.4.2 Modulated Oscillations in the Presence of a Low Barrier

We now turn our attention to the interacting case when the barrier is low, $J \gg N|U|$, in a symmetric potential, $\Delta V = 0$. Whereas a single frequency $2J/\hbar$ characterizes $\bar{n}_L(t)$ when $U = 0$, the average occupation of the left well approaches

$$\bar{n}_L(t) \rightarrow (N/2) [1 - \cos(2Jt/\hbar) \cos^{N-1}(Ut/\hbar)], \quad (3.36)$$

as $J/N|U| \rightarrow \infty$. Equation (3.36) is proved for $N = 2$ in Appendix E and has been verified numerically for larger values of N . Here the high frequency carrier depends only on the hopping strength J while the low frequency envelope depends on both the interaction potential U and the total number of particles N . The envelope reaches half its maximum value when

$$t = T_{1/2} \equiv (\hbar/|U|) \cos^{-1}[2^{-1/(N-1)}]. \quad (3.37)$$

At times $t \ll T_{1/2}$, all particles tunnel between wells with period T . At times near $T_{1/2}$, on the other hand, only half the particles tunnel between wells with period T . When $t \simeq 2T_{1/2}$, there is essentially no tunneling. Small interactions thus damp the oscillations between wells. However, tunneling revivals occur periodically with period $T_r \equiv \pi\hbar/U$. The first tunneling revival occurs when $|t - T_r| < T_{1/2}$. The separation of time scales, $T_{1/2} \ll T_r$, occurs only for $N \gg 1$, as evident in Eq. (3.37). The damping effect is shown in Figure 3.13.

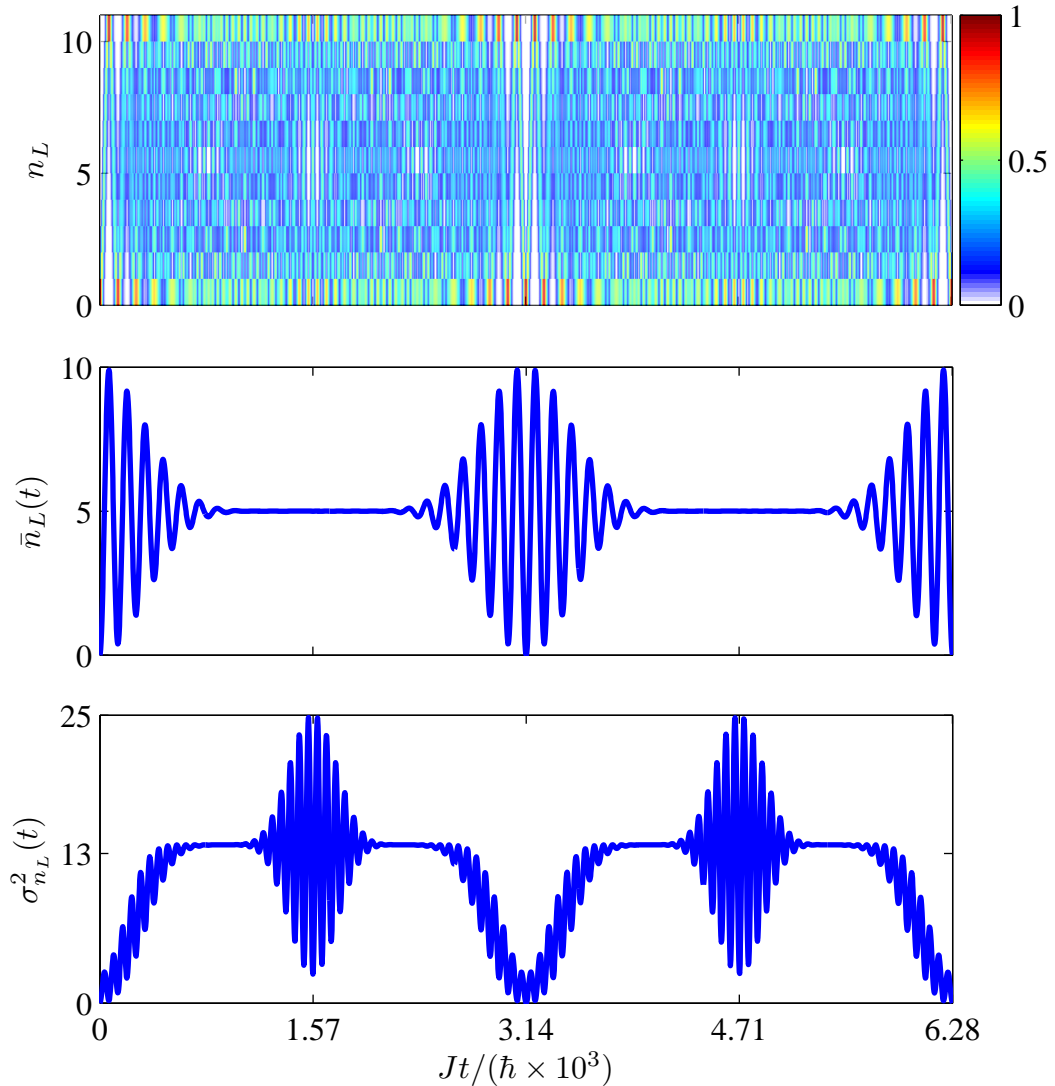


Figure 3.13. *Damped tunneling in the low barrier regime.* Top panel: Shown are the probability densities $P_{n_L}(t)$ for all number states when $N = 10$ and $J/NU = 100$. All particles tunnel between wells with period $T = \pi\hbar/J$ for times $t \ll T_{1/2}$. At later times, interactions cause the pattern to wash out. Middle panel: Average occupation of the left well $\bar{n}_L(t)$. Oscillations between wells are damped by atom-atom interactions. The first tunneling revival occurs when $t = T_r \equiv \pi\hbar/U$.

3.4.3 Ultra-slow Tunneling Through a High Barrier

For the remainder of our discussion, we turn to the high barrier limit, $J \ll |U|$, as it is key to the dynamic production of few-atom entangled states. We assume $U > 0$ without loss of generality with respect to the dynamics. In this regime, the two highest excited eigenstates are nearly-degenerate entangled cat states of the form $|\phi_{\pm}; 0\rangle \equiv (|N, 0\rangle \pm |0, N\rangle)/\sqrt{2}$ to lowest order in J/U . Because the initial state $|\psi(0)\rangle = (|\phi_+; 0\rangle - |\phi_-; 0\rangle)/\sqrt{2}$ is a superposition of two eigenstates, the dynamics are described by the two-state system. The characteristic frequency is $\omega_N = \Delta\varepsilon_N/\hbar$, where $\Delta\varepsilon_N$, given by Equation (3.20), is the energy difference of the states $|\phi_{\pm}; 0\rangle$. As $\Delta\varepsilon_N$ is a very small number, ω_N is also very small.

All particles occupy the right well with probability

$$P_0(t) = 1 - P_N(t) = \cos^2(\omega_N t/2), \quad (3.38)$$

In Fig. 3.14(a), we plot the probability densities $P_{n_L}(t)$ and the average occupation $\bar{n}_L(t)$ as a function of time. The tunneling period is $T_N \equiv 2\pi/\omega_N$. The average occupation and variance are

$$\bar{n}_L(t) = N \sin^2(\omega_N t/2), \quad (3.39)$$

$$\sigma_{n_L}^2(t) = (N^2/4) \sin^2(\omega_N t). \quad (3.40)$$

In this regime, as in the noninteracting case, all N particles oscillate sinusoidally between wells. There are two important differences. The first is that, when $J \ll U$, the period of oscillation depends on N and can become quite small for large values of N . Second, at time $t = T_N/4$, we find that $P_N = P_0 = 1/2$. At this time, all particles simultaneously occupy both wells and the system is described by an

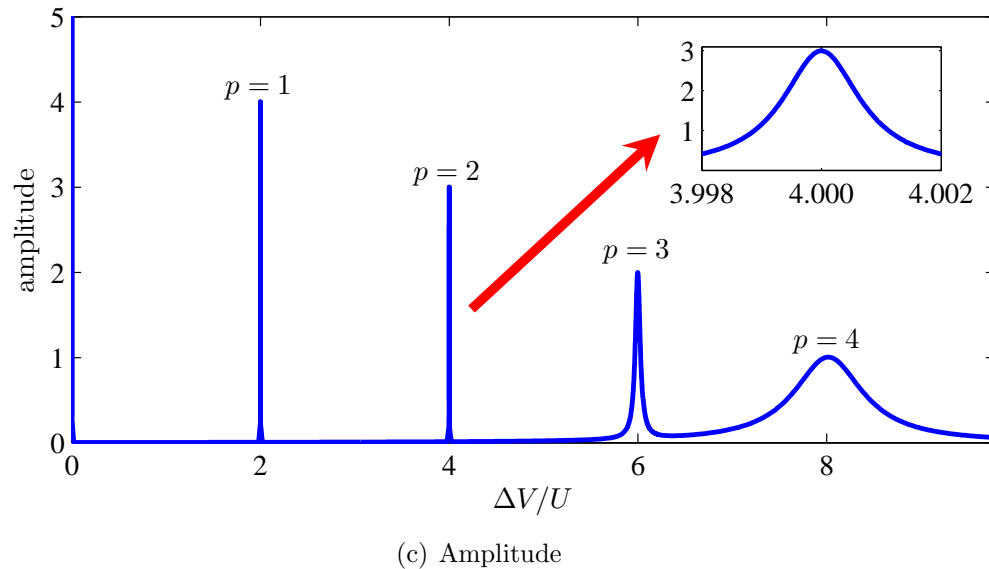
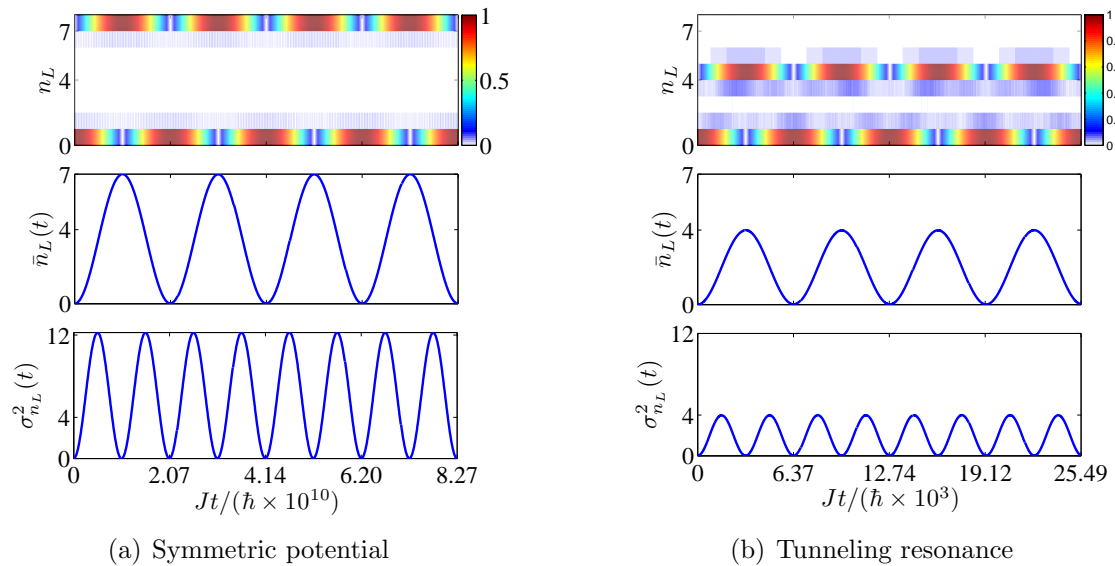


Figure 3.14. *Tunneling resonances in a few-atom system.* Shown are the probability densities $P_{n_L}(t)$ when $N = 7$ and $J/U = 0.1$, for (a) $\Delta V = 0$ and (b) $\Delta V = 6U$. (a) All particles tunnel between wells with period T_N . At time $t = T_N/4$, the system is described by a cat state. (b) Only $N - 3 = 4$ particles tunnel between wells. The oscillation frequency is 6 orders of magnitude faster than the symmetric case. (c) Tunneling amplitude as a function of tilt ΔV for $N = 5$ and $J/U = 0.1$. Tunneling resonances occur when $\Delta V = \Delta V_p \equiv 2pU$. At resonance, $N - p$ particles tunnel between wells. The insert is a zoom around $\Delta V/2U = 2$.

extreme Schrödinger cat-like state.

3.4.4 Tunneling Resonances

When the barrier is high, tunneling between wells is extremely sensitive to tilt ΔV because a small tilt causes the decoherence of the cat-like eigenstates. When $|\Delta V| \gtrsim 2\Delta\varepsilon_N/N$, the highest excited eigenstates become number states of the form $|0, N\rangle$ and $|N, 0\rangle$. In this case, the initial condition $|\psi(0)\rangle$ is stationary and tunneling between wells is therefore suppressed. Tunneling resonances occur when $\Delta V = \Delta V_p$. Then cat-like eigenstates reappear in the form $|\phi_{\pm}; 0, p\rangle \equiv (|N-p, p\rangle \pm |0, N\rangle) / \sqrt{2}$ and the two-state dynamics of the symmetric case are restored. At resonance, the tunneling frequency is $\omega_N^p = \Delta\varepsilon_N^p/\hbar$ where $\Delta\varepsilon_N^p$, given by Equation (3.25) is the level splitting between the states $|\phi_{\pm}; 0, p\rangle$. The average occupation of the left well is

$$\bar{n}_L(t) = (N-p) \sin^2(\omega_N^p t/2). \quad (3.41)$$

Here, $N-p$ particles tunnel between wells with period $T_N^p = 2\pi/\omega_N^p$. At time $t = T_N^p/2$, $N-p$ particles are in the left well. To compensate the tilt, p particles remain in the right well at all times. When $t = T_N^p/4$, the system is described by a partial cat state such that $P_p = P_0 = 1/2$. In Fig. 3.14(b) the tunneling dynamics for the second resonance, i.e., $p = 2$, are illustrated for a system of $N = 7$ particles. Near a resonance, tunneling is suppressed when $|\Delta V - \Delta V_p| \gtrsim 2\Delta\varepsilon_N^p/(N-p)$, as shown in Fig. 3.14(c). Note that tunneling resonances only occur for tilt applied to the left well.

Because $\Delta\varepsilon_N^p$ is greater than $\Delta\varepsilon_N$ by many orders of magnitude, tunneling near resonance is both much faster and less sensitive to tilt than tunneling in a symmetric potential. In Fig. 3.15(a), we show the symmetric tunneling period T_N versus N when

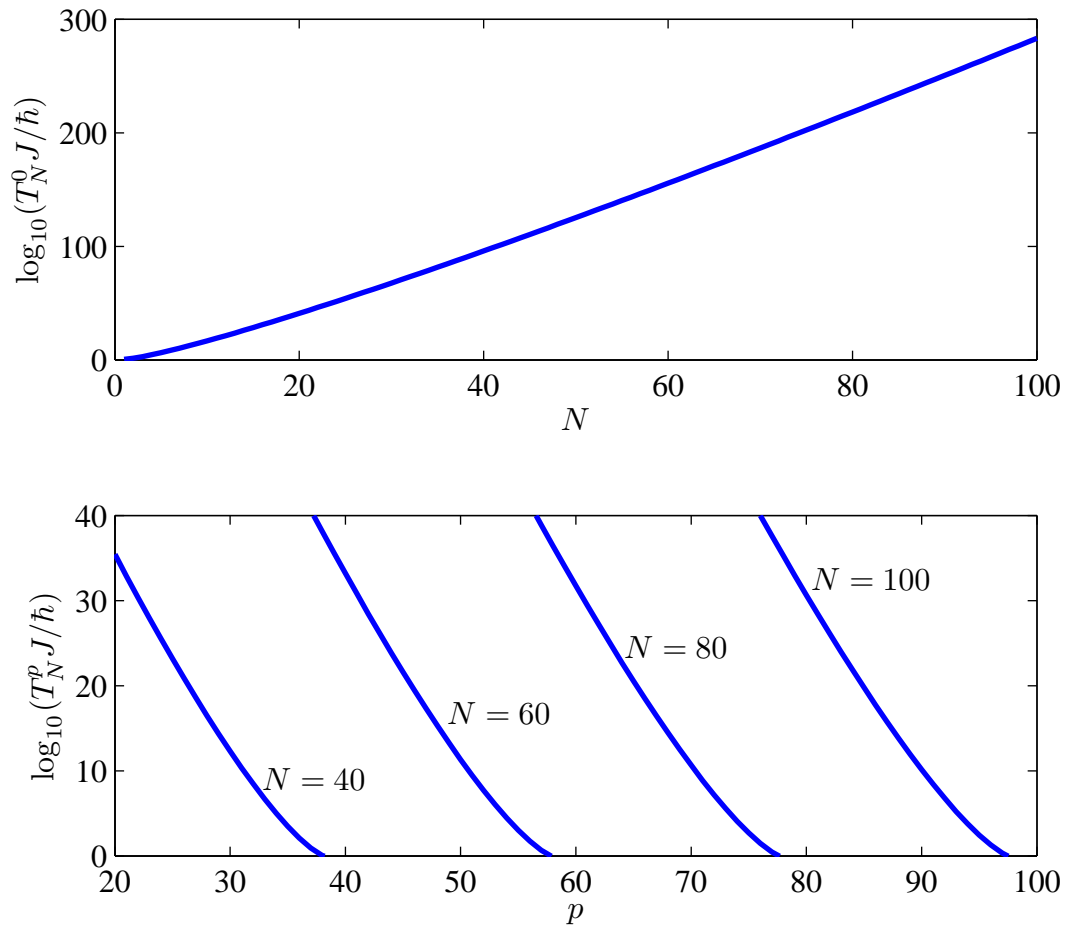


Figure 3.15. *Tunneling periods in a many-body system.* (a) Shown is the tunneling period T_N versus the total number of particles N when $J/U = 0.1$ and $\Delta V = 0$. For large N , tunneling becomes very slow. (b) At resonance, $\Delta V = \Delta V_p \equiv 2pU$, only $N - p$ particles tunnel between wells. Shown are the tunneling periods T_N^p versus p for $N = 40$ to 100 with $J/U = 0.1$. At resonance, the oscillations can be hundreds of orders of magnitude faster than in the symmetric case.

$J/U = 0.1$. Clearly, T_N becomes very long as N becomes large. For instance, consider a system of 200 ^{87}Rb atoms in typical symmetric, one-dimensional double-well trap used in experiments [19],

$$V_1(x) = -v_1 \cos^2(2kx) - v_2 \cos^4(kx - \pi/4), \quad kx \in [-\pi/4, 4\pi/4], \quad (3.42)$$

where $k = 2\pi/\lambda$, $\lambda = 810 \text{ nm}$ is the wavelength of the laser, $v_1 = v_2 = 153 \mu\text{K} \cdot k_B$ is the intensity of the laser, $\omega_\perp = 2\pi \times 91 \text{ Hz}$ is the transverse trapping frequency, and $a_s = 109 a_{\text{Bohr}}$ is the s -wave scattering length of the atoms. Under these conditions, $J/U = 0.0964$ (see Chapter 2) and all 200 atoms tunnel between wells with period $T_{200} = 1.15 \times 10^{635} \text{ ms}$. Furthermore, tunneling is completely suppressed for deviations in the tilt greater than $4.16 \times 10^{-636} \text{ nK} \cdot k_B$. Obviously, one does not expect to observe many-body tunneling in this regime. Under the same conditions, systems with as few as $N = 1, 2$, and 3 ^{87}Rb atoms yield tunneling times as long as $T_1 = 466 \text{ ms}$, $T_2 = 4840 \text{ ms}$, and $T_3 = 134000 \text{ ms}$, respectively. Even in a few-particle system, tunneling times can be prohibitively long.

However, tunneling at resonance can be hundreds of orders of magnitude faster than the symmetric case, as in Fig. 3.15(b). For the 200-atom system discussed above, when $p = 197$, we find that $N - p = 3$ particles tunnel between wells with period $T_{200}^{197} = 117 \text{ ms}$. This resonance occurs when $\Delta V = \Delta V_{197} = 210 \text{ nK} \cdot k_B$. A partial cat state of the form $|\psi\rangle = (|3, 197\rangle - i|0, 200\rangle)/\sqrt{2}$ will be realized at $T_{200}^{197}/4 = 29.25 \text{ ms}$. Likewise, we find that $T_{200}^{198} = 34.3 \text{ ms}$ and $T_{200}^{199} = 33.0 \text{ ms}$ when $\Delta V = \Delta V_{198} = 211 \text{ nK} \cdot k_B$ and $\Delta V_{199} = 212 \text{ nK} \cdot k_B$, respectively. At resonance, this system is sensitive to deviations in the tilt on the order of $0.273 \text{ nK} \cdot k_B$, $1.40 \text{ nK} \cdot k_B$, and $2.90 \text{ nK} \cdot k_B$ for $p = 197, 198$, and 199 , respectively. Thus, the observation of the tunneling of a few ^{87}Rb atoms is made possible by tunneling resonances in a

many-body system.

3.5 Summary

In summary, we used the one-level approximation to develop a Fock space picture of a system of ultracold bosons in a tilted two-well potential. We identified two categories of stationary states: harmonic oscillator-like states and Schrödinger cat-like states. Oscillator-like states dominate the spectrum when the barrier between wells is low. When the barrier is high, the stationary states are primarily cat-like. Both types of states exist when the interaction energy is on the order of the tunneling energy. In the case of repulsive interactions, the low-lying eigenstates are oscillator-like whereas high excited eigenstates are cat-like. The situation is reversed when the interactions are attractive.

Adaptations of two standard measures were used to characterize the entanglement of cat-like states: Meyer's impurity measure and the von Neumann entropy. While both measures yield nonzero values for cat-like states, neither is maximized for such states. Moreover, neither the impurity nor the entropy distinguish between cat-like states with different Fock-space peak separations. Therefore, the expectation value of a Schrödinger cat projection operator was used to provide additional characterization of the cat-like eigenstates. This new measure is maximized for cat-like states with a Fock-space peak separation greater than some prescribed value.

We also studied the quantum sloshing of bosons through the barrier. In the presence of a low barrier, atom-atom interactions damp tunneling between wells. Quantum revivals of tunneling occur periodically at times determined only by the interaction energy. In the high barrier limit, a small tilt causes the collapse of Schrödinger cat-like eigenstates and suppresses tunneling between wells, an effect we call potential

decoherence. However, unlike other forms of decoherence, tunneling resonances occur when the tilt can be exactly compensated by atom-atom interactions. At resonance, cat-like states reappear and a fraction of the atoms tunnel between wells. Resonant tunneling is much faster and less sensitive to tilt than in the symmetric case. Furthermore, tunneling resonances constitute a dynamic scheme for the production of few-atom superposition states in the presence of many bosons. Potential decoherence and tunneling resonances are our main contributions to the dynamics of the double-well system.

Chapter 4

TWO-LEVEL APPROXIMATION

In this chapter, we study the behavior of N ultracold bosons in a tilted, d -dimensional double-well potential in the two-level approximation. When the energy levels are weakly coupled by interactions, stationary states involving no occupation of the excited level closely resemble the eigenstates of the one-level Hamiltonian (see Chapter 3). However, eigenvalue crossings occur even when the energy levels are completely decoupled. These crossings are induced by the presence of the excited level and cannot be described by the one-level approximation. Stationary states which involve nonzero occupation of the excited level emerge among the lowest-lying eigenstates in the weak coupling regime.

4.1 Two-Level Hamiltonians

The two-level Hamiltonians \hat{H}_d for $d = 1, 2$, and 3 dimensions are

$$\hat{H}_1 = \hat{H}_1^A + \hat{H}_1^C + \hat{H}_1^{\text{coup}}, \quad (4.1a)$$

$$\hat{H}_2 = \hat{H}_2^A + \hat{H}_2^B + \hat{H}_2^{\text{coup}}, \quad (4.1b)$$

$$\hat{H}_3 = \hat{H}_3^A + \hat{H}_3^B + \hat{H}_3^C + \hat{H}_3^{\text{coup}}, \quad (4.1c)$$

where

$$\hat{H}_d^A = \hat{H}_d^{(0,0)} + E_d^0 \hat{N}^{(0,0)}, \quad (4.1d)$$

is the Hamiltonian for atoms occupying the lowest energy level,

$$\hat{H}_d^B = \hat{H}_d^{(1,-1)} + \hat{H}_d^{(1,1)} - J_d^{-11} \sum_{j \neq j'} \left\{ \hat{b}_j^{(1,-1)\dagger} \hat{b}_{j'}^{(1,+1)} + \text{h.c.} \right\} + E_d^1 \left(\hat{N}^{(1,1)} + \hat{N}^{(1,-1)} \right), \quad (4.1e)$$

is the Hamiltonian for atoms occupying the excited level with nonzero z angular momentum,

$$\hat{H}_d^C = \hat{H}_d^{(1,0)} + E_d^1 \hat{N}^{(1,0)}. \quad (4.1f)$$

is the Hamiltonian for atoms in the excited level with no angular momentum in the z direction, and

$$\hat{H}_d^{(\ell,m)} \equiv -J_d^{\ell|m|} \sum_{j \neq j'} \hat{b}_j^{(\ell,m)\dagger} \hat{b}_{j'}^{(\ell,m)} + U_d^{\ell|m|} \sum_j \hat{n}_j^{(\ell,m)} \left(\hat{n}_j^{(\ell,m)} - 1 \right) + \frac{\Delta V}{2} \left(\hat{n}_L^{(\ell,m)} - \hat{n}_R^{(\ell,m)} \right), \quad (4.1g)$$

is the one-level Hamiltonian with tilt. In a one-dimensional system, the coupling term is

$$\hat{H}_1^{\text{coup}} = 2U_1^{11} \sum_j \left\{ \sum_{\ell \neq \ell'} \left[\hat{n}_j^{(\ell,0)} \hat{n}_j^{(\ell',0)} \right] \right\} + U_1^{11} \sum_j \left\{ \left(\hat{b}_j^{(0,0)\dagger} \hat{b}_j^{(1,0)} \right)^2 + \text{h.c.} \right\}, \quad (4.1h)$$

in two dimensions, the coupling is given by

$$\begin{aligned} \hat{H}_2^{\text{coup}} = & 2U_2^{11} \sum_j \left\{ \sum_{(\ell,m) \neq (\ell',m')} \left[\hat{n}_j^{(\ell,m)} \hat{n}_j^{(\ell',m')} \right] \right\} \\ & + 2U_2^{11} \sum_j \left\{ \left(\hat{b}_j^{(0,0)\dagger} \right)^2 \hat{b}_j^{(1,-1)} \hat{b}_j^{(1,+1)} + \text{h.c.} \right\}, \end{aligned} \quad (4.1i)$$

and the coupling has the form

$$\begin{aligned} \hat{H}_3^{\text{coup}} = & 2U_3^{11} \sum_j \left\{ \sum_{(\ell,m) \neq (\ell',m')} \left[\epsilon_{\ell m}^{\ell' m'} \hat{n}_j^{(\ell,m)} \hat{n}_j^{(\ell',m')} \right] \right\} \\ & + U_3^{11} \sum_j \left\{ \left(\hat{b}_j^{(0,0)\dagger} \hat{b}_j^{(1,0)} \right)^2 + \left[2 \left(\hat{b}_j^{(0,0)\dagger} \right)^2 + \left(\hat{b}_j^{(1,0)\dagger} \right)^2 \right] \hat{b}_j^{(1,-1)} \hat{b}_j^{(1,+1)} + \text{h.c.} \right\}, \end{aligned} \quad (4.1j)$$

in three dimensions. The element $\epsilon_{\ell m}^{\ell' m'}$ is defined by

$$\epsilon_{\ell m}^{\ell' m'} \equiv \begin{cases} 1/2, & \ell = \ell' = |m + m'| = 1 \\ 1, & \text{otherwise} \end{cases}, \quad (4.1k)$$

and $\hat{N}^{(\ell,m)} \equiv \hat{n}_L^{(j,m)} + \hat{n}_R^{(j,m)}$. Equation (4.1) was derived in Chapter 2, and the one-level Hamiltonian (4.1g) was studied in Chapter 3. For convenience, the discussion from Chapter 2 concerning the two-level Hamiltonian is repeated here.

Recall that $d \in \{1, 2, 3\}$ is the dimensionality of the trapping potential, $j \in \{L, R\}$ is the well index, $\ell \in \{0, 1\}$ is the level index, and m is the z -angular momentum index. The allowed values of m depend on both ℓ and d . The hopping strengths $J_d^{\pm\ell|m|}$ and the interaction energies $U_d^{\ell|m|}$ satisfy

$$J_d^{00} \ll J_d^{-11} < J_d^{10} < J_d^{11} \ll \Delta E_d^{10} \quad \text{and} \quad U_d^{00} = (4/3)U_d^{10} = 2U_d^{11}, \quad (4.2)$$

An arbitrary state vector in Fock space has the form

$$|\Psi_d\rangle = \sum_{n_d=0}^{\Omega_d-1} c_{n_d} |n_d\rangle, \quad |n_d\rangle = \bigotimes_{\ell,m} |n_L^{(\ell,m)}, n_R^{(\ell,m)}\rangle_{(\ell,m)}, \quad (4.3)$$

where n_d is called the *Fock space label* and $n_j^{(\ell,m)}$ represents the number of atoms in the ℓ th energy level of the j th well with z angular momentum $m\hbar$. Here Ω_d is size of the Hilbert space $\{|n_d\rangle\}$. We require the total number of particles $N = \sum_{j,\ell,m} n_j^{(\ell,m)}$ to be constant. Under this restriction, the size of the Hilbert space is given by

$$\Omega_d = \frac{(N + 2d + 1)!}{N!(2d + 1)!}. \quad (4.4)$$

For large N , the multiplicity Ω_d scales like N^{2d+1} .

4.2 Counting Fock States

The Hamiltonian \hat{H}_d , given by Equation (4.1), can be represented as an $\Omega_d \times \Omega_d$ matrix H_d with elements

$$(H_d)_{n_d n'_d} = \langle n_d | \hat{H}_d | n'_d \rangle, \quad (4.5)$$

where the Fock states $|n_d\rangle$ and $|n'_d\rangle$ are given by Equation (4.3). In order to compute the matrix elements $(H_d)_{n_d n'_d}$, we must choose an indexing of Fock space.

We choose the Fock space label $0 \leq n_d \leq \Omega_d - 1$ to increase with increasing number of particles in the left well and increasing number of particles in the excited energy level. Given $n_j^{(\ell,m)}$, the Fock space label n_d in $d = 1, 2$, and 3 dimensions is

given by

$$n_1 = n_L^{(0,0)} + (N^0 + 1)n_L^{(1,0)} + \frac{1}{6}N^1(N^1 + 1)(3N - 2N^1 + 5), \quad (4.6a)$$

$$\begin{aligned} n_2 = & n_L^{(0,0)} + \frac{1}{6}N_L^1(N_L^1 + 1)(N^0 + 1)(3N^1 - 2N_L^1 + 5) \\ & + (N^0 + 1)(N_R^1 + 1)n_L^{(1,+1)} + (N^0 + 1)n_R^{(1,+1)} \\ & + \frac{1}{120}N^1(N^1 + 1)(N^1 + 2)(N^1 + 3)(5N - 4N^1 + 9), \end{aligned} \quad (4.6b)$$

$$\begin{aligned} n_3 = & n_L^{(0,0)} + \frac{1}{2}(N^0 + 1)(N_R^1 + 1)(N_R^1 + 2)n_L^{(1,0)} + (N^0 + 1)n_L^{(1,0)} \\ & + \frac{1}{120}N_L^1(N_L^1 + 1)(N_L^1 + 2)(N^0 + 1) [10(N^1)^2 - 15(N_L^1 - 3)N^1 \\ & + 6(N_L^1)^2 - 33N_L^1 + 47] - \frac{1}{2}(N^0 + 1)(-2N_R^1 + n_R^{(1,-1)} - 3)n_R^{(1,-1)} \\ & - \frac{1}{4}(N^0 + 1)(-2N_L^1 + n_L^{(1,-1)} - 3)(N_R^1 + 1)(N_R^1 + 2)n_L^{(1,-1)} \\ & - \frac{1}{5040}N^1 [(N^1)^5 + 15(N^1)^4 + 85(N^1)^3 + 225(N^1)^2 + 274N^1 \\ & + 120] (6N^1 - 7N - 13), \end{aligned} \quad (4.6c)$$

where $N_j^1 = \sum_m n_j^{(1,m)}$ for $j \in \{L, R\}$, $N^1 = N_L^1 + N_R^1$, and $N^0 = N - N^1$. If there are no atoms in the excited level, i.e., $N^1 = 0$, then $n_d = n_L^{(0,0)}$. Thus, the one-level approximation can be reproduced by truncating the dimensionality of the Fock space to $N + 1$. Algorithms for generating the matrix representation (4.5) are presented in Appendix F.

4.3 Characterization of Stationary States

The energy levels are coupled by the interaction energy U_d^{11} . Energy levels only become completely decoupled when $U_d^{11} = 0$, but the effects of coupling are negligible for $N|U_d^{00}| \ll 2\Delta E_d^{10}$. In the weak coupling regime, the stationary states of the Hamiltonian (4.1) have definite occupation of each energy level and states with no occupation of the excited level are well described by the one-level approximation. Although the energy levels are weakly coupled, eigenvalue crossings are induced by the presence of the excited level when either the number of particles or the interaction energy is greater than some critical value.

Eigenvalue crossings involving the ground state energy occur when $|U_d^{00}| > 0$. Such crossings in the double-well system, which is a finite lattice, provide evidence for the possibility of quantum phase transitions in the limit of an infinite lattice [17], as discussed in Chapter 1. Moreover, we are interested in describing cat-like states which are typically excited eigenstates. Therefore, a characterization of eigenvalue crossings of energies other than the ground state are also relevant.

4.3.1 Eigenvalue Crossings: Decoupled Energy Levels

Consider a system of non-interacting bosons, $U_d^{\ell|m|} = 0$, in a symmetric potential, $\Delta V = 0$. In the non-interacting regime, the Hamiltonians \hat{H}_d reduce to

$$\hat{H}_1 = \hat{H}_1^A + \hat{H}_1^C, \quad \hat{H}_2 = \hat{H}_2^A + \hat{H}_2^B, \quad \text{and} \quad \hat{H}_3 = \hat{H}_3^A + \hat{H}_3^B + \hat{H}_3^C, \quad (4.7a)$$

where

$$\hat{H}_d^A = -J_d^{00} \sum_{j \neq j'} \hat{b}_j^{(0,0)\dagger} \hat{b}_{j'}^{(0,0)} + E_d^0 \hat{N}^{(0,0)}, \quad (4.7b)$$

$$\begin{aligned} \hat{H}_d^B = & -J_d^{11} \sum_{j \neq j'} \left\{ \hat{b}_j^{(1,1)\dagger} \hat{b}_{j'}^{(1,1)} + \hat{b}_j^{(1,-1)\dagger} \hat{b}_{j'}^{(1,-1)} \right\} \\ & - J_d^{-11} \sum_{j \neq j'} \left\{ \hat{b}_j^{(1,-1)\dagger} \hat{b}_{j'}^{(1,+1)} + \text{h.c.} \right\} + E_d^1 \left(\hat{N}^{(1,1)} + \hat{N}^{(1,-1)} \right), \end{aligned} \quad (4.7c)$$

$$\hat{H}_d^C = -J_d^{10} \sum_{j \neq j'} \hat{b}_j^{(1,0)\dagger} \hat{b}_{j'}^{(1,0)} + E_d^1 \hat{N}^{(1,0)}. \quad (4.7d)$$

Clearly, \hat{H}_d is separable and the eigenstates of \hat{H}_d are therefore direct products of the eigenstates of the Hamiltonians \hat{H}_d^A , \hat{H}_d^B , and \hat{H}_d^C .

Since the Hamiltonians $\hat{H}_d^{A,C}$ are non-interacting one-level Hamiltonians, the eigenstates are given by

$$|\phi_k; N\rangle_A = \sum_{n_L=0}^N A_k H_k(n_L|N) \sqrt{P_{1/2}(n_L|N)} |n_L, N - n_L\rangle_{(0,0)}, \quad (4.8)$$

$$|\phi_k; N\rangle_C = \sum_{n_L=0}^N A_k H_k(n_L|N) \sqrt{P_{1/2}(n_L|N)} |n_L, N - n_L\rangle_{(1,0)}, \quad (4.9)$$

with corresponding energy eigenvalues

$$\varepsilon_k^{A,d}(N) = -J_d^{00} (N - 2k) + E_d^0 N, \quad (4.10)$$

$$\varepsilon_k^{C,d}(N) = -J_d^{10} (N - 2k) + E_d^1 N, \quad (4.11)$$

for $0 \leq k \leq N$. Here A_k is a constant of normalization, $H_k(n_L|N)$ is a k th order discrete Hermite polynomial, and $P_{1/2}(n_L|N)$ is the binomial distribution (see

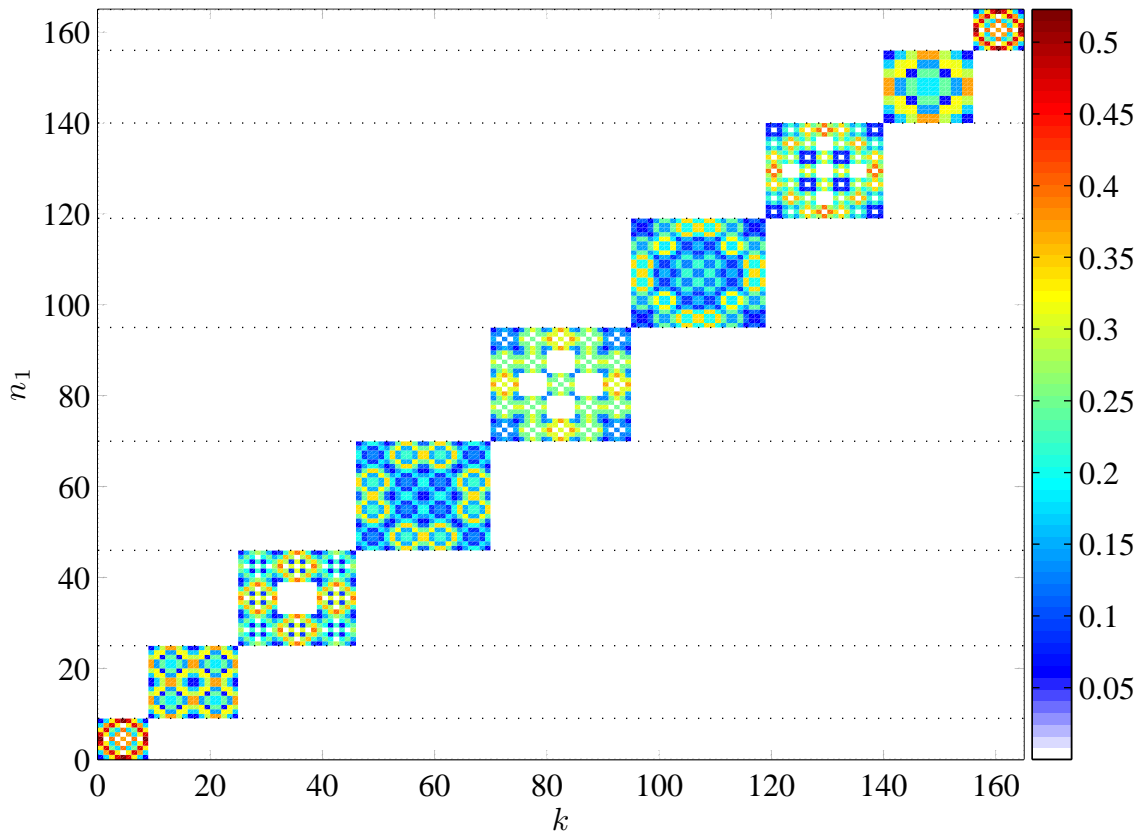


Figure 4.1. *Eigenstate amplitudes: Non-interacting case.* Shown are the eigenstate amplitudes $|c_{n_1}^{(k)}|$ for all values of $n_1, k \in \{0, 1, \dots, \Omega_1 - 1\}$ when $U_1^{00} = 0$, $J_1^{00}/\Delta E_1^{10} \approx 4 \times 10^{-7}$, $J_1^{10}/\Delta E_1^{10} \approx 3 \times 10^{-5}$, and $N = 8$. The number-state label n_1 increases with increasing number of atoms in the excited energy level. For a given value of n_1 , the number of atoms in the excited energy level is equal to the number of dotted horizontal lines below n_1 . The eigenstate label k increases with increasing energy. Eigenstates are grouped according to occupation of the excited level. The $N + 1$ lowest lying states, corresponding to zero occupation of the excited level, are in exact agreement with the harmonic oscillator-like eigenstates of the one-level Hamiltonian (see Chapter 3). The magnitude of $|c_{n_1}^{(k)}|$ is indicated by the colorbar.

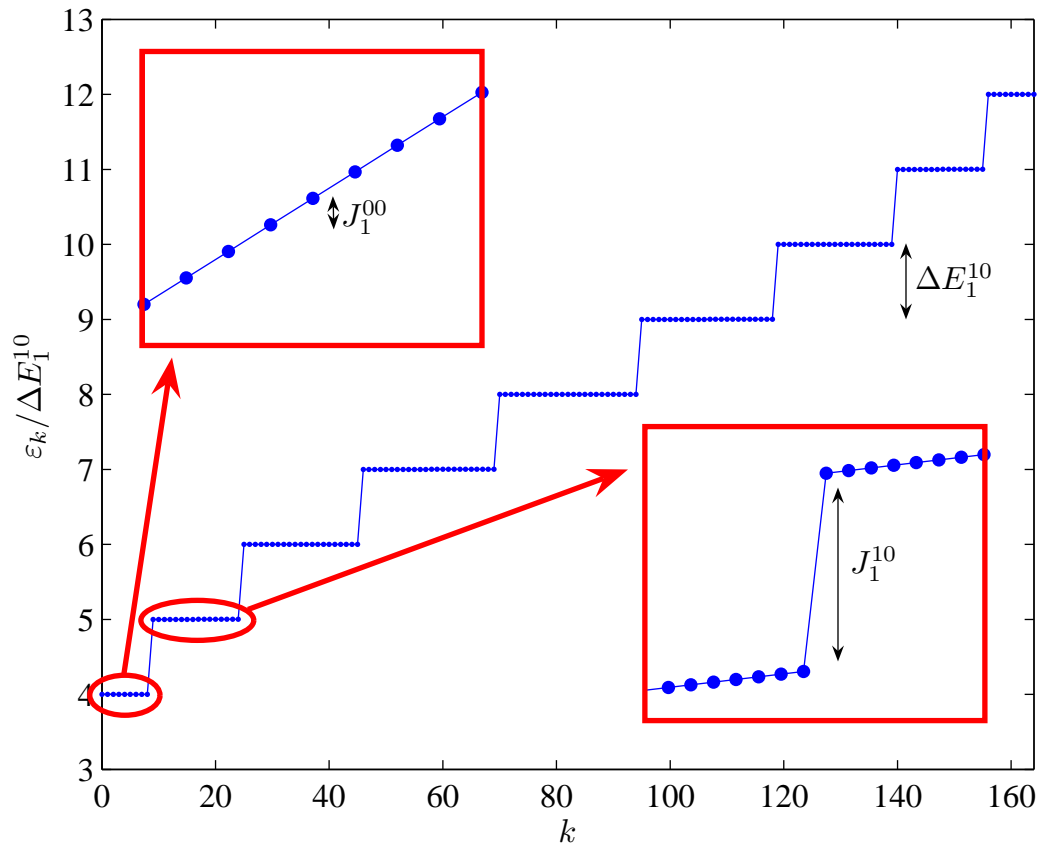


Figure 4.2. *Energy eigenvalues: Non-interacting case.* Shown are the energy eigenvalues ε_k for the same system as in Figure 4.1. The line is a guide to the eye. Eigenvalues occur in groups corresponding to occupation of the excited level. Whereas the energy difference between eigenvalues in the same group is on the order of J_1^{00} and J_1^{10} , the energy difference between groups is on the order of ΔE_1^{10} . The $N + 1$ lowest lying eigenvalues vary linearly in k and are in exact agreement with results from the one-level approximation. The inserts are zooms of the two lowest groups of eigenvalues. Eigenvalue crossings occur when $N > N_1^{\text{crit}}$ because the spread in energy of eigenvalues within each group is large enough to overcome the energy difference ΔE_1^{10} .

Appendix B). The eigenstates of \hat{H}_d^B satisfy

$$\hat{H}_d^B |\phi_k; N\rangle_B = \varepsilon_k^{B,d}(N) |\phi_k; N\rangle_B, \quad (4.12)$$

for $0 \leq k \leq \Omega_1(N) - 1$.

In one dimension, the eigenstates of \hat{H}_1 are given by

$$\hat{H}_1 |\phi_k; N^0\rangle_A \otimes |\phi_{k'}; N^1\rangle_C = \left[\varepsilon_k^{A,1}(N^0) + \varepsilon_{k'}^{C,1}(N^1) \right] |\phi_k; N^0\rangle_A \otimes |\phi_{k'}; N^1\rangle_C, \quad (4.13)$$

for $0 \leq k \leq N^0$ and $0 \leq k' \leq N^1$. Here N^0 and N^1 represent the number of particles in the lowest and excited energy levels, respectively. We require that $N^0 + N^1 = N$, where N is the total number of atoms in the system. Likewise, in two dimensions, we have

$$\hat{H}_2 |\phi_k; N^0\rangle_A \otimes |\phi_{k'}; N^1\rangle_B = \left[\varepsilon_k^{A,2}(N^0) + \varepsilon_{k'}^{B,2}(N^1) \right] |\phi_k; N^0\rangle_A \otimes |\phi_{k'}; N^1\rangle_B, \quad (4.14)$$

for $0 \leq k \leq N^0$ and $0 \leq k' \leq \Omega_1(N^1)$. Again, we impose the constraint $N^0 + N^1 = N$. The eigenstates of the three-dimensional Hamiltonian are given by

$$\begin{aligned} \hat{H}_3 |\phi_k; N^0\rangle_A \otimes |\phi_{k'}; N^B\rangle_B \otimes |\phi_{k''}; N^C\rangle_C \\ = \left[\varepsilon_k^{A,3}(N^0) + \varepsilon_{k'}^{B,3}(N^B) + \varepsilon_{k''}^{C,3}(N^C) \right] |\phi_k; N^0\rangle_A \otimes |\phi_{k'}; N^B\rangle_B \otimes |\phi_{k''}; N^C\rangle_C, \end{aligned} \quad (4.15)$$

for $0 \leq k \leq N^0$, $0 \leq k' \leq \Omega_1(N^B)$, and $0 \leq k'' \leq N^C$. Here $N^1 = N^B + N^C$ represents the number of particles in the excited level.

When $N^0 = N$, all atoms occupy the lowest energy level in each well and the eigenstates and eigenvalues are successfully predicted by the one-level approximation.

The ground state is

$$|g_d\rangle = \frac{1}{2^{N/2}} \sum_{n_L=0}^N \sqrt{\frac{N!}{n_L!(N-n_L)!}} |n_L, N-n_L\rangle_{(0,0)} \bigotimes_m |0, 0\rangle_{(1,m)}, \quad (4.16)$$

with energy

$$\varepsilon_{g_d} = \varepsilon_0^{A,d}(N) = N(-J_d^{00} + E_d^0). \quad (4.17)$$

For small N , the eigenvalues of \hat{H}_d are grouped according to occupation of the excited level. Within each group, eigenvalues are separated by an energy difference on the order of $J_d^{\pm\ell|m|}$ whereas successive groups are separated by the level spacing $\Delta E_d^{10} \gg J_d^{\pm\ell|m|}$. In this case, the eigenstates corresponding to $N^0 = N$ compose the $N + 1$ lowest-lying states as can be seen in Figures 4.1 and 4.2 for a system of $N = 8$ non-interacting atoms in a 1D trap.

However, if N is sufficiently large, the energy difference between groups can become quite small. Consider the case $N^0 = N$, that is, all atoms occupy the lowest energy level in each well. The state

$$|\phi_d^{\max}; N^0 = N\rangle = |\phi_N; N\rangle_A \bigotimes_m |0, 0\rangle_{(1,m)}, \quad (4.18)$$

with eigenvalue

$$\varepsilon_d^{\max} = \varepsilon_N^{A,d}(N) = N(J_1^{00} + E_1^0), \quad (4.19)$$

has the highest energy of all states corresponding to $N^0 = N$. Next suppose a single atom occupies the excited energy level, that is, $N^1 = 1$. In one dimension, $d = 1$, the state

$$|\phi_1^{\min}; N^1 = 1\rangle = |\phi_0; N-1\rangle_A \otimes |\phi_0; 1\rangle_C, \quad (4.20)$$

with eigenvalue

$$\varepsilon_1^{\min} = \varepsilon_0^{A,1}(N-1) + \varepsilon_0^{C,1}(1) = (N-1)(-J_1^{00} + E_1^0) - J_1^{10} + E_1^1, \quad (4.21)$$

has the lowest energy of all states corresponding to $N^1 = 1$. The eigenvalues ε_1^{\max} and ε_1^{\min} are exactly equal to each other and the system undergoes an eigenvalue crossing when the condition

$$N = \frac{1}{2} + \frac{\Delta E_1^{10} - J_1^{10}}{2J_1^{00}}, \quad (4.22)$$

is met. Define N_1^{crit} by

$$N_1^{\text{crit}} = \left\lfloor \frac{1}{2} + \frac{\Delta E_1^{10} - J_1^{10}}{2J_1^{00}} \right\rfloor. \quad (4.23)$$

Then eigenvalue crossings occur in states involving no occupation of the excited level, i.e., in the lowest group of eigenvalues, when

$$N > N_1^{\text{crit}}. \quad (4.24)$$

Because J_1^{00} and J_1^{10} are many orders of magnitude smaller than ΔE_1^{10} , the critical value N_1^{crit} is quite large.

In two and three dimensions, the states

$$|\phi_2^{\min}; N^1 = 1\rangle = |\phi_0; N-1\rangle_A \otimes |\phi_0; 1\rangle_B, \quad (4.25)$$

$$|\phi_3^{\min}; N^1 = 1\rangle = |\phi_0; N-1\rangle_A \otimes |\phi_0; 1\rangle_B \otimes |0, 0\rangle_{(1,0)}, \quad (4.26)$$

with corresponding energy eigenvalues

$$\varepsilon_2^{\min} = \varepsilon_0^{A,2}(N-1) + \varepsilon_0^{B,2}(1), \quad (4.27)$$

$$\varepsilon_3^{\min} = \varepsilon_0^{A,3}(N-1) + \varepsilon_0^{B,3}(1), \quad (4.28)$$

have the lowest energy of all states corresponding to $N^1 = 1$. Here

$$\begin{aligned} |\phi_0; 1\rangle_B = & \frac{1}{2} \left[(|1, 0\rangle_{(1,-1)} + |0, 1\rangle_{(1,-1)}) \otimes |0, 0\rangle_{(1,1)} \right. \\ & \left. + |0, 0\rangle_{(1,-1)} \otimes (|1, 0\rangle_{(1,1)} + |0, 1\rangle_{(1,1)}) \right], \end{aligned} \quad (4.29)$$

is the ground state of \hat{H}_d^B and

$$\varepsilon_0^{B,d} = -J_d^{-11} - J_d^{11} + E_d^1, \quad (4.30)$$

is the energy of the ground state for $N^B = 1$. Thus, eigenvalue crossings occur among the lowest lying states in two and three dimensional systems when

$$N > N_d^{\text{crit}} = \left\lfloor \frac{1}{2} + \frac{\Delta E_d^{10} - J_d^{-11} - J_d^{11}}{2J_d^{00}} \right\rfloor, \quad (4.31)$$

for $d \in \{2, 3\}$. Recall that

$$J_d^{00} = J_1^{00}, \quad J_d^{\pm 11} = (J_1^{10} \pm J_1^{00})/2, \quad J_3^{10} = J_1^{00}, \quad \text{for } d \in \{2, 3\}, \quad (4.32)$$

which was derived in Chapter 2. This implies that

$$N_d^{\text{crit}} = \left\lfloor \frac{1}{2} + \frac{\Delta E_d^{10} - J_1^{10}}{2J_1^{00}} \right\rfloor, \quad (4.33)$$

for $d \in \{1, 2, 3\}$.

Many eigenvalue crossings occur in the non-interacting two-level system. In one-dimension, this happens whenever

$$\varepsilon_k^{A,1}(N^0) + \varepsilon_{k'}^{C,1}(N - N^0) = \varepsilon_q^{A,1}(M^0) + \varepsilon_{q'}^{C,1}(N - M^0), \quad (4.34)$$

where $0 \leq k \leq N^0$, $0 \leq k' \leq N - N^0$, $0 \leq q \leq M^0$, $0 \leq q' \leq N - M^0$ and $\varepsilon_k^\ell(N^\ell)$ is given by Equation (4.10). However, the ground state (4.16) will never undergo a crossing. Setting $N^0 = N$ and $k = k' = 0$, Equation (4.34) yields

$$-2(J_1^{00}q + J_1^{10}q') = (N - M^0)(\Delta E_1^{10} + J_1^{00} - J_1^{10}). \quad (4.35)$$

The left side of Equation (4.35) is less than or equal to zero whereas, for $M^0 < N$, the right side is strictly greater than zero. Therefore, condition (4.35) cannot be met for any allowable values of M^0 , q , and q' and the ground state does not undergo an eigenvalue crossing in the non-interacting case. Similar results hold for two and three dimensions.

4.3.2 Shadows of Schrödinger's Cat

We now turn our attention to the effects of the coupling between energy levels in the regime, $|U_d^{00}| \ll 2\Delta E_d^{10}$. Consider a symmetric 1D potential, $\Delta V = 0$ and $d = 1$, in the high barrier limit, $J_1^{00} \ll U_1^{00}$. Suppose further that $J_1^{10} \ll U_1^{10}$. We will treat the coupling potential \hat{H}_1^{coup} as a perturbation to the decoupled Hamiltonian

$$\hat{H}_1^{\text{decoup}} = \hat{H}_1^A + \hat{H}_1^B. \quad (4.36)$$

Because $\hat{H}_1^{\text{decoup}}$ is separable, its eigenstates are direct products of the eigenstates of \hat{H}_1^A and \hat{H}_1^B .

The eigenstates of the decoupled Hamiltonian are given by

$$\begin{aligned} \hat{H}_1^{\text{decoup}} |\phi_{\pm}; n_L, N^0\rangle_A \otimes |\phi_{\pm}; n'_L, N^1\rangle_C \\ = \left[\varepsilon_{\pm}^{A,1}(n_L, N^0) + \varepsilon_{\pm}^{C,1}(n'_L, N^1) \right] |\phi_{\pm}; n_L, N^0\rangle_A \otimes |\phi_{\pm}; n'_L, N^1\rangle_C, \end{aligned} \quad (4.37)$$

for $0 \leq n_L < N^0/2$ and $0 \leq n'_L \leq N^1/2$. Here the partial Schrödinger cat states

$$|\phi_{\pm}; n_L, N\rangle_A = \frac{1}{\sqrt{2}} \left(|n_L, N - n_L\rangle_{(0,0)} \pm |N - n_L, n_L\rangle_{(0,0)} \right), \quad (4.38)$$

$$|\phi_{\pm}; n_L, N\rangle_C = \frac{1}{\sqrt{2}} \left(|n_L, N - n_L\rangle_{(1,0)} \pm |N - n_L, n_L\rangle_{(1,0)} \right), \quad (4.39)$$

are the eigenstates of \hat{H}_d^A and \hat{H}_d^C with corresponding energy eigenvalues given by

$$\varepsilon_{\pm}^{A,d}(n, N) = U_d^{00} \left[2 \left(n - \frac{N}{2} \right)^2 + N \left(\frac{N}{2} - 1 \right) \right] + N E_d^0 \mp \frac{1}{2} \Delta \varepsilon_n^N(J_d^{00}, U_d^{00}), \quad (4.40)$$

$$\varepsilon_{\pm}^{C,d}(n, N) = U_d^{10} \left[2 \left(n - \frac{N}{2} \right)^2 + N \left(\frac{N}{2} - 1 \right) \right] + N E_d^1 \mp \frac{1}{2} \Delta \varepsilon_n^N(J_d^{10}, U_d^{10}), \quad (4.41)$$

to lowest non-vanishing order in $J_1^{00}/|U_1^{00}|$ and $J_1^{10}/|U_1^{10}|$, respectively. The energy difference between symmetric and antisymmetric states is given by

$$\Delta \varepsilon_n^N(J, U) = 4U \frac{(N - n)!}{n![(N - 2n - 1)!]^2} \left(\frac{J}{2U} \right)^{N-2n}. \quad (4.42)$$

These solutions are derived in Appendix C. When $U_1^{00} \ll 2\Delta E_1^{10}$, the eigenstates and eigenvalues of \hat{H}_1 closely resemble the eigenstates and eigenvalues of the decoupled Hamiltonian $\hat{H}_1^{\text{decoup}}$, as can be seen in Figures 4.3 and 4.4.

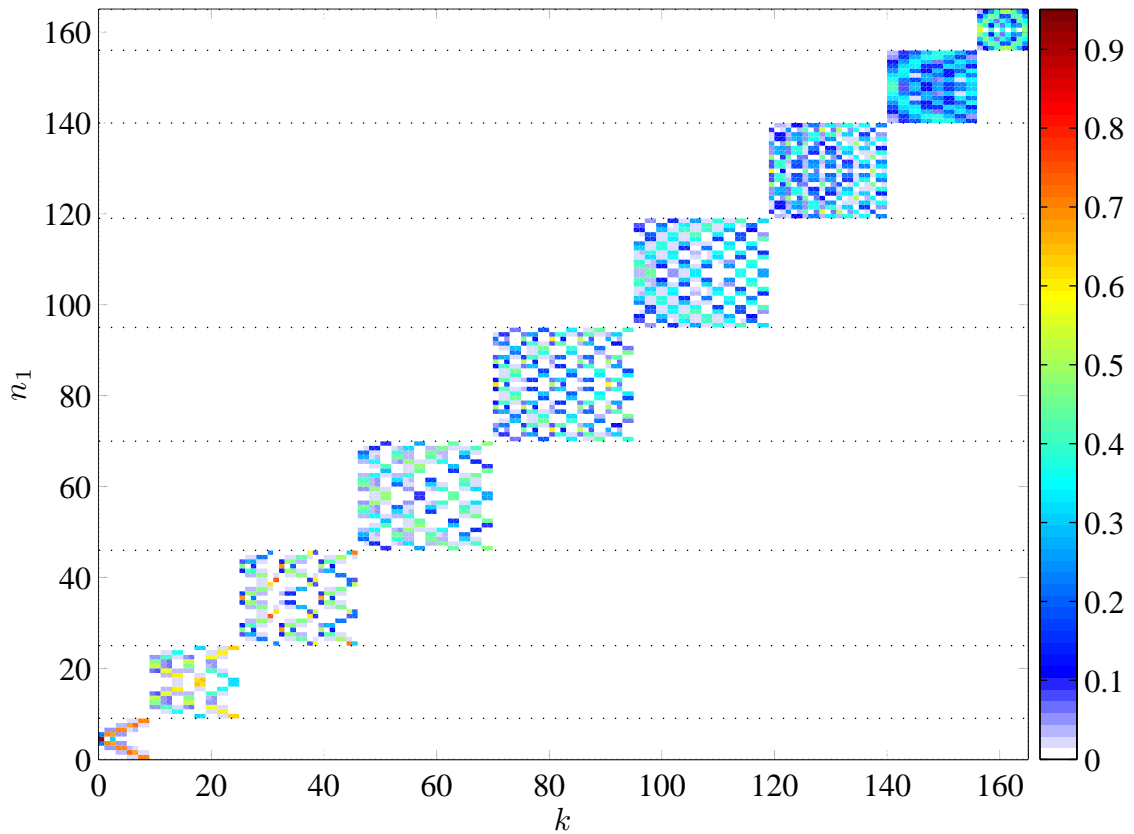


Figure 4.3. *Eigenstate amplitudes: High barrier and weak coupling.* Shown are the eigenstate amplitudes $|c_{n_1}^{(k)}|$ for all values of $n_1, k \in \{0, 1, \dots, \Omega_1 - 1\}$ when $J_1^{00}/U_1^{00} \approx 0.1$, $J_1^{00}/\Delta E_1^{10} \approx 4 \times 10^{-7}$, $J_1^{10}/\Delta E_1^{10} \approx 3 \times 10^{-5}$, and $N = 8$. The number-state and eigenstate labels n_1 and k are described in Figure 4.1. Here $NU_1^{00} \ll 2\Delta E_1^{10}$ and the effects of coupling between energy levels are negligible. Just as in the decoupled case, the eigenstates are grouped according to occupation of the excited level. The $N + 1$ lowest lying states, corresponding to zero occupation of the excited level, closely resemble the Schrödinger cat-like eigenstates of the one-level Hamiltonian (see Chapter 3). The magnitude of $|c_{n_1}^{(k)}|$ is indicated by the colorbar.

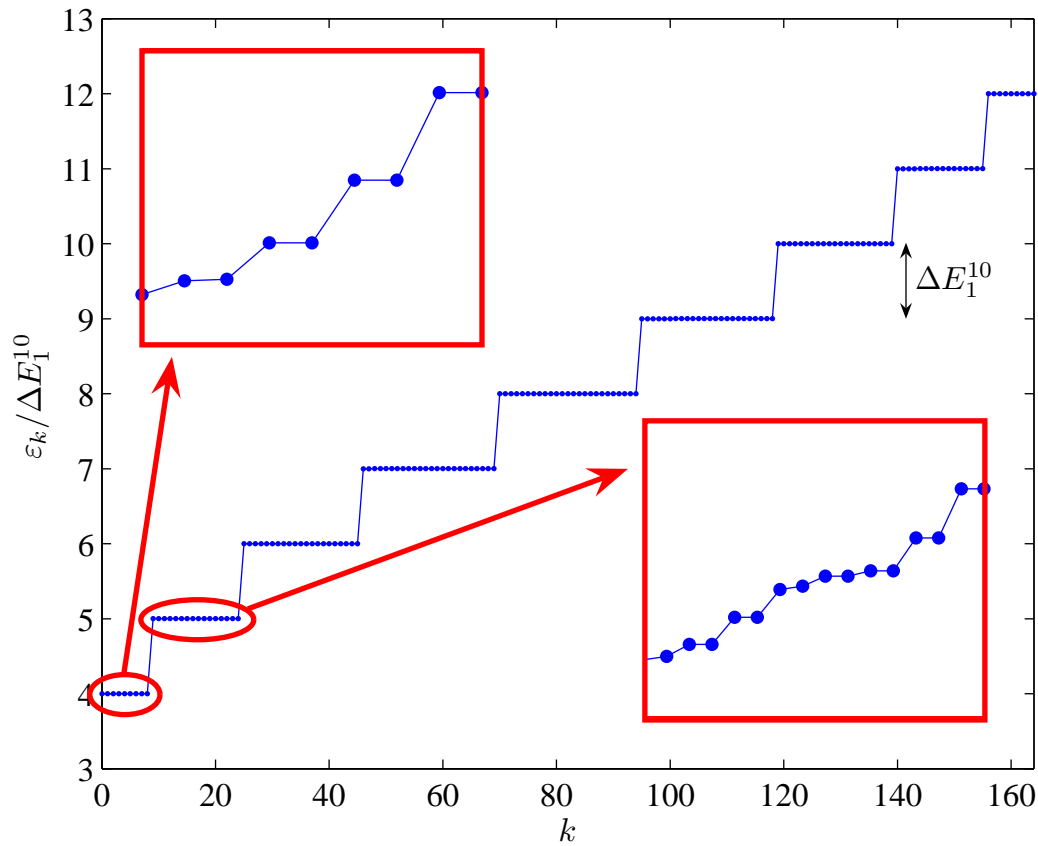


Figure 4.4. *Energy eigenvalues: High barrier and weak coupling.* Shown are the energy eigenvalues ε_k for the same system as in Figure 4.3. The line is a guide to the eye. In the weak coupling regime, eigenvalues occur in groups corresponding to occupation of the excited level. Whereas the energy difference between eigenvalues in the same group is on the order of U_1^{00} and U_1^{10} , the energy difference between groups is on the order of ΔE_1^{10} . The $N + 1$ lowest lying eigenvalues occur in nearly degenerate pairs and vary quadratically with k , as expected from our analysis of the one-level approximation. The inserts are zooms of the two lowest groups of eigenvalues.

Because the eigenstates of $\hat{H}_1^{\text{decoup}}$ are non-degenerate, we employ non-degenerate perturbation theory to study the effects of the coupling potential $\hat{H}_1^{\text{decoup}}$. The full Hamiltonian for the one-dimensional system is

$$\hat{H}_1 = \hat{H}_1^{\text{coup}} + \hat{H}_1^{\text{decoup}}. \quad (4.43)$$

Consider the case $N^0 = N$, that is, all atoms occupy the lowest well. In this case, the eigenstates of the decoupled Hamiltonian $\hat{H}_1^{\text{decoup}}$ are

$$|\phi_{\pm}^{(0)}; n_L\rangle = |\phi_{\pm}; n_L, N\rangle_A \otimes |0, 0\rangle_{(1,0)}, \quad (4.44)$$

with eigenvalues

$$\varepsilon_{\pm}^{(0)}(n_L) = \varepsilon_{\pm}^{A,1}(n_L, N). \quad (4.45)$$

Then, to first order in $|U_1^{00}|/\Delta E_1^{10}$, the eigenstates of the full Hamiltonian \hat{H}_1 are given by

$$|\phi_{\pm}; n_L\rangle = |\phi_{\pm}^{(0)}; n_L\rangle + |\phi_{\pm}^{(1)}; n_L\rangle \pm |\phi_{\pm}^{(1)}; N - n_L\rangle, \quad (4.46)$$

where

$$\begin{aligned} |\phi_{\pm}^{(1)}; n_L\rangle = & \alpha_{n_L} \{ |n_L - 2, N - n_L\rangle_{(0,0)} \otimes |2, 0\rangle_{(1,0)} \\ & \pm |N - n_L, n_L - 2\rangle_{(0,0)} \otimes |0, 2\rangle_{(1,0)} \} \end{aligned} \quad (4.47)$$

with

$$\alpha_{n_L} = \left(\frac{U_1^{00}}{2\Delta E_1^{10}} \right) \left[\frac{\sqrt{n_L(n_L - 1)}}{(U_1^{00}/\Delta E_1^{10})(4n_L - 9) - 2} \right], \quad (4.48)$$

where we have neglected terms on the order of $J_1^{00}/|U_1^{00}|$ and $J_1^{10}/|U_1^{10}|$. To first order

in $|U_1^{00}|/\Delta E_1^{10}$, the corresponding energy eigenvalues are given by

$$\varepsilon_{\pm}(n_L) = \varepsilon_{\pm}^{(0)}(n_L). \quad (4.49)$$

The states $|\phi_{\pm}^{(1)}; n_L\rangle$ and $|\phi_{\pm}^{(1)}; N - n_L\rangle$ appear as shadows of the Schrödinger cat states $|\phi_{\pm}^{(0)}; n_L\rangle$. The eigenstates and eigenvalues of \hat{H}_1 are shown in Figures 4.5 and 4.6 for this case. Similar results hold for cat states with nonzero occupation of the excited level. First order coupling effects also cause the appearance of shadows in two- and three- dimensional systems.

4.3.3 Eigenvalue Crossings: Weakly Coupled Energy Levels

We now turn our attention to the weakly coupled regime, $NU_d^0 \ll 2\Delta E_d^{10}$. In this case, the Hamiltonian \hat{H}_d is given by Equation (4.1). Although the Hamiltonian is no longer separable due to the coupling term \hat{H}_d^{coup} , the constant $\alpha_{n_L} \ll 1/N$ and coupling effects can safely be ignored. In this approximation, the eigenstates closely resemble direct products of the eigenstates of the Hamiltonians $\hat{H}_d^{A,B,C}$.

Consider a system of repulsively interacting bosons, $U_d^{\ell|m|} > 0$, in a symmetric potential with a barrier sufficiently high that no tunneling occurs, $\Delta V = 0$ and $J_d^{\pm\ell|m|} = 0$. The eigenstates of \hat{H}_d^A and \hat{H}_d^C are partial Schrödinger cat-like states given by Equation (4.38) with energies given by Equation (4.40). When all atoms occupy the ground level, i.e., $N^0 = N$, the eigenstates of \hat{H}_d are approximately given by

$$|\phi_{\pm}; n_L\rangle = |\phi_{\pm}; n_L, N\rangle_A \bigotimes_m |0, 0\rangle_{(1,m)}, \quad (4.50)$$

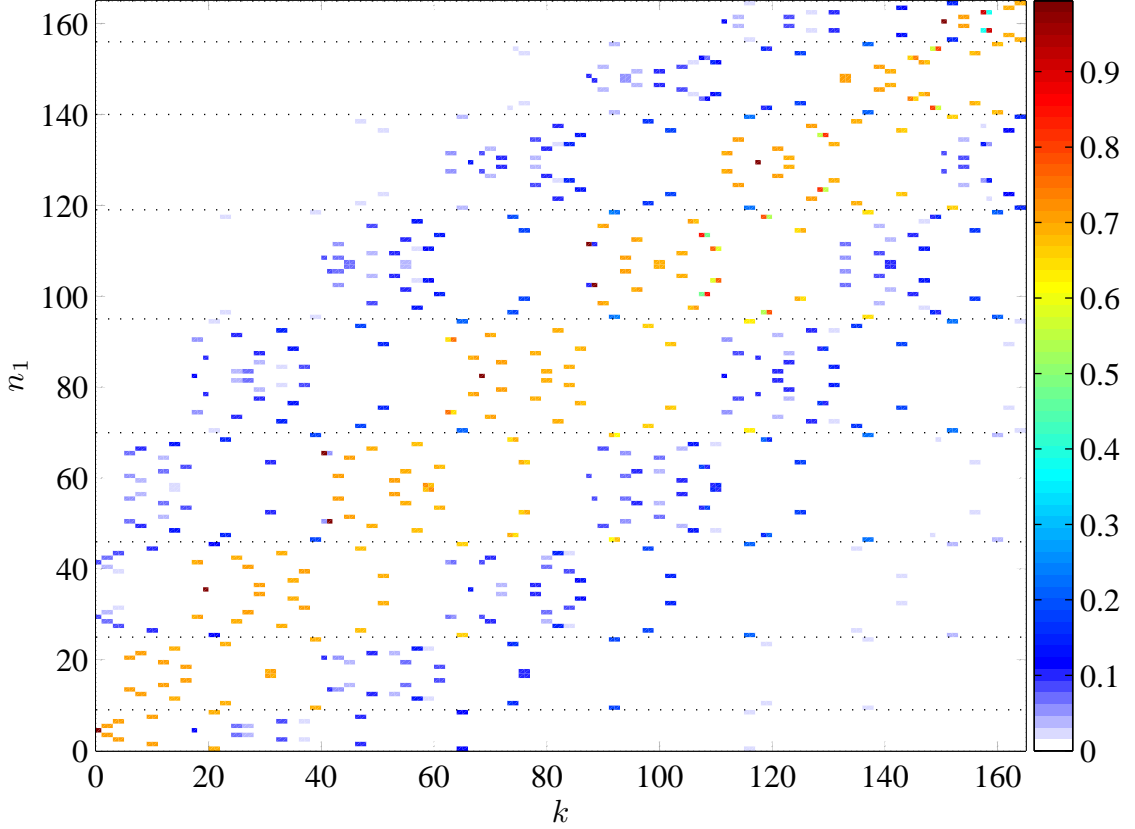


Figure 4.5. *Eigenstate amplitudes: Shadows of Schrödinger cat states.* Shown are the eigenstate amplitudes $|c_{n_1}^{(k)}|$ for all values of $n_1, k \in \{0, 1, \dots, \Omega_1 - 1\}$ when $J_1^{00}/U_1^{00} \approx 6 \times 10^{-6}$, $J_1^{00}/\Delta E_1^{10} \approx 4 \times 10^{-7}$, $J_1^{10}/\Delta E_1^{10} \approx 3 \times 10^{-5}$, and $N = 8$. The number-state and eigenstate labels n_1 and k are described in Figure 4.1. Here $NU_1^{00}/\Delta E_1^{10} \approx 0.5$ and coupling between levels cannot be ignored. The faint blue shadows of the orange Schrodinger cat-like states are a first order effect of level coupling. In this regime, atoms occupying different energy levels are entangled. Moreover, $U_1^{00} = 2U_1^{\text{crit}}$ and the system has passed through multiple eigenvalue crossings. Cat-like states involving definite occupation of the excited level are found among the $N + 1$ lowest eigenstates. In this regime, the one-level approximation is no longer valid. The magnitude of $|c_{n_1}^{(k)}|$ is indicated by the colorbar.

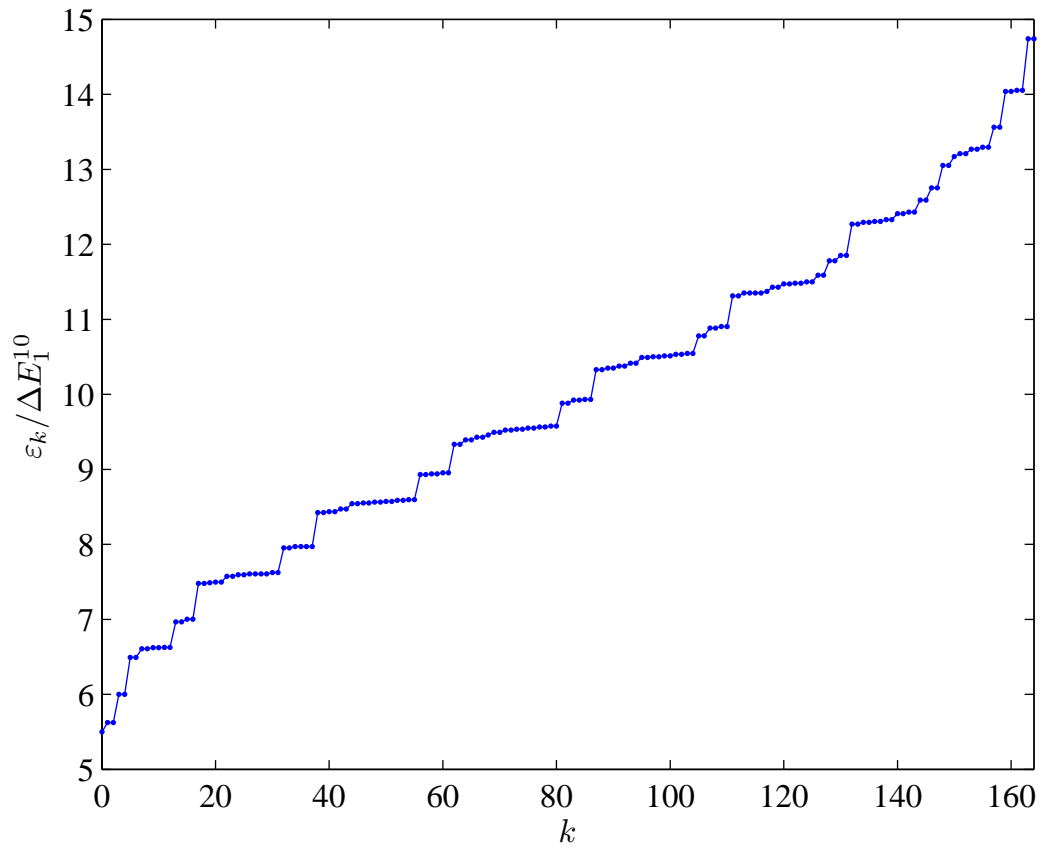


Figure 4.6. *Energy eigenvalues: Shadows of Schrödinger cat states.* Shown are the energy eigenvalues ε_k for the same system as in Figure 4.5. The line is a guide to the eye. In this regime, the magnitude of the interaction energy NU_1^{00} is on the order of energy level spacing ΔE_1^{10} and the eigenvalues are no longer grouped according to occupation of the excited level.

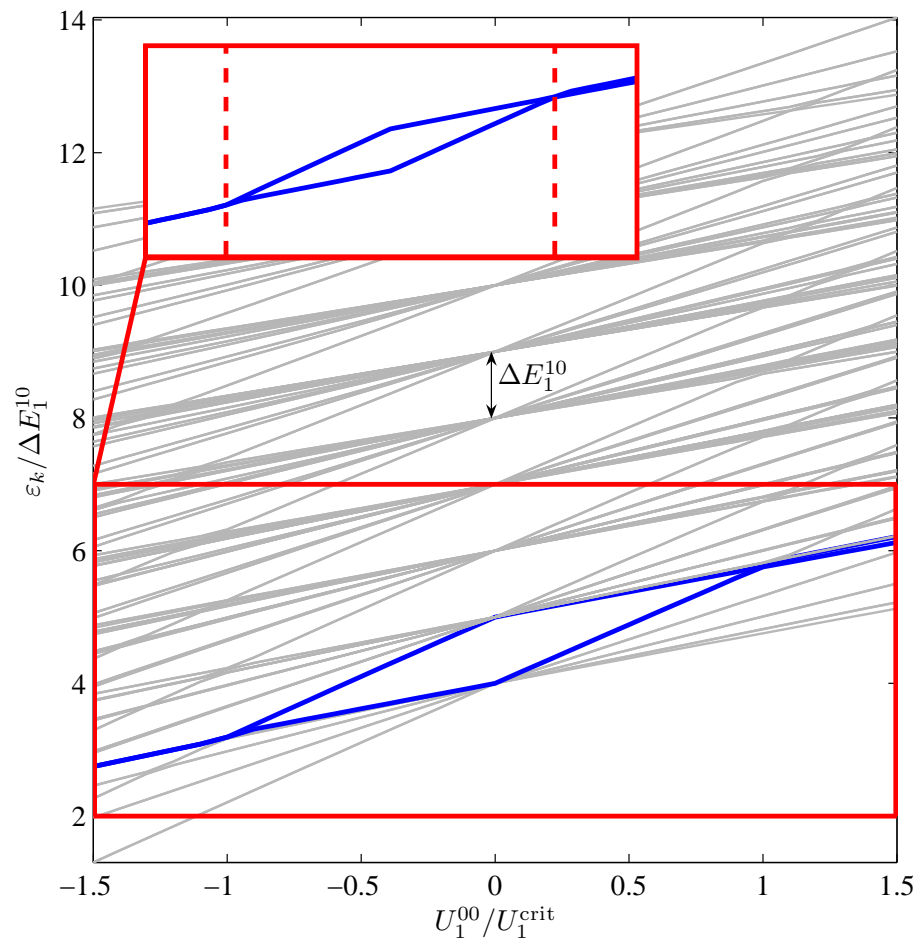


Figure 4.7. *Eigenvalue crossings.* The eigenvalues ε_k are plotted as a function of the interaction energy U_1^{00} for all values of $k \in \{0, 1, \dots, \Omega_1 - 1\}$. When there are no interactions, $U_1^{00} = 0$, the eigenvalues occur in groups separated by the energy level spacing ΔE_1^{10} . As the interaction energy increases, the energy difference between successive groups decreases until there is a crossing of the $(N + 1)$ th and $(N + 2)$ th eigenvalues near $|U_1^{00}| = U_1^{\text{crit}}$. These eigenvalues have been plotted in blue to aid the viewer. The insert is a zoom of the indicated region. Only the $(N + 1)$ th and $(N + 2)$ th eigenvalues are shown in the insert and the dashed vertical lines correspond to $|U_1^{00}| = U_1^{\text{crit}}$. Eigenvalue crossings cause states with definite occupation of the excited level to emerge among the $N + 1$ lowest lying states.

with an average energy

$$\bar{\varepsilon}_{n_L}^{A,d} = \langle \phi_{\pm}; n_L | \hat{H}_d | \phi_{\pm}; n_L \rangle = \varepsilon_{n_L}^{A,d}(N) + NE_d^0. \quad (4.51)$$

The energy

$$\bar{\varepsilon}_d^{\max} = \bar{\varepsilon}_0^{A,d} = U_d^{00}N(N-1) + NE_d^0, \quad (4.52)$$

is the highest such energy. Now suppose one atom occupies the excited level, that is, $N^1 = 1$. In $d = 1, 2$, and 3 dimensions, the states

$$|\phi_1^{\min}; N^1 = 1\rangle = |(N-1)/2, (N-1)/2\rangle_{(0,0)} \otimes |\phi_+; 0, 1\rangle_C, \quad (4.53a)$$

$$|\phi_2^{\max}; N^1 = 1\rangle = |(N-1)/2, (N-1)/2\rangle_{(0,0)} \otimes |\phi_0; 1\rangle_B, \quad (4.53b)$$

$$|\phi_3^{\max}; N^1 = 1\rangle = |(N-1)/2, (N-1)/2\rangle_{(0,0)} \otimes |\phi_0; 1\rangle_B \otimes |0, 0\rangle_{(1,0)}, \quad (4.53c)$$

have the lowest energy of all direct product states corresponding to $N^1 = 1$. The average energy of the state $|\phi_d^{\min}; N^1 = 1\rangle$ is

$$\bar{\varepsilon}_d^{\min} = \langle \phi_d^{\min}; N^1 = 1 | \hat{H}_d | \phi_d^{\min}; N^1 = 1 \rangle = \frac{1}{2}U_d^{00}(N-1)^2 + (N-1)E_d^0 + E_d^1. \quad (4.54)$$

Then $\bar{\varepsilon}_d^{\max} = \bar{\varepsilon}_d^{\min}$ when

$$U_d^{00} = U_d^{\text{crit}} = \frac{2\Delta E_d^{10}}{N^2 - 1}. \quad (4.55)$$

Therefore, we expect an eigenvalue crossing to occur when $U_d^{00} \approx U_d^{\text{crit}}$. To derive condition (4.55), we assumed that $NU_d^{00} \ll 2\Delta E_d^{10}$. Clearly, this condition holds for $U_d^{00} \approx U_d^{\text{crit}}$ when N is large. Moreover, the state $|\phi_d^{\min}; N^1 = 1\rangle$, defined in Equation (4.53), is only a valid state if N is odd. However, Equation (4.55) is also accurate for even values of N when N is large. In the attractive case, $U_d^{\ell|m|} < 0$, we find that a

crossing of eigenvalues occurs when $|U_d^{00}| \approx U_d^{\text{crit}}$.

The eigenvalue crossing near $|U_d^{00}| = U_d^{\text{crit}}$ is the first of many eigenvalue crossings in the interacting system. As the magnitude of the interaction energy $|U_d^{00}|$ increases, the excited states undergo multiple crossings, as demonstrated in Figure 4.7. Unlike the non-interacting case, however, the ground state energy also experiences an eigenvalue crossing for large values of $|U_d^{00}|$. The criterion for eigenvalue crossings in excited states is stronger than for the ground state. Preliminary numerical investigations show that, for small values of N , the ground state energy passes through a crossing when the interaction energy is on the order of the energy level spacing while, for large N , this can occur even for smaller values of $|U_d^{00}|/\Delta E_d^{10}$.

4.4 Summary

In summary, we developed a Fock space picture of the stationary states of a system of ultracold bosons in one-, two-, and three-dimensional double-well potential in a two-level approximation. The energy levels of the double-well are weakly coupled by atom-atom interactions. When the coupling is weak, eigenstates involving no occupation of the excited level are well described by the one-level approximation, which was treated in Chapter 3. However, such states will undergo multiple eigenvalue crossings, which cannot be described by a one-level approximation, when either the number of particles or the interaction energy is greater than some critical value. These crossings cause states with nonzero occupation of the excited level to emerge among the lowest lying eigenstates in a parameter regime where the one-level approximation is typically used. Eigenvalue crossings of the ground state energy of the double-well system suggest that quantum phase transitions may occur in the infinite lattice.

Coupling effects become important and the one-level approximation breaks down

when the interaction energy is comparable to the energy level spacing. In this regime, the interaction energy is much greater than the tunneling energy and the eigenstates are Schrödinger cat states which mix energy levels. First order effects couple states with N^1 atoms in the excited level to states with $N^1 \pm 2$ atoms in the excited level, whereas coupling to states with $N^1 \pm 2p$ atoms in the excited level is a p th order effect. Coupling of energy levels causes shadows of cat-like states to appear in the Fock decomposition of the eigenstates

Chapter 5

CONCLUSIONS AND OUTLOOK

Ultracold bosons in a double-well potential were investigated via exact diagonalization of one- and two-level Bose-Hubbard-like Hamiltonians. Similar studies commonly assume that the double-well is symmetric and that the trapped atoms all occupy the ground level of each well [26, 35, 36, 39, 40, 41, 42, 44, 45, 46]. However, many applications of these systems, such as quantum computing [19, 20] and gravitometry [23, 24], require a multi-level description of bosons in a tilted double-well. In our study, the symmetric trap and one-level assumptions were relaxed in order to provide a better understanding of these systems. Furthermore, orbital angular momentum degrees of freedom were introduced in the two-level approximation for two- and three-dimensional trapping potentials.

Consistent with the results of past studies [40, 42, 44, 45, 46], we identified two types of stationary states in the one-level approximation: harmonic oscillator-like and Schrödinger cat-like states. Oscillator-like states dominate the spectrum when the barrier between wells is low whereas the eigenstates are predominantly cat-like in the presence of a high barrier. For intermediate barrier sizes, both types of states exist. When the atom-atom interactions are repulsive, oscillator-like states compose the low-energy eigenstates. On the other hand, the low lying eigenstates are cat-like for attractive interactions.

Quantum sloshing, i.e., the dynamics of a system in which all atoms initially occupy one well, was studied in various parameter regimes [35, 39, 40, 55]. In the

non-interacting case, the atoms will tunnel sinusoidally between wells with a period that depends only on the hopping strength. The two-well analog of a superfluid state is realized at a quarter period. Interactions damp tunneling between wells when the barrier is low [41, 50, 55]. The damping time decreases with increasing number of particles. However, tunneling revivals occur periodically at times determined solely by the interaction energy.

When the barrier is high, the tunneling period is inversely proportional to the energy difference between symmetric and antisymmetric cat-like eigenstates and depends on the hopping strength, interaction energy, and the total number of atoms in the system. Because the energy difference becomes quite small when the number of particles is large, tunneling times are much longer than the lifetime of typical experiments. Ultralong tunneling times have been attributed to the phenomenon of self-trapping [41] observed in the experiments of Albiez *et al.* [34]. Unlike the low barrier case, the system is described by a Schrödinger cat-like state at a quarter period.

Cat-like states are highly sensitive to tilt; a small potential difference between wells causes their collapse and completely suppresses tunneling between wells [52, 54, 55], an effect which we call potential decoherence. This is quite different from suppression of tunneling due to thermal effects or coupling to a reservoir [47, 49, 51]; our system is closed and suppression is due to an internal parameter, namely, imperfections in the trapping potential. In our case, potential decoherence is induced by a slight misalignment of the energy levels in the left and right wells. Partial cat states are more robust with respect to potential decoherence than extreme cat states. Huang *et al.* demonstrated that partial cat states are also less susceptible to decoherence due to interactions of atoms with the electromagnetic vacuum [45].

Clearly, partial Schrödinger cat states are a better candidate for experiments.

Unlike other sources of decoherence, including the electromagnetic vacuum [45], finite temperature effects [47, 49], and dissipative losses [48, 50], cat-like states reappear and tunneling resonances occur for critical values of the tilt when the barrier is high [52, 54, 55]. At resonance, the potential difference between wells is exactly compensated by atom-atom interactions and only a fraction of the total atoms tunnels between wells. The other atoms remain in one well to counteract the tilt. Resonant tunneling is both much faster and less sensitive to potential decoherence than the symmetric case. Furthermore, tunneling resonances can be used to create robust few-atom superposition states in a many-body system.

To characterize the entanglement of cat-like eigenstates, we adapted two standard entanglement measures: Meyer's measure of the impurity [68, 69] and the von Neumann entropy [70]. Unfortunately, although both measures yield nonzero values for cat states, neither distinguishes between cat states with different Fock space peak separations. The separation of peaks in Fock space is of crucial importance in the decoherence of cat states [45, 54]. A new quantum measure, called the cat measure, was therefore proposed to characterize cat-like states. The cat measure, the expectation value of a Schrödinger cat projection operator, is maximized for cat states with a peak separation greater than some prescribed value.

In the two-level approximation, energy levels are coupled by atom-atom interactions. The coupling between levels is weak when the interaction energy is much less than the energy difference between the ground and first excited levels. In this regime, the eigenstates of the two-level Hamiltonian have definite occupation of each energy level and states with no occupation of the excited level are well described by the one-level approximation. However, if either the number of particles is or the

interaction energy is greater than some critical value, the two-level eigenstates undergo eigenvalue crossings even when the coupling between levels is weak. In the high barrier limit, eigenvalue crossings cause cat-like states with nonzero occupation of the excited level to emerge among the lowest-lying eigenstates. Although eigenvalue crossings occur in the weak coupling regime, they are induced by the presence of the excited energy level and cannot be described by the one-level approximation [54]. Coupling effects become important when the interaction energy is comparable to the energy level spacing. In this case, atoms occupying the ground and first excited level become entangled and coupling effects cannot be neglected.

There is still much to be learned from the two-level approximation. For instance, eigenvalue crossings involving the ground state energy occur when the atom-atom interactions are strong. However, the nature of these crossings has not yet been investigated. Such crossings could become points of non-analyticity in the ground state energy in the limit of an infinite lattice. These points, if they exist, would indicate a quantum phase transition in a lattice with two allowed energy bands [17]. A quantitative treatment of the ground state energy of the two-level approximation therefore requires attention in future studies of the double-well system. Moreover, the quantum sloshing of many bosons undoubtedly deviates from the one-level picture when the energy levels are significantly coupled. Orbital angular momentum degrees of freedom provide new possibilities for the study of the complex quantum dynamics of angular momentum states. The extension of the two-level double-well Hamiltonian to a two-band Bose-Hubbard Hamiltonian can be used to perform a timely and relevant study of ultracold bosons in an optical lattice with two allowed energy bands. Future work could also focus on finite temperature effects and dissipation in the two-level double-well system.

REFERENCES

- [1] S. N. Bose. Plancks gesetz und lichtquantenhypothese. *Zeitschrift für Physik*, 26:178–181, 1924.
- [2] A. Einstein. Quantentheorie des einatomigen idealen gases. *Sitzungsberichte der Preussischen Akademie der Wissenschaften*, page 261, 1924.
- [3] A. Einstein. Quantentheorie des einatomigen idealen gases: Zweite abhandlung. *Sitzungsberichte der Preussischen Akademie der Wissenschaften*, page 3, 1925.
- [4] M. H. Anderson, J. R. Ensher, M. R. Matthews, C. E. Wieman, and E. A. Cornell. Observation of Bose-Einstein condensation in a dilute atomic vapor. *Science*, 269:198–201, 1995.
- [5] K. B. Davis, M. O. Mewes, M. R. Andrews, N. J. van Druten, D. S. Durfee, D. M. Kurn, and W. Ketterle. Bose-Einstein condensation in a gas of sodium atoms. *Physical Review Letters*, 75:3969–3973, 1995.
- [6] C. C. Bradley, C. A. Sackett, J. J. Tollett, and R. G. Hulet. Evidence of Bose-Einstein condensation in an atomic gas with attractive interactions. *Physical Review Letters*, 75(9):1687–1690, Aug 1995.
- [7] M.-O. Mewes, M. R. Andrews, N. J. van Druten, D. S. Durfee, D. M. Kurn, and W. Ketterle. Observation of interference between two Bose condensates. *Science*, 275:637–641, 1997.
- [8] M.-O. Mewes, M. R. Andrews, D. M. Kurn, D. S. Durfee, C. G. Townsend, and W. Ketterle. Output coupler for Bose-Einstein condensed atoms. *Physical Review Letters*, 78(4):582–585, Jan 1997.
- [9] B. P. Anderson and M. A. Kasevich. Macroscopic quantum interference from atomic tunnel arrays. *Science*, 282:1686–9, 1998.
- [10] Immanuel Bloch, Theodor W. Hänsch, and Tilman Esslinger. Atom laser with a cw output coupler. *Physical Review Letters*, 82(15):3008–3011, Apr 1999.
- [11] M. Greiner, O. Mandel, T. Esslinger, T. Hänsch, and I. Bloch. Quantum phase transition from a superfluid to a Mott insulator in a gas of ultracold atoms. *Nature*, 415:39, 2002.

- [12] D. Jaksch, C. Bruder, J. I. Cirac, C. W. Gardiner, and P. Zoller. Cold bosonic atoms in optical lattices. *Phys. Rev. Lett.*, 81:3108–3111, 1998.
- [13] Herman Feshbach. A unified theory of nuclear reactions II. *Annals of Physics*, 19:287–313, 1962.
- [14] E. A. Donley, N. R. Claussen, S. L. Cornish, J. L. Roberts, E. A. Cornell, and C. E. Wieman. Dynamics of collapsing and exploding Bose-Einstein condensates. *Nature*, 412:295, 2001.
- [15] W. K. Hensinger, H. Häffner, A. Browaeys, N. R. Heckenberg, K. Helmerson, C. McKenzie, G. J. Milburn, W. D. Phillips, S. L. Rolston, H. Rubinsztein-Dunlop, and B. Upcroft. Dynamical tunnelling of ultracold atoms. *Nature*, 412:52, 2001.
- [16] D. A. Steck, W. H. Oskay, and M. G. Raizen. Observation of chaos-assisted tunneling between islands of stability. *Science*, 293:279, 2001.
- [17] S. Sachdev. *Quantum phase transitions*. Cambridge University Press, 1999.
- [18] G. K. Brennen, C. M. Caves, P. S. Jessen, and I. H. Deutsch. Quantum logic gates in optical lattices. *Physical Review Letters*, 82:1060, 1999.
- [19] J. Sebby-Strabley, M. Anderlini, P. Jessen, and J. Porto. A lattice of double wells for manipulating pairs of cold atoms. e-print cond-mat/0602103 (2006).
- [20] T. Calarco, U. Domer, P. S. Julienne, C. J. Williams, and P. Zoller. Quantum computations with atoms in optical lattices: Marker qubits and molecular interactions. *Physical Review A*, 70:012306, 2004.
- [21] N. S. Ginsberg, S. R. Garner, and L. Vestergaard Hau. Coherent control of optical information with matter wave dynamics. *Nature*, 445:623–626, 1997.
- [22] A. Peters, K. Y. Chung, and S. Chuo. Measurement of gravitational acceleration by dropping atoms. *Nature*, 400:849, 1999.
- [23] B. V. Hall, S. Whitlock, R. Anderson, P. Hannaford, and A. Sidorov. Condensate splitting in an asymmetric double well for atom chip based sensors. e-print cond-mat/0609014 (2006).
- [24] T. Schumm, S. Hofferberth, L. M. Andersson, S. Wildermuth, S. Groth, I. Bar-Joseph, J. Schmiedmayer, and P. Krüger. Matter-wave interferometry in a double well on an atom chip. *Nature Physics*, 1:57–62, 2005.

- [25] G. Ferrari, N. Poli, F. Sorrentino, and G. M. Tino. Long-lived Bloch oscillations with bosonic Sr atoms and application to gravity measurement at micrometer scale. *Physical Review Letters*, 97:060402, 2006.
- [26] R. Gati, J. Esteve, B. Hemmerling, T. B. Ottenstein, J. Appmeier, A. Weller, and M. K. Oberthaller. A primary noise thermometer for ultracold Bose gases. *New Journal of Physics*, 8:189, 2006.
- [27] L. D. Carr and Y. Castin. Limits of sympathetic cooling of fermions: The role of heat capacity of the coolant. *Physical Review A*, 69:043611, 2004.
- [28] Q. Niu, X.-G. Zhao, G. A. Georgakis, and M. G. Raizen. Atomic Landau-Zener tunneling and Wannier-Stark ladders in optical potentials. *Physical Review Letters*, 76:4504, 1996.
- [29] S. R. Wilkinson, C. F. Bharucha, K. W. Madison, Q. Niu, and M. G. Raizen. Observation of atomic Wannier-Stark ladders in an accelerated optical potential. *Physical Review Letters*, 76:4512, 1996.
- [30] A. Tomadin, R. Mannella, and S. Wimberger. Many-body interband tunneling as a witness of complex dynamics in the Bose-Hubbard model. *Physical Review Letters*, 98:130402, 2007.
- [31] B. T. Seaman, M. Krämer, D. Z. Anderson, and M. J. Holland. Atomtronics: ultracold atom analogs of electronic devices. e-print cond-mat/0606625 (2006).
- [32] J. A. Stickney, D. Z. Anderson, and A. A. Zozulya. Transistor-like behavior of a Bose-Einstein condensate in a triple well potential. e-print cond-mat/0607706 (2006).
- [33] Y. Shin, G.-B. Jo, M. Saba, T. A. Pasquini, W. Ketterle, and D. E. Pritchard. Optical weak link between two spatially separated Bose-Einstein condensates. *Physical Review Letters*, 95:170402, 2005.
- [34] M. Albiez, R. Gati, J. Fölling, S. Hunsmann, M. Cristiani, and M. Oberthaler. Direct observation of tunneling and nonlinear self-trapping in a single bosonic Josephson junction. *Physical Review Letters*, 95:010402, 2005.
- [35] A. Smerzi, S. Fantoni, S. Giovanazzi, and S. R. Shenoy. Quantum coherent atomic tunneling between two trapped Bose-Einstein condensates. *Physical Review Letters*, 79:4950, 1997.
- [36] J. Vidal, G. Palacios, and C. Aslangul. Entanglement dynamics in the Lipkin-Meshkov-Glick model. *Physical Review A*, 70:062304, 2004.

- [37] J. Vidal. Concurrence in collective models. *Physical Review A*, 73:062318, 2006.
- [38] S. Flach, V. Fleurov, and A. A. Ovchinnikov. Tunneling of localized excitations: Giant enhancement due to fluctuations. *Physical Review B*, 63:094304, 2001.
- [39] G. J. Milburn, J. Corney, E. M. Wright, and D. F. Walls. Quantum dynamics of an atomic Bose-Einstein condensate in a double-well potential. *Physical Review A*, 55:4318, 1997.
- [40] A. P. Tonel, J. Links, and A. Foerster. Quantum dynamics of a model for two Josephson-coupled Bose-Einstein condensates. *Journal of Mathematical Physics A*, 38:1235, 2005.
- [41] A. N. Salgueiro, A. F. R. de Toledo Piza, G. B. Lemos, R. Drumond, M. C. Nemes, and M. Weidemuller. Quantum dynamics of bosons in a double-well potential: Josephson oscillations, self-trapping and ultralong tunneling times. e-print quant-ph/06082228 (2006).
- [42] M. Jääskeläinen and P. Meystre. Dynamics of Bose-Einstein condensates in double-well potentials. *Physical Review A*, 71:043603, 2005.
- [43] A. K. Tuchman, C. Orzel, A. Polkovnikov, and M. A. Kasevich. Nonequilibrium coherence dynamics of a soft boson lattice. *Physical Review A*, 74:051601(R), 2006.
- [44] R. W. Spekkens and J. E. Sipe. Spatial fragmentation of a Bose-Einstein condensate in a double-well potential. *Physical Review A*, 59:3868, 1998.
- [45] Y. P. Huang and M. G. Moore. Creation, detection, and decoherence of macroscopic quantum superposition states in double-well Bose-Einstein condensates. *Physical Review A*, 73:023606, 2006.
- [46] K. Mahmud, H. Perry, and W. Reinhardt. Quantum phase-space picture of Bose-Einstein condensates in a double well. *Physical Review A*, 71:023615, 2005.
- [47] L. Pitaevskii and S. Stringari. Thermal vs quantum decoherence in double well trapped Bose-Einstein condensates. *Physical Review Letters*, 87(18):180402, Oct 2001.
- [48] P. J. Y. Louis, P. M. R. Brydon, and C. M. Savage. Macroscopic quantum superposition states in Bose-Einstein condensates: Decoherence and many modes. *Physical Review A*, 64:053613, 2001.

- [49] N. D. Antunes, F. C. Lombardo, D. Monteoliva, and P. I. Villar. Decoherence, tunneling and noise-activation in a double-potential well at high and zero temperature. e-print quant-ph/0508036 (2006).
- [50] I. Zapata, F. Sols, and A. J. Legget. Phase dynamics after connection of two separate Bose-Einstein condensates. *Physical Review A*, 67:021603, 2003.
- [51] J. P. Paz, S. Habib, and W. H. Zurek. Reduction of the wave packet: Preferred observable and decoherence time scale. *Physical Review D*, 47:488, 1993.
- [52] A. P. Tonel, J. Links, and A. Foerster. Behaviour of the energy gap in a model of Josephson coupled Bose-Einstein condensates. *Journal of Mathematical Physics A*, 38:6879, 2005.
- [53] D. Ananikian and T. Bergeman. Gross-Pitaevskii equation for Bose particles in a double-well potential: Two-mode models and beyond. *Physical Review A*, 73:013604, 2006.
- [54] D. R. Dounas-Frazer, A. M. Hermundstad, and L. D. Carr. Ultracold bosons and entanglement in the tilted double-well. e-print quant-ph/0609119 (2006).
- [55] D. R. Dounas-Frazer and L. D. Carr. Tunneling resonances and entanglement dynamics of cold bosons in the double well. e-print quant-ph/0610166 (2006).
- [56] L. D. Landau and E. M. Lifshitz. *Statistical Physics*. Butterworth-Heinemann, 3rd edition, 1980.
- [57] C. J. Pethick and H. Smith. *Bose-Einstein Condensation in Dilute Gases*. Cambridge University Press, 2002.
- [58] Anthony J. Leggett. Bose-Einstein condensation in the alkali gases: Some fundamental concepts. *Reviews of Modern Physics*, 73(2):307–356, Apr 2001.
- [59] Franco Dalfovo, Stefano Giorgini, Lev P. Pitaevskii, and Sandro Stringari. Theory of Bose-Einstein condensation in trapped gases. *Reviews of Modern Physics*, 71(3):463–512, Apr 1999.
- [60] W. Ketterle and N. J. van Druten. Bose-Einstein condensation of a finite number of particles trapped in one or three dimensions. *Physical Review A*, 54:656, 1996.
- [61] L. D. Landau and E. M. Lifshitz. *Quantum Mechanics*. Butterworth-Heinemann, 3rd edition, 1977.
- [62] A. M. Rey. *Ultracold bosonic atoms in optical lattices*. PhD thesis, University of Maryland, 2004.

- [63] A. J. Daley. *Manipulation and Simulation of Cold Atoms in Optical Lattices*. PhD thesis, Leopold-Franzens-Universität Innsbruck, 2005.
- [64] C. P. Friedman and E. F. Taylor. Quantizing angular momentum via the simple harmonic oscillator. *American Journal of Physics*, 39:1073–1078, 1971.
- [65] A. L. Fetter and J. D. Walecka. *Quantum Theory of Many-Particle Systems*. Dover Publications, Inc., 2003.
- [66] L. D. Carr, M. J. Holland, and B. A. Malomed. Macroscopic quantum tunnelling of Bose-Einstein condensates in a finite potential well. *Journal of Physics B*, 38:3217, 2005.
- [67] M. Olshanii. Atomic scattering in the presence of an external confinement and a gas of impenetrable bosons. *Physical Review Letters*, 81:938, 1998.
- [68] D. A. Meyer and N. R. Wallach. Global entanglement in multiparticle systems. *Journal of Mathematical Physics*, 43:4273, 2002.
- [69] G. K. Brennen. An observable measure of entanglement for pure states of multi-qubit systems. *Quantum Information and Computation*, 3:619, 2003.
- [70] C. H. Bennett, H. J. Bernstein, S. Popescu, and B. Schumacher. Concentrating partial entanglement by local operations. *Physical Review A*, 53:2046, 1996.
- [71] J. I. Korsbakken, K. B. Whaley, J. Dubois, and J. I. Cirac. A measurement-based measure of the size of macroscopic quantum superpositions. e-print quant-ph/0611121 (2006).

APPENDIX A

HOPPING STRENGTHS

We are interested in the qualitative behavior of the hopping strengths $J_d^{\ell m}$. As seen in Equation (2.46b), only the 1D parameters J_1^{00} and J_1^{10} need to be computed. These are given by Equation (2.43a), which yields

$$J_1^{00} = - \int_{-\infty}^{\infty} dx \phi_1^{(0,0)}(x+a) \left(-\frac{\hbar^2}{2M} \frac{\partial^2}{\partial x^2} + V_1(x) \right) \phi_1^{(0,0)}(x-a), \quad (\text{A.1})$$

$$J_1^{10} = - \int_{-\infty}^{\infty} dx \phi_1^{(1,0)}(x+a) \left(-\frac{\hbar^2}{2M} \frac{\partial^2}{\partial x^2} + V_1(x) \right) \phi_1^{(1,0)}(x-a), \quad (\text{A.2})$$

where the localized wavefunctions are given by Equation (2.28a) in the harmonic oscillator approximation and the double-well potential V_1 is defined in Chapter 2. The wavefunctions are reproduced below for convenience:

$$\phi_1^{(0,0)}(x) = a_{\text{ho}}^{-1/2} \pi^{-1/4} e^{-x^2/2a_{\text{ho}}^2}, \quad (\text{A.3})$$

$$\phi_1^{(1,0)}(x) = a_{\text{ho}}^{-1/2} 2^{1/2} \pi^{-1/4} (x/a_{\text{ho}}) e^{-x^2/2a_{\text{ho}}^2}. \quad (\text{A.4})$$

To obtain approximate expressions for J_1^{00} and J_1^{10} , we will make use of the fact that the 1D double-well potential $V_1(x)$ reaches a local maximum value of V_0 at $x = 0$. That is, $V_1(0) = V_0$ and $V_1'(0) = 0$.

Upon direct substitution of Equation (A.3) into Equation (A.1), we obtain

$$J_1^{00} = \hbar\omega e^{-a^2/a_{\text{ho}}^2} \left[\frac{1}{4} (2a^2/a_{\text{ho}}^2 - 1) - \pi^{-1/2} \int_{-\infty}^{\infty} d\xi e^{-\xi^2} V_1(\xi)/\hbar\omega \right], \quad (\text{A.5})$$

where $\xi \equiv x/a_{\text{ho}}$. The integral containing $V_1(\xi)$ is approximated as follows. Since $\exp(-\xi^2) \rightarrow 0$ very rapidly as $\xi \rightarrow \infty$, we can reduce the range of integration to a finite interval,

$$\int_{-\infty}^{\infty} d\xi e^{-\xi^2} V_1(\xi) \approx \int_{-1}^1 d\xi e^{-\xi^2} V_1(\xi). \quad (\text{A.6})$$

Expanding $V_1(\xi)$ about $\xi = 0$, we obtain $V_1(\xi) \approx V_0$ for $|\xi| < 1$ up to order ξ^2 . Here $V_1(0) \equiv V_0$ and $V_1'(0) = 0$ since $\xi = 0$ is a local max of $V_1(\xi)$. Then Equation (A.6) becomes

$$\int_{-\infty}^{\infty} d\xi e^{-\xi^2} V_1(\xi) \approx V_0 \int_{-1}^1 d\xi e^{-\xi^2}. \quad (\text{A.7})$$

Finally, we can extend the range of integration to $(-\infty, \infty)$ since the contribution of $\exp(-\xi^2)$ is small for large $|\xi|$. This yields

$$\int_{-\infty}^{\infty} d\xi e^{-\xi^2} V_1(\xi) \approx V_0 \int_{-\infty}^{\infty} d\xi e^{-\xi^2} = V_0 \sqrt{\pi}. \quad (\text{A.8})$$

Then J_1^{00} is approximately

$$J_1^{00} \approx \frac{1}{2} E_r \left\{ \left(\frac{a}{a_{\text{ho}}} \right)^2 \left[\left(\frac{a}{a_{\text{ho}}} \right)^2 - 1/2 \right] - 2V_0/E_r \right\} e^{-a^2/a_{\text{ho}}^2}. \quad (\text{A.9})$$

A similar approach can be used to evaluate J_1^{10} . We find

$$J_1^{10} \approx J_1^{00} \left[\left(\frac{a}{a_{\text{ho}}} \right)^2 - 1 \right] + \frac{1}{2} E_r \left\{ \left(\frac{a}{a_{\text{ho}}} \right)^6 - \frac{9}{2} \left(\frac{a}{a_{\text{ho}}} \right)^4 + \left(\frac{a}{a_{\text{ho}}} \right)^2 \right\} e^{-a^2/a_{\text{ho}}^2}. \quad (\text{A.10})$$

APPENDIX B

HARMONIC-OSCILLATOR-LIKE STATES

We consider the dynamics of a non-interacting Bose-Einstein condensate ($U = 0$) in the single-band model. The Bose-Hubbard Hamiltonian for this system is

$$\hat{H} = -J \left(\hat{b}_L^\dagger \hat{b}_R + \hat{b}_R^\dagger \hat{b}_L \right), \quad (\text{B.1})$$

where the hopping strength J is determined only by the barrier size. We proceed by first finding the Fock-space expansion of the eigenstates of the Hamiltonian (B.1). The eigenstates $|\phi_k\rangle$ satisfy

$$\hat{H}|\phi_k\rangle = \varepsilon_k|\phi_k\rangle, \quad (\text{B.2})$$

for $0 \leq k \leq N$. We will show that

$$\langle n_L, N - n_L | \phi_k \rangle \equiv c_{n_L}^{(k)} = A_k H_k(n_L | N) \sqrt{P_{1/2}(n_L | N)},$$

with corresponding eigenvalues

$$\varepsilon_k = -J(N - 2k),$$

where $H_k(n_L | N)$ are discrete Hermite polynomials and

$$P_{1/2}(n_L | N) = \frac{1}{2^N} \frac{N!}{n_L!(N - n_L)!}, \quad (\text{B.3})$$

is the binomial distribution. Here A_k is a constant of normalization.

Theorem 1. *For a system of non-interacting particles, $\hat{H}|\phi_k\rangle = \varepsilon_k|\phi_k\rangle$ if and only if*

$$-\lambda_k c_{n_L}^{(k)} = \sqrt{n_L(N - n_L + 1)}c_{n_L-1}^{(k)} + \sqrt{(n_L + 1)(N - n_L)}c_{n_L+1}^{(k)}, \quad (\text{B.4})$$

for $0 \leq n_L, k \leq N$ and where $\lambda_k \equiv \varepsilon_k/J$.

Proof. Let $|\phi_k\rangle = \sum_{n_L=0}^N c_{n_L}^{(k)}|n_L, N - n_L\rangle$ where $c_{n_L}^{(k)} \equiv \langle n_L, N - n_L|\phi_k\rangle$. Suppose $\hat{H}|\phi_k\rangle = \varepsilon_k|\phi_k\rangle$. Then $\langle n_L, N - n_L|\hat{H}|\phi_k\rangle = \langle n_L, N - n_L|\varepsilon_k|\phi_k\rangle$ yields (B.4). Suppose instead that $c_{n_L}^{(k)}$ satisfies (B.4). Then it follows that $-\lambda_k|\phi_k\rangle = \left(\hat{b}_L^\dagger \hat{b}_R + \hat{b}_R^\dagger \hat{b}_L\right)|\phi_k\rangle$, thus completing our proof. \square

Our goal is to find a family of sequences that satisfy (B.4) since, by Theorem 1, these sequences must represent the eigenstates of the Hamiltonian \hat{H} .

Definition. We define the discrete Hermite polynomials as

$$H_0(n_L|N) \equiv 1, \quad (\text{B.5a})$$

$$H_1(n_L|N) \equiv 2(N/2 - n_L)H_0(n_L|N), \quad (\text{B.5b})$$

$$H_{k+1}(n_L|N) \equiv 2(N/2 - n_L)H_k(n_L|N) - k(N - k + 1)H_{k-1}(n_L|N), \quad (\text{B.5c})$$

for $0 \leq n_L \leq N$ and $1 \leq k \leq N - 1$.

The definition of the discrete Hermite polynomials $H_k(n_L|N)$ is nearly identical to the definition of the continuous Hermite polynomials $H_k(x)$ under the transformation $N/2 - n_L \rightarrow x$.

Conjecture. The discrete Hermite polynomials satisfy

$$(N - 2k)H_k(n_L|N) = n_L H_k(n_L - 1|N) + (N - n_L)H_k(n_L + 1|N), \quad (\text{B.6})$$

and

$$\sum_{n_L=0}^N H_k(n_L|N)^2 P_{1/2}(n_L|N) = \frac{k!N!}{(N-k)!}, \quad (\text{B.7})$$

for $0 \leq n_L, k \leq N$.

Equations (B.6) and (B.7) can easily be verified for small values of k using the definition (B.5) of the discrete Hermite polynomials. A formal proof by induction of these equations for arbitrary k is quite complicated.

Theorem 2. *Let*

$$c_{n_L}^{(k)} = A_k H_k(n_L|N) \sqrt{P_{1/2}(n_L|N)}, \quad (\text{B.8a})$$

where

$$A_k = \sqrt{\frac{(N-k)!}{k!N!}}, \quad (\text{B.8b})$$

for $0 \leq n_L, k \leq N$. Then the states

$$|\phi_k\rangle = \sum_{n_L=0}^N c_{n_L}^{(k)} |n_L, N - n_L\rangle, \quad (\text{B.8c})$$

are the orthonormal eigenstates of the Hamiltonian (B.1) with corresponding eigenvalues $\varepsilon_k = -J(N - 2k)$.

Proof. Set $\lambda_k = -(N - 2k)$. Using Equation B.6, we have that

$$\begin{aligned} -\lambda_k c_{n_L}^{(k)} &= (N - 2k) A_k H_k(n_L|N) \sqrt{P_{1/2}(n_L|N)} \\ &= (n_L H_k(n_L - 1|N) + (N - n_L) H_k(n_L + 1|N)) A_k \sqrt{P_{1/2}(n_L|N)} \\ &= n_L H_k(n_L - 1|N) A_k \sqrt{\frac{N - n_L + 1}{n_L} P_{1/2}(n_L - 1|N)} \\ &\quad + (N - n_L) H_k(n_L + 1|N) A_k \sqrt{\frac{n_L + 1}{N - n_L} P_{1/2}(n_L + 1|N)} \\ &= \sqrt{n_L(N - n_L + 1)} c_{n_L-1}^{(k)} + \sqrt{(N - n_L)(n_L + 1)} c_{n_L+1}^{(k)} \end{aligned} \quad (\text{B.9})$$

for $0 \leq n_L, k \leq N$. Therefore, $c_{n_L}^{(k)}$ satisfies Equation (B.4) with $\lambda_k = -(N - 2k)$. By Theorem 1, the states $|\phi_k\rangle$ defined by (B.8c) are the eigenstates of the Hamiltonian (B.1) with eigenvalues $-J(N - 2k)$. Because \hat{H} is a hermitian operator, the eigenstates $|\phi_k\rangle$ are orthogonal. That is,

$$\langle \phi_k | \phi_{k'} \rangle = 0 \quad \text{for } k \neq k'. \quad (\text{B.10})$$

Using Equation (B.7), we get

$$\langle \phi_k | \phi_k \rangle = \sum_{n_L=0}^N c_{n_L}^{(k)} c_{n_L}^{(k)} = A_k^2 \sum_{n_L=0}^N H_k(n_L|N)^2 P_{1/2}(n_L|N) = 1, \quad (\text{B.11})$$

completing our proof. \square

From Theorem 2, the states $|\phi_k\rangle$ defined by Equation (B.8) are the orthogonal eigenstates of the Hamiltonian (B.1). Using the recursive definition of the discrete Hermite polynomials, we can derive a recursion relation for the eigenstates.

Corollary 1. *The eigenstates satisfy the recursion relation*

$$(\hat{N} - 2\hat{n}_L)|\phi_k\rangle = \sqrt{k(N - k + 1)}|\phi_{k-1}\rangle + \sqrt{(k + 1)(N - k)}|\phi_{k+1}\rangle, \quad (\text{B.12})$$

for $0 \leq k \leq N$.

The recursion relation (B.12) is extremely useful as it provides a simple method for determining the matrix elements of the number operator \hat{n}_L .

Lemma 1. *The matrix elements of the number operator \hat{n}_L are*

$$(\hat{n}_L)_{k'k} = \frac{N}{2}\delta_{k,k'} - \frac{1}{2}\sqrt{k(N - k + 1)}\delta_{k',k-1} - \frac{1}{2}\sqrt{(k + 1)(N - k)}\delta_{k',k+1}, \quad (\text{B.13})$$

where $(\hat{n}_L)_{k'k} = \langle \phi_{k'} | \hat{n}_L | \phi_k \rangle$ and $0 \leq k, k' \leq N$.

Lemma 1 is easily proved by multiplying Equation (B.12) by $\langle \phi_{k'} |$ on the left. We are finally in a position to describe the dynamics of a system in which n_L particles initially occupy the left well.

Theorem 3. *Suppose a system is described by state $|\Psi\rangle = |n_L, N - n_L\rangle$ at time $t = 0$. Then the average number of particles in the left well at some time $t > 0$ is given by*

$$\bar{n}_L(t) = \frac{N}{2} + \left(n_L - \frac{N}{2} \right) \cos(2Jt/\hbar), \quad (\text{B.14})$$

where

$$\bar{n}_L(t) = \langle \Psi | \hat{U}^\dagger(t) \hat{n}_L \hat{U}(t) | \Psi \rangle, \quad (\text{B.15})$$

and $\hat{U}(t) = \exp(-i\hat{H}t/\hbar)$ is the time evolution operator.

Proof. Consider the number operator $\hat{n}_L(t) = \hat{U}^\dagger(t) \hat{n}_L \hat{U}(t)$ in the Heisenberg picture. Inserting closure twice yields

$$\hat{n}_L(t) = \sum_{k,k'=0}^N e^{i\omega_{k'k}t} (\hat{n}_L)_{k'k} |\phi'_k\rangle \langle \phi_k|, \quad (\text{B.16})$$

where $\omega_{k'k} \equiv (\varepsilon_{k'} - \varepsilon_k)/\hbar = -2J(k' - k)$. Using Lemma 1, we find

$$\begin{aligned} \hat{n}_L(t) = & \frac{\hat{N}}{2} - \frac{1}{2} \sum_{k=0}^N \left[e^{i2Jt/\hbar} \sqrt{k(N-k+1)} |\phi_{k-1}\rangle \right. \\ & \left. + e^{-i2Jt/\hbar} \sqrt{(k+1)(N-k)} |\phi_{k+1}\rangle \right] \langle \phi_k|, \end{aligned} \quad (\text{B.17})$$

where we used $\sum_{k=0}^N |\phi_k\rangle\langle\phi_k| = 1$. Recursion relation (B.12) gives us

$$\begin{aligned} \hat{n}_L(t) = & \frac{\hat{N}}{2} - \frac{1}{2} \sum_{k=0}^N e^{i2Jt/\hbar} \left[(\hat{N} - 2\hat{n}_L)|\phi_k\rangle - \sqrt{(k+1)(N-k)}|\phi_{k+1}\rangle \right] \langle\phi_k| \\ & - \frac{1}{2} \sum_{k=0}^N e^{-i2Jt/\hbar} \left[(\hat{N} - 2\hat{n}_L)|\phi_k\rangle - \sqrt{k(N-k+1)}|\phi_{k-1}\rangle \right] \langle\phi_k|, \end{aligned} \quad (\text{B.18})$$

which can be rewritten as

$$\begin{aligned} \hat{n}_L(t) = & \hat{N} - (\hat{N} - 2\hat{n}_L) \cos(2Jt/\hbar) - \left\{ \frac{\hat{N}}{2} - \frac{1}{2} \sum_{k=0}^N \left[e^{-i2Jt/\hbar} \sqrt{k(N-k+1)}|\phi_{k-1}\rangle \right. \right. \\ & \left. \left. + e^{i2Jt/\hbar} \sqrt{(k+1)(N-k)}|\phi_{k+1}\rangle \right] \langle\phi_k| \right\}. \end{aligned} \quad (\text{B.19})$$

Together, Equations (B.17) and (B.19) imply that

$$\bar{n}_L(t) = N - (N - 2n_L) \cos(2Jt/\hbar) - \bar{n}_L^*(t), \quad (\text{B.20})$$

which, upon recognizing that $\bar{n}_L^*(t) = \bar{n}_L(t)$, completes our proof. \square

Finally, we consider the dynamics of a system in which all N atoms initially occupy the right well. We are interested in the probability that the system remains in the initial state as a function of time.

Theorem 4. *Suppose a system is described by state $|\Psi\rangle = |0, N\rangle$ at time $t = 0$. The probability of finding all N atoms in the right well at some time $t > 0$ is*

$$P_R(t) = \cos^{2N}(Jt/\hbar), \quad (\text{B.21})$$

where $P_R(t) = |\langle 0, N | \Psi(t) \rangle|^2$ and $|\Psi(t)\rangle = \hat{U}(t)|\Psi\rangle$ is the time-evolved ket.

Proof. Expanding the initial condition in an energy eigenbasis yields

$$|\Psi\rangle = |0, N\rangle = \sum_{k=0}^N \sqrt{P_{1/2}(k|N)} |\phi_k\rangle, \quad (\text{B.22})$$

where $c_0^{(k)} = \sqrt{P_{1/2}(k|N)}$. Then $\langle 0, N|\Psi(t)\rangle$ is

$$\langle 0, N|\Psi(t)\rangle = \sum_{k=0}^N P_{1/2}(k|N) e^{-i\varepsilon_k t/\hbar} = \sum_{k=0}^N P_{1/2}(k|N) e^{iJt/\hbar(N-2k)}, \quad (\text{B.23})$$

where we used $\varepsilon_k = -J(N - 2k)$. We can rewrite Equation (B.23) as

$$\langle 0, N|\Psi(t)\rangle = \frac{1}{2^N} \sum_{k=0}^N \frac{N!}{k!(N-k)!} (e^{-iJt/\hbar})^k (e^{iJt/\hbar})^{N-k}. \quad (\text{B.24})$$

Using the Binomial Theorem and Euler's Formula, this reduces to

$$\langle 0, N|\Psi(t)\rangle = \frac{1}{2^N} (e^{-iJt/\hbar} + e^{iJt/\hbar})^N = \cos^N(Jt/\hbar), \quad (\text{B.25})$$

which, after squaring both sides, is what we wanted to show. \square

APPENDIX C

SCHRÖDINGER CAT-LIKE STATES

We consider the stationary states of a system of N ultracold bosons in a tilted double-well with a very high barrier. In the one-level approximation, the Hamiltonian for this system is

$$\hat{H} = -J \sum_{j \neq j'} \hat{b}_j^\dagger \hat{b}_{j'} + U \sum_j \hat{n}_j (\hat{n}_j - 1) + \frac{\Delta V}{2} (\hat{n}_L - \hat{n}_R). \quad (\text{C.1})$$

Equation (C.1) was derived in Chapter 2. Because there are no angular momentum degrees of freedom in the lowest energy level, the cumbersome sub- and super-scripts of Equation (2.52) have been dropped. Recall that the subscript $j \in \{L, R\}$ is the well index, J is the hopping strength, U is the interaction potential, and ΔV is the potential difference between wells, or tilt.

For convenience, we define the following operators,

$$\hat{H}_U \equiv U \sum_j \hat{n}_j (\hat{n}_j - 1), \quad \hat{H}_J \equiv -J \sum_{j \neq j'} \hat{b}_j^\dagger \hat{b}_{j'}, \quad \text{and} \quad \hat{H}_{\Delta V} \equiv \frac{\Delta V}{2} (\hat{n}_L - \hat{n}_R). \quad (\text{C.2})$$

The Hamiltonian can then be written $\hat{H} = \hat{H}_U + \hat{H}_J + \hat{H}_{\Delta V}$. We consider the high barrier case, $J \ll |U|$.

C.1 Cat-Like States in a Symmetric Potential

Consider a symmetric potential, $\Delta V = 0$. Suppose further that the barrier is sufficiently high that $J \ll |U|$ so that we can treat \hat{H}_J as a perturbation to \hat{H}_U . The eigenstates and eigenvalues of \hat{H}_U are given by

$$\hat{H}_U |n_L, N - n_L\rangle = \varepsilon_{n_L}^{(0)} |n_L, N - n_L\rangle, \quad (\text{C.3})$$

with

$$\varepsilon_{n_L}^{(0)} = U [2(n_L - N/2)^2 + N(N/2 - 1)]. \quad (\text{C.4})$$

Because $\varepsilon_{N-n_L}^{(0)} = \varepsilon_{n_L}^{(0)}$, the states $|n_L, N - n_L\rangle$ and $|N - n_L, n_L\rangle$ are degenerate and we employ degenerate perturbation theory.

The first step is to diagonalize the perturbing potential \hat{H}_J in the degenerate subspace. In the case of two-fold degeneracies, the perturbation matrix P is given by the following 2×2 matrix:

$$P = \begin{pmatrix} 0 & \langle n_L, N - n_L | \hat{H}_J | N - n_L, n_L \rangle \\ \langle N - n_L, n_L | \hat{H}_J | n_L, N - n_L \rangle & 0 \end{pmatrix}. \quad (\text{C.5})$$

The off-diagonal elements of the matrix P are zero for $n_L \neq N/2 \pm 1$ implying that we must turn to higher order perturbations. Because

$$\langle n_L, N - n_L | \left(\hat{H}_J \right)^x | n_L, N - n_L \rangle = \langle n_L, N - n_L | \left(\hat{H}_J \right)^x | N - n_L, n_L \rangle = 0, \quad (\text{C.6})$$

for $x < N - 2n_L$, the effects of the perturbing potential \hat{H}_J require $(N - 2n_L)$ th order

degenerate perturbation theory. In this case, the perturbation matrix becomes

$$P' = \begin{pmatrix} 0 & P'_{12} \\ P'_{12} & 0 \end{pmatrix}, \quad (\text{C.7})$$

where

$$\begin{aligned} P'_{12} &= \frac{\langle n_L, N - n_L | (\hat{H}_J)^{N-2n_L} | N - n_L, n_L \rangle}{\prod_{n'_L=n_L+1}^{N-n_L-1} (\varepsilon_{n'_L}^{(0)} - \varepsilon_{n_L}^{(0)})} \\ &= 2U \frac{(N - n_L)!}{n_L! [(N - 2n_L - 1)!]^2} \left(\frac{J}{2U} \right)^{N-2n_L}, \end{aligned} \quad (\text{C.8})$$

and $\varepsilon_{n_L}^{(0)}$ is given by Equation (C.4). The eigenvectors and eigenvalues of the perturbation matrix P' are

$$\chi_{\pm} = \begin{pmatrix} 1 \\ \mp 1 \end{pmatrix} \quad \text{and} \quad \lambda_{\pm} = \pm P'_{12}, \quad (\text{C.9})$$

which implies that the eigenstates of the perturbed matrix are

$$|\phi_{\pm}^{(0)}; n_L\rangle = \frac{1}{\sqrt{2}} (|n_L, N - n_L\rangle \pm |N - n_L, n_L\rangle), \quad \text{for } 0 \leq n_L < N/2. \quad (\text{C.10})$$

to $(N - 2n_L - 1)$ th order $J/|U|$ and the energy difference between states is

$$\Delta\varepsilon_{n_L} = 2P'_{12} = 4U \frac{(N - n_L)!}{n_L! [(N - 2n_L - 1)!]^2} \left(\frac{J}{2U} \right)^{N-2n_L}, \quad (\text{C.11})$$

to $(N - 2n_L)$ th order in $J/|U|$. Therefore, the eigenstates of the Hamiltonian $\hat{H} = \hat{H}_U + \hat{H}_J$ are nearly degenerate pairs of partial Schrödinger cat states in the high barrier limit, $J \ll |U|$.

C.2 Potential Decoherence

We now investigate the effects of a small tilt, $\Delta V \ll J$ in the presence of a high barrier, $J \ll |U|$. The eigenstates $|\phi_{\pm}^{(0)}; n_L\rangle$ of the Hamiltonian $\hat{H} = \hat{H}_U + \hat{H}_J$ are given by Equation (C.10) with a level splitting $\Delta\varepsilon_{n_L}$ given by Equation (C.11). Here the superscript (0) indicates the zeroth order eigenstate with respect to both hopping J and tilt ΔV . We now introduce a small tilt $|\Delta V| \ll J$ by taking $\hat{H} \rightarrow \hat{H} + \hat{H}_{\Delta V}$. Because \hat{H}_J lifts all degeneracies, we can use non-degenerate perturbation theory to find the approximate eigenstates. Furthermore, because the level splitting between entangled pairs ΔE_{n_L} is much smaller than all other energy differences, the first- and second- order corrections to the state $|\phi_{+}^{(0)}; n_L\rangle$ are given by

$$|\phi_{+}^{(1)}; n_L\rangle = |\phi_{-}^{(0)}; n_L\rangle \frac{H_{\mp; n_L}^{(\Delta V)}}{\Delta\varepsilon_{n_L}}, \quad (\text{C.12})$$

and

$$|\phi_{+}^{(2)}; n_L\rangle = |\phi_{-}^{(0)}; n_L\rangle \frac{H_{-; n_L}^{(\Delta V)} H_{\mp; n_L}^{(\Delta V)} - H_{\mp; n_L}^{(\Delta V)} H_{+; n_L}^{(\Delta V)}}{\Delta\varepsilon_{n_L}^2}, \quad (\text{C.13})$$

where

$$H_{-; n_L}^{(\Delta V)} \equiv \langle \phi_{-}^{(0)}; n_L | \hat{H}_{\Delta V} | \phi_{-}^{(0)}; n_L \rangle = N\Delta V, \quad (\text{C.14})$$

$$H_{+; n_L}^{(\Delta V)} \equiv \langle \phi_{+}^{(0)}; n_L | \hat{H}_{\Delta V} | \phi_{+}^{(0)}; n_L \rangle = N\Delta V, \quad (\text{C.15})$$

and

$$H_{\mp; n_L}^{(\Delta V)} \equiv \langle \phi_{-}^{(0)}; n_L | \hat{H}_{\Delta V} | \phi_{+}^{(0)}; n_L \rangle = \Delta V (n_L - N/2). \quad (\text{C.16})$$

To second order, the eigenstates satisfy

$$|\phi_+; n_L\rangle \approx |\phi_+^{(2)}; n_L\rangle - |\phi_+^{(2)}; n_L\rangle \Delta V \frac{N/2 - n_L}{\Delta \varepsilon_{n_L}}. \quad (\text{C.17})$$

The eigenstate $|\phi_+; n_L\rangle$ becomes a number state of the form $|n_L, N - n_L\rangle$ when

$$|\Delta V| = \frac{\Delta \varepsilon_{n_L}}{N/2 - n_L}, \quad (\text{C.18})$$

for $n_L < N/2$. A small tilt thus destroys the entangled eigenstates in the presence of a high barrier. If we let $N = 1$ particle, then the eigenstates become localized when $\Delta V = 2\Delta \varepsilon_0$ which is agreement with results obtained from an exact treatment of the Schrödinger equation (see Appendix D).

C.3 Tunneling Resonances

Consider $J = 0$ and $\Delta V = \Delta V_p \equiv 2pU$ where $p \leq N - 1$ is an integer. In this case, the Hamiltonian is $\hat{H} = \hat{H}_U + \hat{H}_{\Delta V_p}$. The eigenstates are number states $|n_L, N - n_L\rangle$ with corresponding energy eigenvalues

$$\varepsilon_{n_L}^p = U [2(n_L - N/2 + p/2)^2 + N(N/2 - 1) - p^2/2 + pN]. \quad (\text{C.19})$$

In this case, the states $|n_L, N - n_L\rangle$ and $|N - p - n_L, n_L + p\rangle$ are degenerate for $0 \leq n_L \leq N - p$.

Now consider $\hat{H} \rightarrow \hat{H} + \hat{H}_J$ with $J \ll |U|$. Similar to the treatment in Section C.1, we employ degenerate perturbation theory to $(N - 2n_L - p)$ th order. The

eigenstates of the perturbed matrix are therefore

$$|\phi_{\pm}; n_L, p\rangle \equiv \frac{1}{\sqrt{2}} (|n_L, N - n_L\rangle \pm |N - p - n_L, n_L + p\rangle), \quad (\text{C.20})$$

to $(N - 2n_L - p - 1)$ th order $J/|U|$ and the energy difference between states is

$$\Delta\varepsilon_{n_L}^p = 2 \frac{\langle n_L, N - n_L | (\hat{H}_J)^{N-2n_L-p} | N - p - n_L, n_L + p \rangle}{\prod_{n'_L=n_L+1}^{N-n_L-p-1} (\varepsilon_{n'_L}^p - \varepsilon_{n_L}^p)}, \quad (\text{C.21})$$

to $(N - 2n_L - p)$ th order in $J/|U|$ where $\varepsilon_{n_L}^p$ is given by Equation (C.19). Thus, partial cat states reappear for critical values of the tilt given by

$$\Delta V = \Delta V_p \equiv 2pU, \quad p \in \{1, 2, \dots, N - 1\}. \quad (\text{C.22})$$

Furthermore, the procedure for determining the maximum deviation from ΔV_p for which the entangled eigenstates still exist is the same as in Section C.2. The stationary states will become localized when

$$|\Delta V - \Delta V_p| = \frac{2\Delta\varepsilon_{n_L}^p}{N - 2n_L - p}, \quad (\text{C.23})$$

where $\Delta\varepsilon_{n_L}^p$ is defined in (C.21). For the special case $n_L = 0$, we find that

$$\Delta\varepsilon_0^p = \frac{4U(J/2U)^{N-p}(N-p)}{(N-p-1)!} \sqrt{\frac{N!}{p!(N-p)!}}. \quad (\text{C.24})$$

APPENDIX D

LOCALIZATION OF A SINGLE PARTICLE IN A TILTED SQUARE
TWO-WELL POTENTIAL

Consider a single particle in a square two-well potential of the form

$$V(x) = \begin{cases} V_0 & , \quad |x| < a/2 \\ 0 & , \quad a/2 < |x| < b/2 \\ \infty & , \quad |x| > b/2 \end{cases} \quad (\text{D.1})$$

The Hamiltonian for this system is given by

$$H = -\frac{\hbar^2}{2m} \frac{\partial^2}{\partial x^2} + V(x) \quad (\text{D.2})$$

where m is the mass of the particle. The ground state $\psi_0^{(0)}(x)$ of (D.2) is symmetric and the first excited state $\psi_1^{(0)}(x)$ is antisymmetric. If we assume that the barrier is high, then the probability density inside the barrier is negligible. That is,

$$\int dx \psi_0^{(0)}(x)^2 \approx \int_L dx \psi_0^{(0)}(x)^2 + \int_R dx \psi_0^{(0)}(x)^2, \quad (\text{D.3})$$

where $\int_L dx \equiv \int_{-b/2}^{-a/2} dx$ and $\int_R dx \equiv \int_{a/2}^{b/2} dx$. Furthermore, because the ground state is symmetric, we have that

$$\int_L dx \psi_0^{(0)}(x)^2 = \int_R dx \psi_0^{(0)}(x)^2 \approx \frac{1}{2}. \quad (\text{D.4})$$

We introduce a small tilt by taking

$$H \rightarrow H + \Delta V(x) \quad (\text{D.5})$$

where

$$\Delta V(x) = \begin{cases} +\Delta V/2 & , \quad -b/2 < x < -a/2 \\ -\Delta V/2 & , \quad a/2 < x < b/2 \\ 0 & \text{otherwise} \end{cases} \quad (\text{D.6})$$

This system represents a tilted two-well system in one dimension. Suppose $\Delta V \ll V_0$. Then we can use non-degenerate perturbation theory to investigate the stationary states of a tilted two-well system. The first-order correction to the ground state is

$$\psi_0^{(1)}(x) = \sum_{n \neq 0} \psi_n^{(0)}(x) \frac{\int dx' \psi_n^{(0)}(x') \Delta V(x') \psi_0^{(0)}(x')}{E_0^{(0)} - E_n^{(0)}}. \quad (\text{D.7})$$

If the barrier is high, it is safe to assume that the level splitting between the first two excited states is very small. That is,

$$E_1^{(0)} - E_0^{(0)} \ll E_n^{(0)} - E_0^{(0)}, \quad (\text{D.8})$$

for $n > 1$. Then Eq. (D.7) becomes

$$\psi_0^{(1)}(x) \approx \psi_1^{(0)}(x) \frac{\int dx' \psi_1^{(0)}(x') \Delta V(x') \psi_0^{(0)}(x')}{E_0^{(0)} - E_1^{(0)}}, \quad (\text{D.9})$$

where

$$\int dx \psi_1^{(0)}(x) \Delta V(x) \psi_0^{(0)}(x) = \frac{\Delta V}{2} \left[\int_L dx \psi_1^{(0)}(x) \psi_0^{(0)}(x) - \int_R dx \psi_1^{(0)}(x) \psi_0^{(0)}(x) \right]. \quad (\text{D.10})$$

Because $\psi_1^{(0)}(x)$ is the antisymmetric compliment to $\psi_0^{(0)}(x)$, we have

$$\begin{aligned}\int_L dx \psi_1^{(0)}(x)\psi_0^{(0)}(x) &\approx \int_L dx \psi_0^{(0)}(x)^2, \\ \int_R dx \psi_1^{(0)}(x)\psi_0^{(0)}(x) &\approx - \int_R dx \psi_0^{(0)}(x)^2.\end{aligned}\quad (\text{D.11})$$

Substituting (D.11) into (D.10) yields

$$\int dx \psi_1^{(0)}(x)\Delta V(x)\psi_0^{(0)}(x) \approx \Delta V/2, \quad (\text{D.12})$$

and Eq. (D.9) becomes

$$\psi_0^{(1)}(x) \approx -\frac{\Delta V/2}{E_1^{(0)} - E_0^{(0)}}\psi_1^{(0)}(x) = -\frac{\Delta V}{2\Delta E_{10}}\psi_1^{(0)}(x), \quad (\text{D.13})$$

where $\Delta E_{10}^{(0)} \equiv E_1^{(0)} - E_0^{(0)}$. The second order correction to the ground state is given by

$$\psi_0^{(2)}(x) = \sum_{i \neq 0} \left[\sum_{j \neq 0} \frac{\Delta V_{ij}\Delta V_{j0}}{(E_0^{(0)} - E_i^{(0)})(E_0^{(0)} - E_j^{(0)})} - \frac{\Delta V_{i0}\Delta V_{00}}{(E_0^{(0)} - E_i^{(0)})^2} \right] \psi_i^{(0)}(x), \quad (\text{D.14})$$

where

$$\Delta V_{ij} \equiv \int dx \psi_i^{(0)}(x)\Delta V(x)\psi_j^{(0)}(x). \quad (\text{D.15})$$

Condition (D.8) reduces Eq. (D.14) to

$$\psi_0^{(2)}(x) \approx \frac{\Delta V_{11}\Delta V_{10} - \Delta V_{10}\Delta V_{00}}{(E_0^{(0)} - E_1^{(0)})^2}\psi_1^{(0)}(x). \quad (\text{D.16})$$

By symmetry considerations alone, since $\psi_0^{(0)}(x)$ is even and $\psi_1^{(0)}(x)$ and $\Delta V(x)$ are

odd, we see immediately that $\Delta V_{00} = \Delta V_{11} = 0$ and

$$\psi_0^{(2)}(x) \approx 0. \quad (\text{D.17})$$

The true ground state of Hamiltonian (D.5) is given by

$$\psi_0(x) \approx \psi_0^{(0)}(x) + \psi_0^{(1)}(x) + \psi_0^{(2)}(x) = \psi_0^{(0)}(x) - \frac{\Delta V}{2\Delta E_{10}} \psi_1^{(0)}(x), \quad (\text{D.18})$$

to second order. Therefore, the single particle ground state is localized when

$$|\Delta V| = \delta V_{\text{critical}} \equiv 2\Delta E_{10}^{(0)}. \quad (\text{D.19})$$

This result is consistent with the results obtained in Appendix C.

APPENDIX E

EXACT SOLUTIONS FOR THE ONE-LEVEL APPROXIMATION

In the one-level approximation, the Hamiltonian for N weakly interacting bosons in a double-well potential is

$$\hat{H} = -J \sum_{j \neq j'} \hat{b}_j^\dagger \hat{b}_{j'} + U \sum_j \hat{n}_j (\hat{n}_j - 1) + \frac{\Delta V}{2} (\hat{n}_L - \hat{n}_R). \quad (\text{E.1})$$

where the subscript $j \in \{L, R\}$ is the well index, J is the hopping strength, U is the interaction potential, and ΔV is the tilt. The energy eigenstates of the one-level Hamiltonian \hat{H} satisfy

$$\hat{H}|\phi_k\rangle = \varepsilon_k|\phi_k\rangle, \quad (\text{E.2})$$

and can be expanded in terms of the number states $|n_L, N - n_L\rangle$ as

$$|\phi_k\rangle = \sum_{n_L=0}^N c_{n_L}^{(k)} |n_L, N - n_L\rangle. \quad (\text{E.3})$$

Here $|c_{n_L}^{(k)}|^2$ is the probability of finding n_L particles in the left well when the system is in the k th excited state.

In particular, we are interested in the dynamics of a system in which all particles initially occupy the right well, i.e., $|\psi\rangle = |0, N\rangle$. At a later time $t > 0$, the system is described in the Schrödinger picture by the time-evolved state

$$|\psi(t)\rangle \equiv e^{-i\hat{H}t/\hbar}|\psi\rangle. \quad (\text{E.4})$$

The average occupation of the left well at some time $t > 0$ is given by

$$\bar{n}_L(t) \equiv \langle \psi(t) | \hat{n}_L | \psi(t) \rangle. \quad (\text{E.5})$$

We provide exact solutions expressions for $\bar{n}_L(t)$ for systems of $N = 1$ and 2 atoms.

E.1 One Atom

Consider a single atom, $N = 1$, in a double well potential. The energy eigenstates and eigenvalues are given by

$$\chi_{\pm} = \frac{1}{Z_{\pm}} \begin{pmatrix} \Delta V/(2J) - \varepsilon_{\pm} \\ 1 \end{pmatrix} \quad \text{and} \quad \varepsilon_{\pm} = \pm J \sqrt{1 + [\Delta V/(2J)]^2}, \quad (\text{E.6})$$

where

$$Z_{\pm} = \sqrt{[\Delta V/(2J) - \varepsilon_{\pm}]^2 + 1}, \quad (\text{E.7})$$

is a constant of normalization. The Fock space probability amplitudes are the elements of the vectors χ_{\pm} . That is, $c_{n_L}^{(\pm)} = (\chi_{\pm})_{n_L}$ for $n_L \in \{0, 1\}$. The average occupation of the left well is

$$\bar{n}_L(t) = A \sin^2(\omega t/2), \quad (\text{E.8})$$

where the amplitude and frequency of oscillation are

$$A = 1/[1 + (\Delta V/2J)^2] \quad \text{and} \quad \omega = (2J/\hbar) \sqrt{1 + (\Delta V/2J)^2}. \quad (\text{E.9})$$

For a system of N non-interacting bosons, we find that the average occupation of the left well is simply given by $[\bar{n}_L(t)]^N$.

E.2 Two Atoms

Next, consider two atoms, $N = 2$, in a symmetric potential, $\Delta V = 0$. The eigenvalues are given by

$$\varepsilon_{\pm} = U \left[1 \pm \sqrt{4 \left(\frac{J}{U} \right)^2 + 1} \right] \quad \text{and} \quad \varepsilon_0 = 2U, \quad (\text{E.10})$$

with corresponding eigenvectors

$$\chi_{\pm} = \frac{1}{Z_{\pm}} \begin{pmatrix} 1/\sqrt{2} \\ \varepsilon_{\mp}/(2J) \\ 1/\sqrt{2} \end{pmatrix} \quad \text{and} \quad \chi_0 = \begin{pmatrix} -1/\sqrt{2} \\ 0 \\ 1/\sqrt{2} \end{pmatrix}, \quad (\text{E.11})$$

where

$$Z_{\pm} = \sqrt{[\varepsilon_{\mp}/(2J)]^2 + 1}, \quad (\text{E.12})$$

is a constant of normalization. The average occupation of the left well is

$$\bar{n}_L(t) = 1 - A_+ \cos(\omega_+ t/2) + A_- \cos(\omega_- t/2), \quad (\text{E.13})$$

where the amplitudes and frequencies of oscillation are

$$A_{\pm} = \frac{1}{2} \left(\frac{\varepsilon_{\pm} - \varepsilon_0}{2\varepsilon_+ - \varepsilon_0} \right) \quad \text{and} \quad \hbar\omega_{\pm} = |\varepsilon_{\pm} - \varepsilon_0|. \quad (\text{E.14})$$

Note that $A_{\pm} \approx 1/2$ when $J/|U| \gg 1$. Then

$$\begin{aligned} \bar{n}_L(t) &\approx 1 - \frac{1}{2} [\cos(\omega_+ t/2) + \cos(\omega_- t/2)] \\ &= 1 - \cos[(\omega_+ + \omega_-)t/2] \cos[(\omega_+ - \omega_-)t/2], \end{aligned} \quad (\text{E.15})$$

where we used a sum-to-product trigonometric identity. Since $\omega_+ + \omega_- \approx 4J/\hbar$ and $\omega_+ - \omega_- \approx 2U/\hbar$ when $J/|U| \gg 1$, Equation (E.2) becomes

$$\bar{n}_L(t) \approx 1 - \cos(2Jt/\hbar) \cos(Ut/\hbar) \quad \text{for } J/|U| \gg 1. \quad (\text{E.16})$$

Thus, a pair of interacting atoms will undergo modulated oscillations between wells in the low barrier limit.

APPENDIX F

MATLAB CODE FOR GENERATING TWO-LEVEL HAMILTONIANS

In this section, we present MATLAB code for generating the two-level Hamiltonians \hat{H}_d , given by Equation (4.1), for $d = 1, 2$, and 3 dimensions. The function `colindex.m` takes the values $n_j^{(\ell,m)}$ as input and computes the corresponding Fock state label $n_d \in \{0, 1, \dots, \Omega_d - 1\}$ where the multiplicity Ω_d is given by Equation (4.4) and computed in the function `multiModeMultiplicity.m`. The Fock state label is given by Equation (4.6) for $d = 1, 2$, and 3 dimensions. The function `operators.m` generates the Fock space matrix representation of the operators $\hat{b}_j^{(\ell,m)\dagger} \hat{b}_{j'}^{(\ell',m')}$ for a system with N total atoms in d dimensions. These operators are represented as $\Omega_d \times \Omega_d$ square, Hermitian matrices. As $\Omega_d \propto N^{2d+1}$, these matrices are quite large even for small values of N .

The interaction energies $U_d^{\ell|m|}$ and the hopping strengths $J_d^{\pm\ell|m|}$ are computed by the function `params.m`. The input to this function are the barrier size $V_1''(a)a^2/E_r$ and the coupling constants G_d (see Chapter 2). All energies are in units of the level spacing ΔE_1^{10} . The interaction energies have a power law dependence on the barrier size whereas the hopping strengths decay exponentially with increasing barrier size.

Finally, the matrix representation $(H_d)_{n_d n'_d}$ of the two-level Hamiltonian, given by Equation (4.5), is generated by the function `twoLevelHamiltonian.m`. In Figure F.1, we show the time required to generate and diagonalize the matrix $(H_d)_{n_d n'_d}$. For $N = 6, 9$, and 22, diagonalization takes approximately two minutes in $d = 1, 2$, and 3 dimensions, respectively.

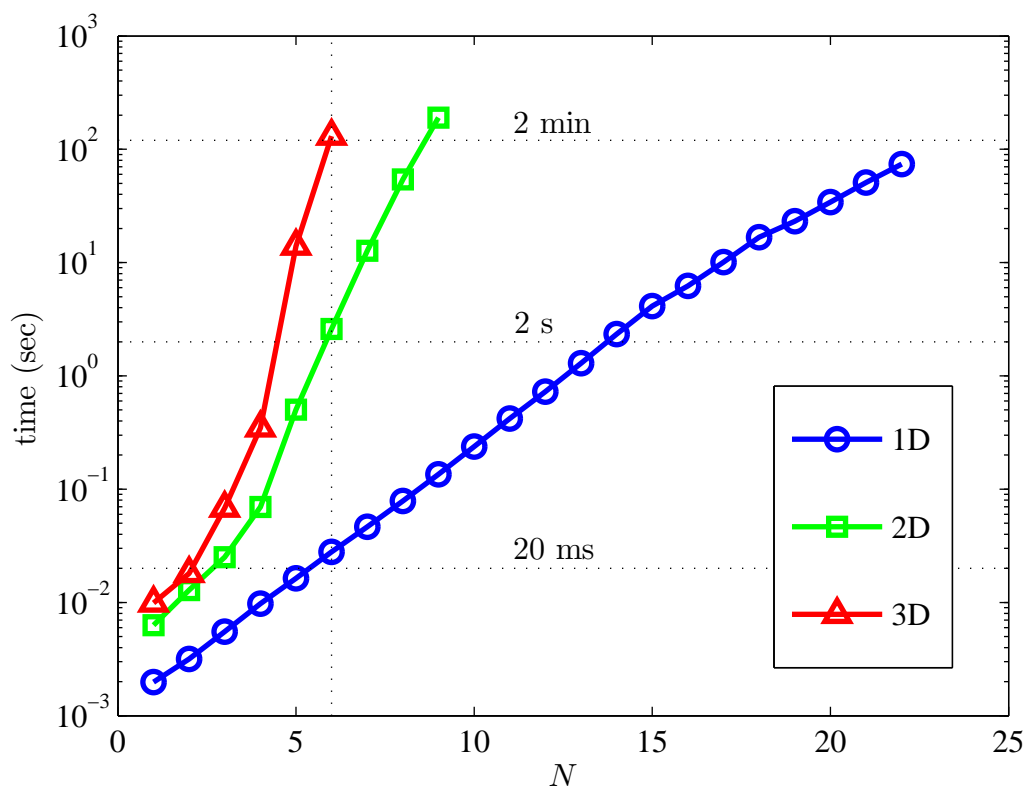


Figure F.1. *Time required to generate and diagonalize the two-level Hamiltonian.* The time required to generate and diagonalize the two-level Hamiltonian \hat{H}_d is plotted versus the total number of atoms N . Results for $d = 1, 2$, and 3 are plotted in blue circles, green squares, and red triangles, respectively. The multiplicity of the d -dimensional system scales like N^{2d+1} . In 1D, the Hamiltonian for a 6-atom system can be diagonalized in about 20 ms whereas this process takes over 2 minutes for the 3D case. The curves are a guide to the eye.

F.1 MultiModeMultiplicity.m

```
function omega = multiModeMultiplicity(N, M)
% omega = multiModeMultiplicity(N, M)
%
% omega is the multiplicity of a double-well system with N total particles
% allowed to occupy M total single-particle energy levels.

omega = binomial(N + 2.*M - 1, N); %%% compute the multiplicity
omega = floor(omega); %%% to avoid doubles, i.e., 61.0000)

function y = binomial(n, r) %%% subfunction
% y = binomial(n, r)
%
% y = n!/r!(n-r)! is the binomial coefficient
y = factorial(n)./( factorial(r).*factorial(n-r) );
```

F.2 Colindex.m

```
function j = colindex(data, D)
%j = colindex(data, D)
%
%j is the column (or row) index. the form of the data used to compute j
%depends on the number of dimensions D.
% D = 1: data = [mL0, mR0, mL1, mR1]
% D = 2: data = [mL0, mR0, mLp, mRp, mLm, mRm]
% D = 3: data = [mL0, mR0, mL1p, mR1p, mL10, mR10, mL1m, mR1m]

switch D
case 1 %one dimension
    N = sum( data );
    M1 = sum( data([3:4]) );
    mL0 = data(1);
    mL1 = data(3);
    %compute j
    j0 = (1/6) * M1 * (M1+1) * (5 + 3*N - 2*M1) + 1;
    j1 = j0 + mL1*(N-M1+1);
```

```

j2 = j1 + mL0;
j  = int16(j2);
return

case 2 %two dimensions
N   = sum( data );
M1  = sum( data([3:6]) );
M0  = N-M1;
ML  = sum( data([3,5]) ); %in 1st level of L
MR  = sum( data([4,6]) ); %in 1st level of R
mLp = data(3);
mRp = data(4);
mL0 = data(1);
%compute j
j0  = (1/120)*M1*(M1+1)*(M1+2)*(M1+3)*(9+5*N-4*M1) + 1;
j1  = j0 + (1/6)*(M0+1)*ML*(ML+1)*(5+3*M1-2*ML);
j2  = j1 + mLp*(MR+1)*(M0+1);
j3  = j2 + mRp*(M0+1);
j4  = j3 + mL0;
j   = int16(j4);
return

case 3 %three dimensions
N   = sum( data );
M1  = sum( data([3:8]) );
M0  = N-M1;
ML  = sum( data([3,5,7]) ); %in 1st level of L
MR  = sum( data([4,6,8]) ); %in 1st level of R
mL1m = data(3);
mL10 = data(7);
mR1m = data(4);
mR10 = data(8);
mL0  = data(1);
%compute j
j0  = 1 - (M1*(120+274*M1+225*M1^2+85*M1^3+15*M1^4+M1^5)* ...
        (-13+6*M1-7*N))/5040;
j1  = j0 + ((1+M0)*ML*(1+ML)*(2+ML)* ...
        (47+10*M1^2-15*M1*(ML-3)-33*ML+6*ML^2))/120;
j2  = j1 - ((1+M0)*mL1m*(-3-2*ML+mL1m)*(1+MR)*(2+MR))/4;
j3  = j2 + ((1+M0)*mL10*(1+MR)*(2+MR))/2;

```

```

        j4 = j3 - ((1+M0)*mR1m*(-3-2*MR+mR1m))/2;
        j5 = j4 + ((1+M0)*mR10);
        j6 = j5 + mL0;
        j = int16(j6);
        return
    end

```

F.3 Operators.m

```

function ops = operators(N, D)
%ops = operators(N, D)

switch D
    case 0 %two mode approximation
        ops = operators_twoMode(N); %see subfunction below
    case 1 %one dimension
        ops = operators1D(N); %see subfunction below
        return
    case 2 %two dimensions
        ops = operators2D(N); %see subfunction below
        return
    case 3 %three dimensions
        ops = operators3D(N); %see subfunction below
        return
end

%%%%%%%%%%%%%%%%%%%%%%%%%%%%%%%%%%%%%%%%%%%%%%%%%%%%%%%%%%%%%%%%%%%%%%%%%%%%%%
%%%%%%%%%%%%%%%%%%%%%%%%%%%%%%%%%%%%%%%%%%%%%%%%%%%%%%%%%%%%%%%%%%%%%%%%%%%%%%
%%%%%%%%%%%%%%%%%%%%%%%%%%%%%%%%%%%%%%%%%%%%%%%%%%%%%%%%%%%%%%%%%%%%%%%%%%%%%%
%%
%%                                SUBFUNCTION: two mode                                %%
%%%%%%%%%%%%%%%%%%%%%%%%%%%%%%%%%%%%%%%%%%%%%%%%%%%%%%%%%%%%%%%%%%%%%%%%%%%%%%

function ops = operators_twoMode(N) %subfunction

i      = 0:N-1;
bRbdL = sparse(2:N+1, 1:N, sqrt( (i+1).*(N-i) ), N+1, N+1);
i      = 0:N;
nR     = sparse(1:N+1, 1:N+1, N-i, N+1, N+1);
nL     = sparse(1:N+1, 1:N+1, i, N+1, N+1);

```

```

ops = {nL,    bRbdL';
      bRbdL, nR    };

%%%%%%%%%%%%%%%%%%%%%%%%%%%%%%%%%%%%%%%%%%%%%%%%%%%%%%%%%%%%%%%%%%%%%%%%
%%%%%%%%%%%%%%%%%%%%%%%%%%%%%%%%%%%%%%%%%%%%%%%%%%%%%%%%%%%%%%%%%%%%%%%%
%%%%%%%%%%%%%%%%%%%%%%%%%%%%%%%%%%%%%%%%%%%%%%%%%%%%%%%%%%%%%%%%%%%%%%%%
%%                                SUBFUNCTION: 1D                                %%

function ops = operators1D(N) %subfunction

omega = multiModeMultiplicity(N, 2); %omega is four-mode multiplicity
L00L00 = spalloc(omega,omega,omega); %allocate space for the operators
R00L00 = spalloc(omega,omega,omega);
R00R00 = spalloc(omega,omega,omega);
L10L00 = spalloc(omega,omega,omega);
L10R00 = spalloc(omega,omega,omega);
L10L10 = spalloc(omega,omega,omega);
R10L00 = spalloc(omega,omega,omega);
R10R00 = spalloc(omega,omega,omega);
R10L10 = spalloc(omega,omega,omega);
R10R10 = spalloc(omega,omega,omega);

for nL00 = 0:N %cycle through all possible combinations
for nR00 = 0:N-nL00
for nL10 = 0:N-nL00-nR00
nR10 = N - nL00 - nR00 - nL10; %number conserving: sum(njlm = N)

n    = [nL00, nR00, nL10, nR10]; %fock-state
i    = colindex(n,1); %compute the row index: see colindex.m

%NOTE: we have to compute 10 matrices

%number operators are diagonal
L00L00(i,i) = nL00; %1
R00R00(i,i) = nR00; %2
L10L10(i,i) = nL10; %3
R10R10(i,i) = nR10; %4

%compute bdR00*bL00

```

```

if nL00 < N & nR00 > 0 %5
    K    = 1;
    L    = 2;
    m    = n;
    m(K) = m(K)+1;
    m(L) = m(L)-1;
    j    = colindex(m,1);

    R00L00(i,j) = sqrt( m(K) )*sqrt( m(L) + 1 );
end

%compute bdL10*bL00
if nL00 < N & nL10 > 0 %6
    K    = 1;
    L    = 3;
    m    = n;
    m(K) = m(K)+1;
    m(L) = m(L)-1;
    j    = colindex(m,1);

    L10L00(i,j) = sqrt( m(K) )*sqrt( m(L) + 1 );
end

%compute bdR10*bL00
if nL00 < N & nR10 > 0 %8
    K    = 1;
    L    = 4;
    m    = n;
    m(K) = m(K)+1;
    m(L) = m(L)-1;
    j    = colindex(m,1);

    R10L00(i,j) = sqrt( m(K) )*sqrt( m(L) + 1 );
end

%compute bdL10*bR00
if nR00 < N & nL10 > 0 %7
    K    = 2;
    L    = 3;
    m    = n;

```

```

    m(K) = m(K)+1;
    m(L) = m(L)-1;
    j     = colindex(m,1);

    L1OR00(i,j) = sqrt( m(K) )*sqrt( m(L) + 1 );
end

%compute bdR10*bR00
if nR00 < N & nR10 > 0 %9
    K     = 2;
    L     = 4;
    m     = n;
    m(K) = m(K)+1;
    m(L) = m(L)-1;
    j     = colindex(m,1);

    R1OR00(i,j) = sqrt( m(K) )*sqrt( m(L) + 1 );
end

%compute bdR10*bL10
if nL10 < N & nR10 > 0 %10
    K     = 3;
    L     = 4;
    m     = n;
    m(K) = m(K)+1;
    m(L) = m(L)-1;
    j     = colindex(m,1);

    R1OL10(i,j) = sqrt( m(K) )*sqrt( m(L) + 1 );
end

end %nL10 loop
end %nR00 loop
end %nL00 loop

%note that bJLM*bdJLM = (bdJLM*bJLM)'
ops = {L00L00, R00L00', L10L00', R10L00';
       R00L00, R00R00, L10R00', R10R00';
       L10L00, L10R00, L10L10, R10L10';
       R10L00, R10R00, R10L10, R10R10};

```

```

%%%%%%%%%%%%%%%%%%%%%%%%%%%%%%%%%%%%%%%%%%%%%%%%%%%%%%%%%%%%%%%%%%%%%%%%%
%%%%%%%%%%%%%%%%%%%%%%%%%%%%%%%%%%%%%%%%%%%%%%%%%%%%%%%%%%%%%%%%%%%%%%%%%
%%%%%%%%%%%%%%%%%%%%%%%%%%%%%%%%%%%%%%%%%%%%%%%%%%%%%%%%%%%%%%%%%%%%%%%%%
%%
                                SUBFUNCTION: 2D                                %%

function ops = operators2D(N) %subfunction

omega = multiModeMultiplicity(N, 3); %omega is six-mode multiplicity
L00L00 = spalloc(omega,omega,omega); %allocate space for the operators
R00L00 = spalloc(omega,omega,omega);
R00R00 = spalloc(omega,omega,omega);
L1mL00 = spalloc(omega,omega,omega);
L1mR00 = spalloc(omega,omega,omega);
L1mL1m = spalloc(omega,omega,omega);
R1mL00 = spalloc(omega,omega,omega);
R1mR00 = spalloc(omega,omega,omega);
R1mL1m = spalloc(omega,omega,omega);
R1mR1m = spalloc(omega,omega,omega);
L1pL00 = spalloc(omega,omega,omega);
L1pR00 = spalloc(omega,omega,omega);
L1pL1m = spalloc(omega,omega,omega);
L1pR1m = spalloc(omega,omega,omega);
L1pL1p = spalloc(omega,omega,omega);
R1pL00 = spalloc(omega,omega,omega);
R1pR00 = spalloc(omega,omega,omega);
R1pL1m = spalloc(omega,omega,omega);
R1pR1m = spalloc(omega,omega,omega);
R1pL1p = spalloc(omega,omega,omega);
R1pR1p = spalloc(omega,omega,omega);

for nL00 = 0:N %cycle through all possible combinations
for nR00 = 0:N-nL00
for nL1m = 0:N-nL00-nR00
for nR1m = 0:N-nL00-nR00-nL1m;
for nL1p = 0:N-nL00-nR00-nL1m-nR1m;
nR1p = N - nL00 - nR00 - nL1m - nR1m - nL1p; %number conserving: sum(njlm = N)

n = [nL00, nR00, nL1p, nR1p, nL1m, nR1m]; %fock-state

```



```
i = colindex(n,2); %compute the row index: see colindex.m
```

```
%NOTE: we have to compute 21 matrices
```

```
%number operators are diagonal
```

```
L00L00(i,i) = nL00; %1
```

```
R00R00(i,i) = nR00; %2
```

```
L1mL1m(i,i) = nL1m; %3
```

```
R1mR1m(i,i) = nR1m; %4
```

```
L1pL1p(i,i) = nL1p; %5
```

```
R1pR1p(i,i) = nR1p; %6
```

```
%compute bdR00*bL00
```

```
if nL00 < N & nR00 > 0 %7
```

```
    K = 1;
```

```
    L = 2;
```

```
    m = n;
```

```
    m(K) = m(K)+1;
```

```
    m(L) = m(L)-1;
```

```
    j = colindex(m,2);
```

```
    R00L00(i,j) = sqrt( m(K) ) * sqrt( m(L) + 1 );
```

```
end
```

```
%compute bdL1p*bL00
```

```
if nL00 < N & nL1p > 0 %8
```

```
    K = 1;
```

```
    L = 3;
```

```
    m = n;
```

```
    m(K) = m(K)+1;
```

```
    m(L) = m(L)-1;
```

```
    j = colindex(m,2);
```

```
    L1pL00(i,j) = sqrt( m(K) ) * sqrt( m(L) + 1 );
```

```
end
```

```
%compute bdR1p*bL00
```

```
if nL00 < N & nR1p > 0 %9
```

```
    K = 1;
```

```
    L = 4;
```

```

    m    = n;
    m(K) = m(K)+1;
    m(L) = m(L)-1;
    j    = colindex(m,2);

    R1pL00(i,j) = sqrt( m(K) )*sqrt( m(L) + 1 );
end

%compute bdL1m*bL00
if nL00 < N & nL1m > 0 %10
    K    = 1;
    L    = 5;
    m    = n;
    m(K) = m(K)+1;
    m(L) = m(L)-1;
    j    = colindex(m,2);

    L1mL00(i,j) = sqrt( m(K) )*sqrt( m(L) + 1 );
end

%compute bdR1m*bL00
if nL00 < N & nR1m > 0 %11
    K    = 1;
    L    = 6;
    m    = n;
    m(K) = m(K)+1;
    m(L) = m(L)-1;
    j    = colindex(m,2);

    R1mL00(i,j) = sqrt( m(K) )*sqrt( m(L) + 1 );
end

%compute bdL1p*bR00
if nR00 < N & nL1p > 0 %12
    K    = 2;
    L    = 3;
    m    = n;
    m(K) = m(K)+1;
    m(L) = m(L)-1;
    j    = colindex(m,2);

```

```

    L1pR00(i,j) = sqrt( m(K) )*sqrt( m(L) + 1 );
end

```

```

%compute bdR1p*bR00
if nR00 < N & nR1p > 0 %13
    K    = 2;
    L    = 4;
    m    = n;
    m(K) = m(K)+1;
    m(L) = m(L)-1;
    j    = colindex(m,2);

```

```

    R1pR00(i,j) = sqrt( m(K) )*sqrt( m(L) + 1 );
end

```

```

%compute bdL1m*bR00
if nR00 < N & nL1m > 0 %14
    K    = 2;
    L    = 5;
    m    = n;
    m(K) = m(K)+1;
    m(L) = m(L)-1;
    j    = colindex(m,2);

```

```

    L1mR00(i,j) = sqrt( m(K) )*sqrt( m(L) + 1 );
end

```

```

%compute bdR1m*bR00
if nR00 < N & nR1m > 0 %15
    K    = 2;
    L    = 6;
    m    = n;
    m(K) = m(K)+1;
    m(L) = m(L)-1;
    j    = colindex(m,2);

```

```

    R1mR00(i,j) = sqrt( m(K) )*sqrt( m(L) + 1 );
end

```

```

%compute bdR1m*bL1m
if nL1m < N & nR1m > 0 %21
    K    = 5;
    L    = 6;
    m    = n;
    m(K) = m(K)+1;
    m(L) = m(L)-1;
    j    = colindex(m,2);

    R1mL1m(i,j) = sqrt( m(K) )*sqrt( m(L) + 1 );
end

%compute bdL1p*bL1m
if nL1m < N & nL1p > 0 %17
    K    = 5;
    L    = 3;
    m    = n;
    m(K) = m(K)+1;
    m(L) = m(L)-1;
    j    = colindex(m,2);

    L1pL1m(i,j) = sqrt( m(K) )*sqrt( m(L) + 1 );
end

%compute bdR1p*bL1m
if nL1m < N & nR1p > 0 %19
    K    = 5;
    L    = 4;
    m    = n;
    m(K) = m(K)+1;
    m(L) = m(L)-1;
    j    = colindex(m,2);

    R1pL1m(i,j) = sqrt( m(K) )*sqrt( m(L) + 1 );
end

%compute bdL1p*bR1m
if nR1m < N & nL1p > 0 %18
    K    = 6;
    L    = 3;

```

```

    m    = n;
    m(K) = m(K)+1;
    m(L) = m(L)-1;
    j    = colindex(m,2);

    L1pR1m(i,j) = sqrt( m(K) )*sqrt( m(L) + 1 );
end

%compute bdR1p*bR1m
if nR1m < N & nR1p > 0 %20
    K    = 6;
    L    = 4;
    m    = n;
    m(K) = m(K)+1;
    m(L) = m(L)-1;
    j    = colindex(m,2);

    R1pR1m(i,j) = sqrt( m(K) )*sqrt( m(L) + 1 );
end

%compute bdR1p*bL1p
if nL1p < N & nR1p > 0 %16
    K    = 3;
    L    = 4;
    m    = n;
    m(K) = m(K)+1;
    m(L) = m(L)-1;
    j    = colindex(m,2);

    R1pL1p(i,j) = sqrt( m(K) )*sqrt( m(L) + 1 );
end

end %nL1p loop
end %nR1m loop
end %nL1m loop
end %nR00 loop
end %nL00 loop

%note that bjl m*bdJLM = (bdjlm*bJLM)'
ops = {'L00L00', 'R00L00', 'L1mL00', 'R1mL00', 'L1pL00', 'R1pL00'};

```



```

R1pR1p = spalloc(omega,omega,omega);

L10L1m = spalloc(omega,omega,omega);
L10R1m = spalloc(omega,omega,omega);
R10L1m = spalloc(omega,omega,omega);
R10R1m = spalloc(omega,omega,omega);
L1pL10 = spalloc(omega,omega,omega);
L1pR10 = spalloc(omega,omega,omega);
R1pL10 = spalloc(omega,omega,omega);
R1pR10 = spalloc(omega,omega,omega);

for nL00 = 0:N                                %cycle through all possible combinations
for nR00 = 0:N-nL00
for nL1m = 0:N-nL00-nR00
for nR1m = 0:N-nL00-nR00-nL1m
for nL10 = 0:N-nL00-nR00-nL1m-nR1m
for nR10 = 0:N-nL00-nR00-nL1m-nR1m-nL10
for nL1p = 0:N-nL00-nR00-nL1m-nR1m-nL10-nR10
nR1p = N - nL00 - nR00 - nL1m - nR1m - nL10 - nR10 - nL1p;

n = [nL00, nR00, nL1p, nR1p, nL10, nR10, nL1m, nR1m]; %fock-state
i = colindex(n,3); %compute the row index: see colindex.m

%number operators are diagonal
L00L00(i,i) = nL00; %1
R00R00(i,i) = nR00; %2
L10L10(i,i) = nL10; %3
R10R10(i,i) = nR10; %4
L1mL1m(i,i) = nL1m; %5
R1mR1m(i,i) = nR1m; %6
L1pL1p(i,i) = nL1p; %7
R1pR1p(i,i) = nR1p; %8

%compute bdR00*bL00
if nL00 < N & nR00 > 0 %5
    K    = 1;
    L    = 2;
    m    = n;
    m(K) = m(K)+1;

```

```

    m(L) = m(L)-1;
    j     = colindex(m,3);

    R00L00(i,j) = sqrt( m(K) )*sqrt( m(L) + 1 );
end

%compute bdL10*bL00
if nL00 < N & nL10 > 0 %6
    K     = 1;
    L     = 5;
    m     = n;
    m(K) = m(K)+1;
    m(L) = m(L)-1;
    j     = colindex(m,3);

    L10L00(i,j) = sqrt( m(K) )*sqrt( m(L) + 1 );
end

%compute bdR10*bL00
if nL00 < N & nR10 > 0 %8
    K     = 1;
    L     = 6;
    m     = n;
    m(K) = m(K)+1;
    m(L) = m(L)-1;
    j     = colindex(m,3);

    R10L00(i,j) = sqrt( m(K) )*sqrt( m(L) + 1 );
end

%compute bdL10*bR00
if nR00 < N & nL10 > 0 %7
    K     = 2;
    L     = 5;
    m     = n;
    m(K) = m(K)+1;
    m(L) = m(L)-1;
    j     = colindex(m,3);

    L10R00(i,j) = sqrt( m(K) )*sqrt( m(L) + 1 );

```



```

end

%compute bdR10*bR00
if nR00 < N & nR10 > 0 %9
    K    = 2;
    L    = 6;
    m    = n;
    m(K) = m(K)+1;
    m(L) = m(L)-1;
    j    = colindex(m,3);

    R10R00(i,j) = sqrt( m(K) )*sqrt( m(L) + 1 );
end

%compute bdR10*bL10
if nL10 < N & nR10 > 0 %10
    K    = 5;
    L    = 6;
    m    = n;
    m(K) = m(K)+1;
    m(L) = m(L)-1;
    j    = colindex(m,3);

    R10L10(i,j) = sqrt( m(K) )*sqrt( m(L) + 1 );
end

%compute bdL1p*bL00
if nL00 < N & nL1p > 0 %8
    K    = 1;
    L    = 3;
    m    = n;
    m(K) = m(K)+1;
    m(L) = m(L)-1;
    j    = colindex(m,3);

    L1pL00(i,j) = sqrt( m(K) )*sqrt( m(L) + 1 );
end

%compute bdR1p*bL00
if nL00 < N & nR1p > 0 %9

```

```

K    = 1;
L    = 4;
m    = n;
m(K) = m(K)+1;
m(L) = m(L)-1;
j    = colindex(m,3);

R1pL00(i,j) = sqrt( m(K) )*sqrt( m(L) + 1 );
end

%compute bdL1m*bL00
if nL00 < N & nL1m > 0 %10
    K    = 1;
    L    = 7;
    m    = n;
    m(K) = m(K)+1;
    m(L) = m(L)-1;
    j    = colindex(m,3);

    L1mL00(i,j) = sqrt( m(K) )*sqrt( m(L) + 1 );
end

%compute bdR1m*bL00
if nL00 < N & nR1m > 0 %11
    K    = 1;
    L    = 8;
    m    = n;
    m(K) = m(K)+1;
    m(L) = m(L)-1;
    j    = colindex(m,3);

    R1mL00(i,j) = sqrt( m(K) )*sqrt( m(L) + 1 );
end

%compute bdL1p*bR00
if nR00 < N & nL1p > 0 %12
    K    = 2;
    L    = 3;
    m    = n;
    m(K) = m(K)+1;

```

```

    m(L) = m(L)-1;
    j     = colindex(m,3);

    L1pR00(i,j) = sqrt( m(K) )*sqrt( m(L) + 1 );
end

%compute bdR1p*bR00
if nR00 < N & nR1p > 0 %13
    K     = 2;
    L     = 4;
    m     = n;
    m(K) = m(K)+1;
    m(L) = m(L)-1;
    j     = colindex(m,3);

    R1pR00(i,j) = sqrt( m(K) )*sqrt( m(L) + 1 );
end

%compute bdL1m*bR00
if nR00 < N & nL1m > 0 %14
    K     = 2;
    L     = 7;
    m     = n;
    m(K) = m(K)+1;
    m(L) = m(L)-1;
    j     = colindex(m,3);

    L1mR00(i,j) = sqrt( m(K) )*sqrt( m(L) + 1 );
end

%compute bdR1m*bR00
if nR00 < N & nR1m > 0 %15
    K     = 2;
    L     = 8;
    m     = n;
    m(K) = m(K)+1;
    m(L) = m(L)-1;
    j     = colindex(m,3);

    R1mR00(i,j) = sqrt( m(K) )*sqrt( m(L) + 1 );

```

```

end

%compute bdR1m*bL1m
if nL1m < N & nR1m > 0 %21
    K    = 7;
    L    = 8;
    m    = n;
    m(K) = m(K)+1;
    m(L) = m(L)-1;
    j    = colindex(m,3);

    R1mL1m(i,j) = sqrt( m(K) )*sqrt( m(L) + 1 );
end

%compute bdL1p*bL1m
if nL1m < N & nL1p > 0 %17
    K    = 7;
    L    = 3;
    m    = n;
    m(K) = m(K)+1;
    m(L) = m(L)-1;
    j    = colindex(m,3);

    L1pL1m(i,j) = sqrt( m(K) )*sqrt( m(L) + 1 );
end

%compute bdR1p*bL1m
if nL1m < N & nR1p > 0 %19
    K    = 7;
    L    = 4;
    m    = n;
    m(K) = m(K)+1;
    m(L) = m(L)-1;
    j    = colindex(m,3);

    R1pL1m(i,j) = sqrt( m(K) )*sqrt( m(L) + 1 );
end

%compute bdL1p*bR1m
if nR1m < N & nL1p > 0 %18

```

```

K    = 8;
L    = 3;
m    = n;
m(K) = m(K)+1;
m(L) = m(L)-1;
j    = colindex(m,3);

L1pR1m(i,j) = sqrt( m(K) )*sqrt( m(L) + 1 );
end

%compute bdR1p*bR1m
if nR1m < N & nR1p > 0 %20
    K    = 8;
    L    = 4;
    m    = n;
    m(K) = m(K)+1;
    m(L) = m(L)-1;
    j    = colindex(m,3);

    R1pR1m(i,j) = sqrt( m(K) )*sqrt( m(L) + 1 );
end

%compute bdR1p*bL1p
if nL1p < N & nR1p > 0 %16
    K    = 3;
    L    = 4;
    m    = n;
    m(K) = m(K)+1;
    m(L) = m(L)-1;
    j    = colindex(m,3);

    R1pL1p(i,j) = sqrt( m(K) )*sqrt( m(L) + 1 );
end

%L10L1m
%L10R1m
%R10L1m
%R10R1m
%L1pL10
%L1pR10

```

```

%R1pL10
%R1pR10

end
end
end
end
end
end %nR00 loop
end %nL00 loop

ops = {L00L00, R00L00', L1mL00', R1mL00', L10L00', R10L00', L1pL00', R1pL00';
       R00L00, R00R00, L1mR00', R1mR00', L10R00', R10R00', L1pR00', R1pR00';
       L1mL00, L1mR00, L1mL1m, R1mL1m', L10L1m', R10L1m', L1pL1m', R1pL1m';
       R1mL00, R1mR00, R1mL1m, R1mR1m, L10R1m', R10R1m', L1pR1m', R1pR1m';
       L10L00, L10R00, L10L1m, L10R1m, L10L10, R10L10', L1pL10', R1pL10';
       R10L00, R10R00, R10L1m, R10R1m, R10L10, R10R10, L1pR10', R1pR10';
       L1pL00, L1pR00, L1pL1m, L1pR1m, L1pL10, L1pR10, L1pL1p, R1pL1p';
       R1pL00, R1pR00, R1pL1m, R1pR1m, R1pL10, R1pR10, R1pL1p, R1pR1p};

```

F.4 Params.m

```

function [E0,E1,J0,J1,J11,U00,U11,U10] = parameters(B, L, D)
%[E0,E1,J0,J1,J11,U00,U11,U10] = parameters(B, L, D)
%
%E0,E1 are the energies of the 0th,1st levels. J0,J1 are the hopping
%strengths between L and R wells in the 0th,1st levels. J11 is the hopping
%strength between +/-1 angular momentum states in the 1st level. U00 is
%the on-site interaction potential in the (0,0) mode. U11 is the on-site
%potential in the (1,+/-1) mode; U10 in the (1,0) mode; and U01 is the
%inter-mode interaction potential between (1,0) and (1,+/-1) modes.

%barrier size:          B = M * Vx''(a) * a^4 / hbar^2
%interaction strength: L = a * as / aperp^2
%where a is such that Vx'(a) = 0.

%energy is in units of hbar*omega where omega is the effective trapping
%frequency of the wells

```

```
%parameters obtained analytically by using a SHO approximation
```

```
E0 = D/2;      %zero-point energy
E1 = D/2 + 1; %first excited energy level
```

```
J0 = 1/2 .* exp( -sqrt(B) );
```

```
switch D
```

```
  case 1 %one dimension
```

```
    %define the hopping terms
```

```
    J1 = J0 .* ( 6 * sqrt(B) - 3 );
```

```
    J11 = 0;
```

```
    %define the interaction terms
```

```
    U00 = L .* B.^(-1/4) / sqrt(2*pi);
```

```
  case 2 %two dimensions
```

```
    %define the hopping terms
```

```
    J1 = +J0 .* ( 3 * sqrt(B) - 1 );
```

```
    J11 = -J0 .* ( 3 * sqrt(B) - 2 );
```

```
    %define the interaction terms
```

```
    U00 = L / sqrt(2*pi);
```

```
  case 3%three dimensions
```

```
    %define the hopping terms
```

```
    J1 = +J0 .* ( 3 * sqrt(B) - 1 );
```

```
    J11 = -J0 .* ( 3 * sqrt(B) - 2 );
```

```
    %define the interaction terms
```

```
    U00 = L .* B.^(1/4) / sqrt(2*pi);
```

```
end
```

```
U11 = (1/2)*U00;
```

```
U10 = (3/4)*U00;
```

F.5 TwoLevelHamiltonian.m

```
function H = twoLevelHamiltonian(B, L, V, ops)
```

```
%H = twoLevelHamiltonian(B, L, V, ops)
```

```
%
```

```
%H is the Hamiltonian for N weakly interacting bosons in a D-dimensional
```

%double-well potential with two allowed energy levels. B is the
 %dimensionless "barrier size" and L is the dimensionless "interaction
 %strength".

%barrier size: B = M * Vx''(a) * a^4 / hbar^2
 %interaction strength: L1 = a * as / aperp^2
 % L2 = as / az
 % L3 = as / a
 %where a is such that Vx'(a) = 0.

%energy is in units of hbar*omega where omega is the effective trapping
 %frequency of the wells

%NOTE: B > Bmin where Bmin = ((D/2) * V''(a) * a^2 / V0)^2. For a
 %sinusoidal potential, we have that Bmin = (D*pi^2/4)^2

number_of_modes = length(ops);

```
switch number_of_modes
  case 2 %two mode approximation
    H = H_twoMode(B, L, V, ops); %see subfunction below
  case 4 %four modes = one dimension
    H = H1D(B, L, V, ops); %see subfunction below
    return
  case 6 %six modes = two dimensions
    H = H2D(B, L, V, ops);
    return
  case 8 %eight modes = three dimensions
    H = H3D(B, L, V, ops);
    return
end
```

```
%%%%%%%%%%%%%%%%%%%%%%%%%%%%%%%%%%%%%%%%%%%%%%%%%%%%%%%%%%%%%%%%%%%%%%%%%%%%%%
%%%%%%%%%%%%%%%%%%%%%%%%%%%%%%%%%%%%%%%%%%%%%%%%%%%%%%%%%%%%%%%%%%%%%%%%%%%%%%
%%%%%%%%%%%%%%%%%%%%%%%%%%%%%%%%%%%%%%%%%%%%%%%%%%%%%%%%%%%%%%%%%%%%%%%%%%%%%%
%%                                SUBFUNCTION: 1D                                %%
```

```
function H = H_twoMode(B, L, V, ops) %subfunction
```



```

J = B;
U = L;

nL      = cell2mat( ops(1,1) ); %see operators.m
bdRbL   = cell2mat( ops(1,2) );
bRbdL   = cell2mat( ops(2,1) );
nR      = cell2mat( ops(2,2) );

I        = speye( size(nL) ); %identity

%compute two-mode hamiltonian
H = -J*(bdRbL+bRbdL) + U*(nL*(nL-I) + nR*(nR-I)) + (V/2)*(nL-nR);

%%%%%%%%%%%%%%%%%%%%%%%%%%%%%%%%%%%%%%%%%%%%%%%%%%%%%%%%%%%%%%%%%%%%%%%%%%%%%%
%%%%%%%%%%%%%%%%%%%%%%%%%%%%%%%%%%%%%%%%%%%%%%%%%%%%%%%%%%%%%%%%%%%%%%%%%%%%%%
%%%%%%%%%%%%%%%%%%%%%%%%%%%%%%%%%%%%%%%%%%%%%%%%%%%%%%%%%%%%%%%%%%%%%%%%%%%%%%
%%%%%%%%%%%%%%%%%%%%%%%%%%%%%%%%%%%%%%%%%%%%%%%%%%%%%%%%%%%%%%%%%%%%%%%%%%%%%%
%%                                SUBFUNCTION: 1D                                %%

function H = H1D(B, L, V, ops) %subfunction

%compute 1D hopping/interaction parameters
[E0,E1,J0,J1,J11,U00,U11,U10] = parameters(B, L, 1);

nL00      = cell2mat( ops(1,1) ); %see operators.m
bR00bdL00 = cell2mat( ops(1,2) );
bL10bdL00 = cell2mat( ops(1,3) );
bR10bdL00 = cell2mat( ops(1,4) );

bdR00bL00 = cell2mat( ops(2,1) );
nR00      = cell2mat( ops(2,2) );
bL10bdR00 = cell2mat( ops(2,3) );
bR10bdR00 = cell2mat( ops(2,4) );

bdL10bL00 = cell2mat( ops(3,1) );
bdL10bR00 = cell2mat( ops(3,2) );
nL10      = cell2mat( ops(3,3) );
bR10bdL10 = cell2mat( ops(3,4) );

bdR10bL00 = cell2mat( ops(4,1) );
bdR10bR00 = cell2mat( ops(4,2) );

```

```

bdR10bL10 = cell2mat( ops(4,3) );
nR10      = cell2mat( ops(4,4) );

I = speye( size(nL00) ); %identity

%compute two-mode hamiltonians
H00 = -J0*(bR00bdL00 + bdR00bL00) + U00*(nL00*(nL00-I) + nR00*(nR00-I)) ...
      + (V/2)*(nL00-nR00);

H10 = -J1*(bR10bdL10 + bdR10bL10) + U10*(nL10*(nL10-I) + nR10*(nR10-I)) ...
      + (V/2)*(nL10-nR10);

%compute energy of levels 0 and 1
E = E0*(nL00 + nR00) + E1*(nL10 + nR10);

%compute inter-level, same site interactions
Uint = 4*U11*(nL00*nL10 + nR00*nR10);

%compute inter-level, same site hopping
Uhop = U11*(bL10bdL00^2 + bdL10bL00^2 + bR10bdR00^2 + bdR10bR00^2);

%compute 1D hamiltonian
H = H00 + H10 + E + Uint + Uhop;

%%%%%%%%%%%%%%%%%%%%%%%%%%%%%%%%%%%%%%%%%%%%%%%%%%%%%%%%%%%%%%%%%%%%%%%%%%%%%%
%%%%%%%%%%%%%%%%%%%%%%%%%%%%%%%%%%%%%%%%%%%%%%%%%%%%%%%%%%%%%%%%%%%%%%%%%%%%%%
%%%%%%%%%%%%%%%%%%%%%%%%%%%%%%%%%%%%%%%%%%%%%%%%%%%%%%%%%%%%%%%%%%%%%%%%%%%%%%
%%                                SUBFUNCTION: 2D                                %%
function H = H2D(B, L, V, ops) %subfunction

%compute 2D hopping/interaction parameters
[E0,E1,J0,J1,J11,U00,U11,U10] = parameters(B, L, 2);

nL00      = cell2mat( ops(1,1) ); %see operators.m
bR00bdL00 = cell2mat( ops(1,2) );
bL1mbdL00 = cell2mat( ops(1,3) );
bR1mbdL00 = cell2mat( ops(1,4) );
bL1pbdL00 = cell2mat( ops(1,5) );
bR1pbdL00 = cell2mat( ops(1,6) );

```

```

bdR00bL00 = cell2mat( ops(2,1) );
nR00      = cell2mat( ops(2,2) );
bL1mbdR00 = cell2mat( ops(2,3) );
bR1mbdR00 = cell2mat( ops(2,4) );
bL1pbdR00 = cell2mat( ops(2,5) );
bR1pbdR00 = cell2mat( ops(2,6) );

bdL1mbL00 = cell2mat( ops(3,1) );
bdL1mbR00 = cell2mat( ops(3,2) );
nL1m      = cell2mat( ops(3,3) );
bR1mbdL1m = cell2mat( ops(3,4) );
bL1pbdL1m = cell2mat( ops(3,5) );
bR1pbdL1m = cell2mat( ops(3,6) );

bdR1mbL00 = cell2mat( ops(4,1) );
bdR1mbR00 = cell2mat( ops(4,2) );
bdR1mbL1m = cell2mat( ops(4,3) );
nR1m      = cell2mat( ops(4,4) );
bL1pbdR1m = cell2mat( ops(4,5) );
bR1pbdR1m = cell2mat( ops(4,6) );

bdL1pbL00 = cell2mat( ops(5,1) );
bdL1pbR00 = cell2mat( ops(5,2) );
bdL1pbL1m = cell2mat( ops(5,3) );
bdL1pbR1m = cell2mat( ops(5,4) );
nL1p      = cell2mat( ops(5,5) );
bR1pbdL1p = cell2mat( ops(5,6) );

bdR1pbL00 = cell2mat( ops(6,1) );
bdR1pbR00 = cell2mat( ops(6,2) );
bdR1pbL1m = cell2mat( ops(6,3) );
bdR1pbR1m = cell2mat( ops(6,4) );
bdR1pbL1p = cell2mat( ops(6,5) );
nR1p      = cell2mat( ops(6,6) );

I = speye( size(nL00) ); %identity

%compute two-mode hamiltonians
H00 = -J0*(bR00bdL00 + bdR00bL00) + U00*(nL00*(nL00-I) + nR00*(nR00-I)) ...
      + (V/2)*(nL00-nR00);

```

```

H1m = -J1*(bR1mbdL1m + bdR1mbL1m) + U11*(nL1m*(nL1m-I) + nR1m*(nR1m-I)) ...
      + (V/2)*(nL1m-nR1m);

H1p = -J1*(bR1pbdL1p + bdR1pbL1p) + U11*(nL1p*(nL1p-I) + nR1p*(nR1p-I)) ...
      + (V/2)*(nL1p-nR1p);

%compute energy of levels 0 and 1
E = E0*(nL00 + nR00) + E1*(nL1m + nR1m + nL1p + nR1p);

%compute inter-level, same site interactions
Uint = 4*U11*(nL00*nL1m + nL00*nL1p + nL1m*nL1p ...
          + nR00*nR1m + nR00*nR1p + nR1m*nR1p);

%compute inter-level, same site hopping
Uhop = 2*U11*(bdL1mbL00*bdL1pbL00 + bL1mbdL00*bL1pbdL00...
          + bR1mbdR00*bR1pbdR00 + bdR1mbR00*bdR1pbR00);

%compute diagonal hopping: from (1,+/-1) to (1,-/+1)
Jdia = -J11*(bdL1pbR1m + bL1pbdR1m + bR1pbdL1m + bdR1pbL1m);

%compute 2D hamiltonian
H = H00 + H1m + H1p + E + Uint + Uhop + Jdia;

%%%%%%%%%%%%%%%%%%%%%%%%%%%%%%%%%%%%%%%%%%%%%%%%%%%%%%%%%%%%%%%%%%%%%%%%%%%%%%
%%%%%%%%%%%%%%%%%%%%%%%%%%%%%%%%%%%%%%%%%%%%%%%%%%%%%%%%%%%%%%%%%%%%%%%%%%%%%%
%%%%%%%%%%%%%%%%%%%%%%%%%%%%%%%%%%%%%%%%%%%%%%%%%%%%%%%%%%%%%%%%%%%%%%%%%%%%%%
%%                                SUBFUNCTION: 3D                                %%
function H = H3D(B, L, V, ops) %subfunction

%compute 2D hopping/interaction parameters
[E0,E1,J0,J1,J11,U00,U11,U10] = parameters(B, L, 3);

nL00      = cell2mat( ops(1,1) ); %see operators.m
bR00bdL00 = cell2mat( ops(1,2) );
bL1mbdL00 = cell2mat( ops(1,3) );
bR1mbdL00 = cell2mat( ops(1,4) );
bL10bdL00 = cell2mat( ops(1,5) );
bR10bdL00 = cell2mat( ops(1,6) );
bL1pbdL00 = cell2mat( ops(1,7) );

```

```
br1pbdL00 = cell2mat( ops(1,8) );

bdR00bL00 = cell2mat( ops(2,1) );
nR00      = cell2mat( ops(2,2) );
bL1mbdR00 = cell2mat( ops(2,3) );
bR1mbdR00 = cell2mat( ops(2,4) );
bL10bdR00 = cell2mat( ops(2,5) );
bR10bdR00 = cell2mat( ops(2,6) );
bL1pbdR00 = cell2mat( ops(2,7) );
bR1pbdR00 = cell2mat( ops(2,8) );

bdL1mbL00 = cell2mat( ops(3,1) );
bdL1mbR00 = cell2mat( ops(3,2) );
nL1m      = cell2mat( ops(3,3) );
bR1mbdL1m = cell2mat( ops(3,4) );
bL10bdL1m = cell2mat( ops(3,5) );
bR10bdL1m = cell2mat( ops(3,6) );
bL1pbdL1m = cell2mat( ops(3,7) );
bR1pbdL1m = cell2mat( ops(3,8) );

bdR1mbL00 = cell2mat( ops(4,1) );
bdR1mbR00 = cell2mat( ops(4,2) );
bdR1mbL1m = cell2mat( ops(4,3) );
nR1m      = cell2mat( ops(4,4) );
bL10bdR1m = cell2mat( ops(4,5) );
bR10bdR1m = cell2mat( ops(4,6) );
bL1pbdR1m = cell2mat( ops(4,7) );
bR1pbdR1m = cell2mat( ops(4,8) );

bdL10bL00 = cell2mat( ops(5,1) );
bdL10bR00 = cell2mat( ops(5,2) );
bdL10bL1m = cell2mat( ops(5,3) );
bdL10bR1m = cell2mat( ops(5,4) );
nL10      = cell2mat( ops(5,5) );
bR10bdL10 = cell2mat( ops(5,6) );
bL1pbdL10 = cell2mat( ops(5,7) );
bR1pbdL10 = cell2mat( ops(5,8) );

bdR10bL00 = cell2mat( ops(6,1) );
bdR10bR00 = cell2mat( ops(6,2) );
```

```

bdR10bL1m = cell2mat( ops(6,3) );
bdR10bR1m = cell2mat( ops(6,4) );
bdR10bL10 = cell2mat( ops(6,5) );
nR10       = cell2mat( ops(6,6) );
bL1pbdR10 = cell2mat( ops(6,7) );
bR1pbdR10 = cell2mat( ops(6,8) );

```

```

bdL1pbL00 = cell2mat( ops(7,1) );
bdL1pbR00 = cell2mat( ops(7,2) );
bdL1pbL1m = cell2mat( ops(7,3) );
bdL1pbR1m = cell2mat( ops(7,4) );
bdL1pbL10 = cell2mat( ops(7,5) );
bdL1pbR10 = cell2mat( ops(7,6) );
nL1p      = cell2mat( ops(7,7) );
bR1pbdL1p = cell2mat( ops(7,8) );

```

```

bdR1pbL00 = cell2mat( ops(8,1) );
bdR1pbR00 = cell2mat( ops(8,2) );
bdR1pbL1m = cell2mat( ops(8,3) );
bdR1pbR1m = cell2mat( ops(8,4) );
bdR1pbL10 = cell2mat( ops(8,5) );
bdR1pbR10 = cell2mat( ops(8,6) );
bdR1pbL1p = cell2mat( ops(8,7) );
nR1p      = cell2mat( ops(8,8) );

```

```
I = speye( size(nL00) ); %identity
```

```
%compute two-mode hamiltonians
```

```
H00 = -J0*(bR00bdL00 + bdR00bL00) + U00*(nL00*(nL00-I) + nR00*(nR00-I)) ...
      + (V/2)*(nL00-nR00);
```

```
H1m = -J1*(bR1mbdL1m + bdR1mbL1m) + U11*(nL1m*(nL1m-I) + nR1m*(nR1m-I)) ...
      + (V/2)*(nL1m-nR1m);
```

```
H10 = -J0*(bR10bdL10 + bdR10bL10) + U10*(nL10*(nL10-I) + nR10*(nR10-I)) ...
      + (V/2)*(nL10-nR10);
```

```
H1p = -J1*(bR1pbdL1p + bdR1pbL1p) + U11*(nL1p*(nL1p-I) + nR1p*(nR1p-I)) ...
      + (V/2)*(nL1p-nR1p);
```

```

%compute energy of levels 0 and 1
E = E0*(nL00 + nR00) + E1*(nL1m + nR1m + nL10 + nR10 + nL1p + nR1p);

%compute inter-level, same site interactions
Uint = 4*U11*(nL00*nL1m + nL00*nL10 + nL00*nL1p + nL1m*nL1p ...
          + nR00*nR1m + nR00*nR10 + nR00*nR1p + nR1m*nR1p) ...
        + 2*U11*(nL10*nL1m + nL10*nL1p + nR10*nR1m + nR10*nR1p);

%compute inter-level, same site hopping
Uhop = 2*U11*(bdL1mbL00*bdL1pbL00 + bL1mbdL00*bL1pbdL00...
          + bR1mbdR00*bR1pbdR00 + bdR1mbR00*bdR1pbR00)...
        + U11*(bL10bdL00^2 + bdL10bL00^2 + bR10bdR00^2 + bdR10bR00^2);

%compute same-level, same site hopping: from (1,0) to (1,+/-1)
Uhop_2 = U11*(bdL1mbL10*bdL1pbL10 + bL1mbdL00*bL1pbdL10...
          + bR1mbdR00*bR1pbdR10 + bdR1mbR00*bdR1pbR10);

%compute diagonal hopping: from (1,+/-1) to (1,-/+1)
Jdia = -J11*(bdL1pbR1m + bL1pbdR1m + bR1pbdL1m + bdR1pbL1m);

%compute 3D hamiltonian
H = H00 + H1m + H10 + H1p + E + Uint + Uhop + Uhop_2 + Jdia;

```